Technical Report Documentation Page

1. Report No.	2. Government Accession No.	3. Recipient's Catalog No.
FHWA/TX-96/1335-2		

4. Title and Subtitle	5. Report Date
EVALUATION OF PAVEMENT BASE AND SUBGRADE MATERIAL PROPERTIES AND TEST PROCEDURES	November 1995
	6. Performing Organization Code

7. Author(s)	8. Performing Organization Report No.
Leslie Titus-Glover and Emmanuel G. Fernando	Research Report 1335-2

9. Performing Organization Name and Address	10. Work Unit No. (TRAIS)
Texas Transportation Institute The Texas A&M University System College Station, Texas 77843-3135	11. Contract or Grant No. Study No. 0-1335

12. Sponsoring Agency Name and Address	13. Type of Report and Period Covered
Texas Department of Transportation Research and Technology Transfer Office P. O. Box 5080 Austin, Texas 78763-5080	Interim: March 1994 - August 1995
	14. Sponsoring Agency Code

15. Supplementary Notes

Research performed in cooperation with the Texas Department of Transportation and the U.S. Department of Transportation, Federal Highway Administration.
Research Study Title: Movement of Superheavy Loads Over the State Highway System

16. Abstract

The objective of this research was to develop simpler and less expensive procedures for characterizing the resilient properties, K_1 to K_3; the strength parameters, cohesion, C; and angle of internal friction, ϕ, of base and subgrade materials. Researchers accomplished this by developing prediction equations which use easy to obtain soil properties and by evaluating a modified Texas triaxial test procedure which can be used to determine both the strength and resilient properties of pavement materials. Researchers tested five subgrade soils, i.e., sand, lean clay, fat clay, silt, and sandy gravel, and four base materials, i.e., crushed limestone, caliche, shellbase, and iron ore gravel, according to Texas specifications to obtain a database of material properties for developing the prediction equations. In developing this database, the strength parameters, C, and ϕ, of the Mohr-Coulomb yield criterion, were obtained from standard Texas triaxial tests. For the resilient properties, compressive creep and recovery tests were run using AASHTO T-274 as a guide, to obtain the resilient moduli and Poisson's ratios of the materials tested at different stress states and moisture contents. The standard Texas triaxial test procedure, TEX-117-E, was modified to include a creep and recovery cycle before the test sample is loaded monotonically to failure. This loading sequence produced test data that allowed the estimation of the K_1 to K_3 resilient properties in addition to the strength parameters, C, and ϕ. The strength and resilient parameters obtained from the modified Texas triaxial test were compared to those obtained from the standard Texas triaxial test and the compressive creep and recovery test. Researchers document the results of these comparisons, as well as the development of the equations for predicting the strength and resilient parameters of base and subgrade materials, in this report.

17. Key Words	18. Distribution Statement
Triaxial Test, Compressive Creep and Recovery Test, Nonlinear Material Properties, Resilient Properties, Strength Properties, Cohesion, Angle of Internal Friction	No restrictions. This document is available to the public through NTIS: National Technical Information Service 5285 Port Royal Road Springfield, Virginia 22161

19. Security Classif.(of this report)	20. Security Classif.(of this page)	21. No. of Pages	22. Price
Unclassified	Unclassified	126	

EVALUATION OF PAVEMENT BASE AND SUBGRADE MATERIAL PROPERTIES AND TEST PROCEDURES

by

Leslie Titus-Glover
Graduate Research Assistant
Texas Transportation Institute

and

Emmanuel G. Fernando
Assistant Research Engineer
Texas Transportation Institute

Research Report 1335-2
Research Study Number 0-1335
Research Study Title: Movement of Superheavy Loads
Over the State Highway System

Sponsored by the
Texas Department of Transportation
In Cooperation with
U. S. Department of Transportation
Federal Highway Administration

November 1995

TEXAS TRANSPORTATION INSTITUTE
The Texas A&M University System
College Station, Texas 77843-3135

IMPLEMENTATION STATEMENT

The procedures for determining the resilient and strength parameters of base and subgrade materials should be implemented within the Texas Department of Transportation (TxDOT). TTI researchers can assist with this implementation. While the procedures utilize test methods and equipment already established within the Department, there will be a need for training with respect to measuring soil suction and dielectric properties, and for conducting the modified Texas triaxial test and the compressive creep and recovery test. There is also a need to establish standard TxDOT procedures for these new tests. This can be done as part of the implementation effort. In the development of standard test procedures, researchers recommend the following tasks:

1. Further testing should be done with the modified Texas triaxial test procedure to obtain a broader database to establish the effect of moisture on determining K_1 and K_2, and to investigate further the relationships between the resilient parameters from the modified test procedure and the compressive creep and recovery test.
2. A laboratory program should be established and executed to compare resilient parameters from the compressive creep and recovery test to the corresponding parameters determined from the resilient modulus test described in AASHTO T-274.
3. The resilient parameters estimated from the modified Texas triaxial test should also be compared with corresponding parameters from the resilient modulus test (AASHTO T-274).
4. A laboratory program should be conducted to evaluate the resilient and strength parameters for TxDOT asphalt concrete mixtures and stabilized base materials.

DISCLAIMER

The contents of this report reflect the views of the authors, who are responsible for the facts and the accuracy of the data presented herein. The contents do not necessarily reflect the official view or policies of the Texas Department of Transportation (TxDOT), or the Federal Highway Administration (FHWA). This report does not constitute a standard, specification or regulation, nor is it intended for construction, bidding, or permit purposes. The engineer in charge of the project was Dr. Emmanuel G. Fernando, P.E. # 69614.

ACKNOWLEDGMENTS

The work reported herein was conducted as part of a research study sponsored by TxDOT and the Federal Highway Administration, U.S. Department of Transportation. The objective of the study was to develop a procedure for evaluating the structural adequacy of pavement sections along a proposed superheavy load route. The researchers gratefully acknowledge the support and guidance of the Project Director, Mr. Michael Murphy. The researchers extend a sincere note of appreciation to the following Districts for their assistance in the collection of data on superheavy load routes: Atlanta, Austin, Beaumont, Houston, Tyler, and Yoakum.

TABLE OF CONTENTS

Page

LIST OF FIGURES xi

LIST OF TABLES xv

SUMMARY xvii

CHAPTER 1. INTRODUCTION 1

BACKGROUND 1
RESEARCH OBJECTIVE 2
RESEARCH APPROACH 2

CHAPTER 2. LITERATURE REVIEW 5

OVERVIEW 5
PAVEMENT MATERIAL RESPONSE MODEL 5
STRENGTH PARAMETERS 16
SOIL SUCTION 17

CHAPTER 3. LABORATORY INVESTIGATION AND RESULTS 23

INTRODUCTION 23
SPECIFIC GRAVITY 24
PARTICLE SIZE ANALYSIS 24
MOISTURE-DENSITY CHARACTERISTICS 30
ATTERBERG LIMITS 32
MEASUREMENT OF SOIL SUCTION (FILTER PAPER METHOD) 33
MEASUREMENT OF SOIL SUCTION (PRESSURE PLATE METHOD) . . 36
TEXAS TRIAXIAL TEST (MONOTONIC LOADING) 42
MODIFIED TEXAS TRIAXIAL TEST 48
COMPRESSIVE CREEP AND RECOVERY TEST 55
DIELECTRIC AND CONDUCTIVITY TEST 60

CHAPTER 4. ANALYSIS OF THE MODIFIED TEXAS TRIAXIAL TEST RESULTS 63

INTRODUCTION 63
STATISTICAL ANALYSIS 67

CHAPTER Page

CHAPTER 5. PREDICTIVE RELATIONSHIPS 75

INTRODUCTION 75
EXPLORATORY ANALYSIS 77
TEST FOR NORMALITY, INDEPENDENCE AND CONSTANT VARIANCE 77
DIAGNOSTIC STATISTICS 77
MODEL SELECTION 78
RESILIENT PARAMETER K_1 79
SUMMARY 80
RESILIENT PARAMETER K_2 81
SUMMARY 81
RESILIENT PARAMETER K_3 82
SUMMARY 83
EFFECT OF LOADING TIME ON THE RESILIENT MODULUS OF PAVEMENT MATERIALS 84
STRENGTH PARAMETER COHESION, C 86
SUMMARY 88
STRENGTH PARAMETER ANGLE OF INTERNAL FRICTION, ϕ 88
SUMMARY 89

CHAPTER 6. CONCLUSIONS AND RECOMMENDATIONS 91

CONCLUSIONS 91
RECOMMENDATIONS 92

REFERENCES 93

APPENDIX 97

LIST OF FIGURES

FIGURE		Page
1.	Visco-Elasto-Plastic Model (2)	6
2.	Observed Versus Predicted Resilient Modulus	11
3.	Observed Versus Predicted Poisson's Ratio	12
4.	Vertical Creep Compliance Curve from Laboratory Data and Fitted Compliance Equation	14
5.	Radial Creep Compliance Curve from Laboratory Data and Fitted Compliance Equation	14
6.	Vertical Creep Compliance from Laboratory Data and Compliance Equation	15
7.	Radial Creep Compliance from Laboratory Data and Compliance Equation	15
8.	Mohr Circles and Failure Envelope	17
9.	Gradation Curve of Limestone	26
10.	Gradation Curve of Iron Ore Gravel	26
11.	Gradation Curve of Sandy Gravel	27
12.	Gradation Curve of Caliche	27
13.	Gradation Curve of Shellbase	28
14.	Gradation Curve of Sand	28
15.	Gradation Curve of Silt	29
16.	Gradation Curve of Lean Clay	29
17.	Gradation Curve of Fat Clay	30
18.	Moisture Density Curve for Caliche	31

FIGURE Page

19. Moisture Density Curve for Lean Clay 32

20. Soil Sample with Filter Papers 34

21. Suction Versus Moisture Content of Filter Paper (calibration curve 1) 35

22. Suction Versus Moisture Content of Filter Paper (calibration curve 2) 35

23. Suction Versus Moisture Content for Limestone 37

24. Suction Versus Moisture Content for Iron Ore Gravel 38

25. Suction Versus Moisture Content for Sandy Gravel 38

26. Suction Versus Moisture Content for Caliche 39

27. Suction Versus Moisture Content for Shellbase 39

28. Suction Versus Moisture Content for Sand 40

29. Suction Versus Moisture Content for Silt 40

30. Suction Versus Moisture Content for Lean Clay 41

31. Suction Versus Moisture Content for Fat Clay 41

32. Mohr Failure Envelopes for Limestone 43

33. Mohr Failure Envelopes for Iron Ore Gravel 43

34. Mohr Failure Envelopes for Sandy Gravel 44

35. Mohr Failure Envelopes for Caliche 44

36. Mohr Failure Envelopes for Shellbase 45

37. Mohr Failure Envelopes for Sand 45

38. Mohr Failure Envelopes for Silt 46

39. Mohr Failure Envelopes for Lean Clay 46

FIGURE Page

40. Mohr Failure Envelopes for Fat Clay 47

41. Mohr Failure Envelope for Limestone 48

42. Mohr Failure Envelope for Iron Ore Gravel 49

43. Mohr Failure Envelope for Sandy Gravel 49

44. Mohr Failure Envelope for Caliche 50

45. Mohr Failure Envelope for Shellbase 50

46. Mohr Failure Envelope for Sand 51

47. Mohr Failure Envelope for Silt 51

48. Mohr Failure Envelope for Lean Clay 52

49. Mohr Failure Envelope for Fat Clay 52

50. Load and Deformation Profiles for Modified Texas Triaxial Test 54

51. Pressure Chamber with Specimen 56

52. Specimen with Vertical and Radial LVDT's 56

53. Vertical Displacement Measuring System 58

54. Radial Displacement Measuring System 58

55. Dielectric Probe Used to Measure Dielectric Constants of Laboratory Molded Specimens 61

56. Cohesion Results from Standard and Modified Texas Triaxial Tests for Caliche, Shellbase and Sand 64

57. Cohesion Results from Standard and Modified Texas Triaxial Tests for Limestone, Iron Ore Gravel and Sandy Gravel 64

58. Cohesion Results from Standard and Modified Texas Triaxial Tests for Silt, Lean Clay and Fat Clay 65

FIGURE Page

59. Angle of Internal Friction Results from Standard and Modified Texas Triaxial Tests for Limestone, Iron Ore Gravel and Sandy Gravel 65

60. Angle of Internal Friction Results from Standard and Modified Texas Triaxial Tests for Caliche, Silt and Sand 66

61. Angle of Internal Friction Results from Standard and Modified Texas Triaxial Tests for Silt, Lean Clay and Fat Clay 66

62. Standard Cohesion Versus Modified Cohesion 68

63. Standard Friction Angle Versus Modified Friction Angle 68

64. Modified Texas Triaxial Test K_1 Versus Compressive Creep and Recovery Test K_1 70

65. Modified Texas Triaxial Test K_2 Versus Compressive Creep and Recovery Test K_2 70

66. Measured K_1 from Compressive Creep and Recovery Test Versus Predicted K_1 from Calibration Equation 72

67. Measured K_2 from Compressive Creep and Recovery Test Versus Predicted K_2 from Calibration Equation 72

68. Flow Chart of Regression Analysis (22) 76

69. Measured Versus Predicted K_1 Values 80

70. Measured Versus Predicted K_2 Values 82

71. Measured Versus Predicted K_3 Values 83

72. Measured Versus Predicted Natural Logarithm of Resilient Modulus 85

73. Measured Versus Predicted Cohesion 87

74. Measured Versus Predicted Angle of Internal Friction, ϕ, Values 89

LIST OF TABLES

TABLE		Page
1.	Specific Gravity of Binder Content for Each Soil Type Tested	24
2.	Sieve Analysis of Base Materials	25
3.	Sieve Analysis of Subgrade Materials	25
4.	Optimum Moisture Content and Maximum Dry Density	31
5.	Atterberg Limits of Base and Subgrade Materials	33
6.	Value of Constants A and B for Suction Curves	37
7.	Cohesion and Angle of Internal Friction Results for Materials	47
8.	Summary of Strength and Resilient Parameters from Modified Texas Triaxial Test	53
9.	Material Properties K_1 to K_5 and Suction for Material at -2% of Optimum	59
10.	Material Properties K_1 to K_5 and Suction for Material at Optimum	59
11.	Material Properties K_1 to K_5 and Suction for Material at +2% Optimum	60
12.	Dielectric and Conductivity Values for Materials Tested	62
13.	Typical Dielectric Constants	62
14.	Calibrated K_1 and K_2 Values from Modified Texas Triaxial Test	71
15.	Critical Values of Diagnostic Statistics	78
A.1	Analysis of Variance for Cohesion	99
A.2	Analysis of Variance for Angle of Internal Friction	100
A.3	Analysis of Variance for Resilient Parameter K_1	101
A.4	Analysis of Variance for Resilient Parameter K_2	102

TABLE Page

A.5 Regression and General Linear Model Output for K_1 103

A.6 Regression and General Linear Model Output for K_2 104

A.7 Regression and General Linear Model Output for K_3 105

A.8 Regression and General Linear Model Output for $\ln(E_{r,t})$ 106

A.9 Regression and General Linear Model Output for Cohesion, C 107

A.10 Regression and General Linear Model Output for Angle of Internal Friction, ϕ 108

SUMMARY

This report forms part of the work done under TxDOT Study 1335 which investigated the movement of superheavy loads over the state highway system. During the course of this project, researchers performed a laboratory investigation and an analysis of test data. This report describes the test procedures and the underlying theory and presents an analysis of the data obtained together with the development of regression equations to estimate the strength and resilient parameters of base and subgrade materials.

Nine different base and subgrade materials were tested to set up a database of material properties for developing prediction equations. The materials tested were crushed limestone, caliche, iron ore gravel, shellbase, sandy gravel, sand, silt, lean clay, and fat clay. These materials were selected because they are found in pavements in the southeastern region of Texas where most superheavy load moves take place. The tests performed included the standard Texas triaxial test and the compressive creep and recovery test. The procedure for this latter test generally follows AASHTO T-274 except that a different loading sequence is used. In addition, researchers evaluated a modified Texas triaxial test wherein a creep and recovery cycle is run prior to loading the test specimen monotonically to failure. Researchers analyzed the resulting creep and recovery data to estimate the resilient parameters of pavement materials. Results from this evaluation demonstrated the feasibility of using the modified Texas triaxial test for characterizing not only the strength properties of soils but also the resilient properties. This finding is of practical significance.

Using the database of material properties, the research team developed regression equations to estimate the resilient parameters K_1, K_2, and K_3, which determine the resilient modulus of materials under different stress states. Similar prediction equations were developed for cohesion and angle of internal friction, which are parameters of the Mohr-Coulomb yield criterion that is the basis for the structural assessment of superheavy load routes. Researchers also developed resilient modulus transformation equations to take the effect of time of loading into account in the characterization of the resilient properties of base and subgrade materials.

CHAPTER 1
INTRODUCTION

BACKGROUND

Several elements are critical to highway pavement performance. These elements include traffic loading, the properties of the materials comprising the pavement system, and the climatic and moisture conditions to which the materials are subject. The increase in the frequency of heavier traffic loads and superheavy loads in the last few years has made it critical for the strength and resilient properties of these materials to be determined with reasonable accuracy and cost to enable the pavement engineer to predict the effect of increased loads on the pavement materials, and hence, the pavement system as a whole. There are several methods to determine these properties; however, some of the methods currently in use are time consuming, expensive and require sophisticated test equipment.

The Texas Department of Transportation (TxDOT) is the sponsor of a project to investigate the movement of superheavy loads over the state highway system. The objective of this study is to develop a procedure for assessing the structural adequacy of pavement sections along a proposed superheavy load route prior to the move. If the route is deemed adequate, the move can proceed as planned. Otherwise, alternative routes will have to be identified or temporary strengthening measures applied on weak segments of the route.

The evaluation of structural adequacy requires determining the strength and resilient properties of the pavement materials found along the proposed route. This report documents the research work conducted to develop simple and practical procedures for estimating these material properties. The results from this work have been incorporated into the procedure developed for structural evaluation of superheavy load routes.

RESEARCH OBJECTIVE

The research work documented herein focuses on predicting the strength and resilient properties of the materials (base and subgrade) that make up the foundation of the highway pavement by considering alternative and more simple procedures and analysis as compared to the traditional methods for obtaining these properties.

Material strength parameters, specifically cohesion, **C**, and the angle of internal friction, ϕ, are obtained by using traditional test methods such as the standard Texas triaxial test. Recent mechanistic analyses have established that these parameters have a good correlation with soil properties such as Atterberg limits, suctions, gradation and others, that are obtained from simple and inexpensive laboratory tests and analysis (1). This was also realized for the resilient modulus and the Poisson's ratio, which are some of the resilient properties of materials.

This research seeks to identify elastic constitutive relationships that best model the actual stress and recoverable strain states in base and subgrade materials. This will be used to obtain the resilient parameters K_1, K_2, and K_3 which are material constants used in the models to predict the resilient modulus and Poisson's ratios for various stress states (2). The strength parameters C, and ϕ, are also predicted based on a model developed from the Mohr-Coulomb failure criterion (1). Finally, researchers evaluated a modification to the Texas triaxial test procedure with the aim of obtaining both the strength and the resilient properties of soils from the Texas triaxial test. This report presents the results from the research.

RESEARCH APPROACH

The approach used in this investigation compares the strength parameters obtained from the standard Texas triaxial test to those from prediction equations and models, and the modified Texas triaxial test. Also, the resilient properties, K_1 to K_3, obtained from the compressive creep and recovery test, are compared to those from the modified Texas triaxial test and prediction equations.

Nine different soil types, ranging from fine grained to granular materials, were used in the laboratory investigation. The materials tested were crushed limestone,

caliche, iron ore gravel, shellbase, sandy gravel, sand, silt, lean clay, and fat clay. These materials were selected because they are representative of those found in pavements in the southeastern region of Texas where most superheavy load moves take place. Triaxial tests were conducted following the standard Texas test method except that compacted specimens were prepared and tested at three moisture contents corresponding to the optimum, and plus and minus two percent of the optimum, in lieu of saturating the specimens by capillary absorption. In this way, the effects of moisture on Mohr-Coulomb strength parameters can be evaluated and considered in developing the structural evaluation procedure for superheavy load routes. Finally, a statistical analysis of the various comparisons was made to determine their significance.

CHAPTER 2
LITERATURE REVIEW

OVERVIEW

There are a variety of material properties that can be used to characterize the behavior of pavement materials. As defined in the discipline of mechanics, material properties are those characteristics of materials that do not depend upon the testing apparatus, procedure or conditions (3). Instead, they are test-independent relationships between causative and response quantities that can be observed or measured. Thus an elastic modulus is a relationship between the applied stress and an observed strain. A Poisson's ratio is a relationship between strains measured at right angles. Material properties are important to define because they permit the use of mechanics in predicting the behavior of a pavement under the service conditions of traffic and weather.

PAVEMENT MATERIAL RESPONSE MODEL

Most paving materials can be described as visco-elasto-plastic (2). They have an elastic, viscous and plastic strain response when stressed. Figure 1 shows the loading profile and corresponding strain response of a visco-elasto-plastic material. The upper part of Figure 1 shows a constant load, σ_0, applied for a fixed time. The material is then unloaded. An instantaneous and time dependent strain response is observed. This is shown in the bottom part of the figure. The instantaneous response at the time of loading is made up of the elastic, ε_e, and plastic, ε_p, strains. The time dependent strain, $\varepsilon(t)$, under a constant stress, σ_0, is made up of the visco-elastic, ε_{ve}, and visco-plastic, ε_{vp}, strains. The instantaneous response which is observed when the material is unloaded is the elastic strain, ε_e. A long time after unloading, the response of the material tends to be asymptotic to the sum of the plastic, ε_p, and visco-plastic, ε_{vp}, strains which are the irrecoverable components of the strain. The meanings of the components in Figure 1 are as follows:

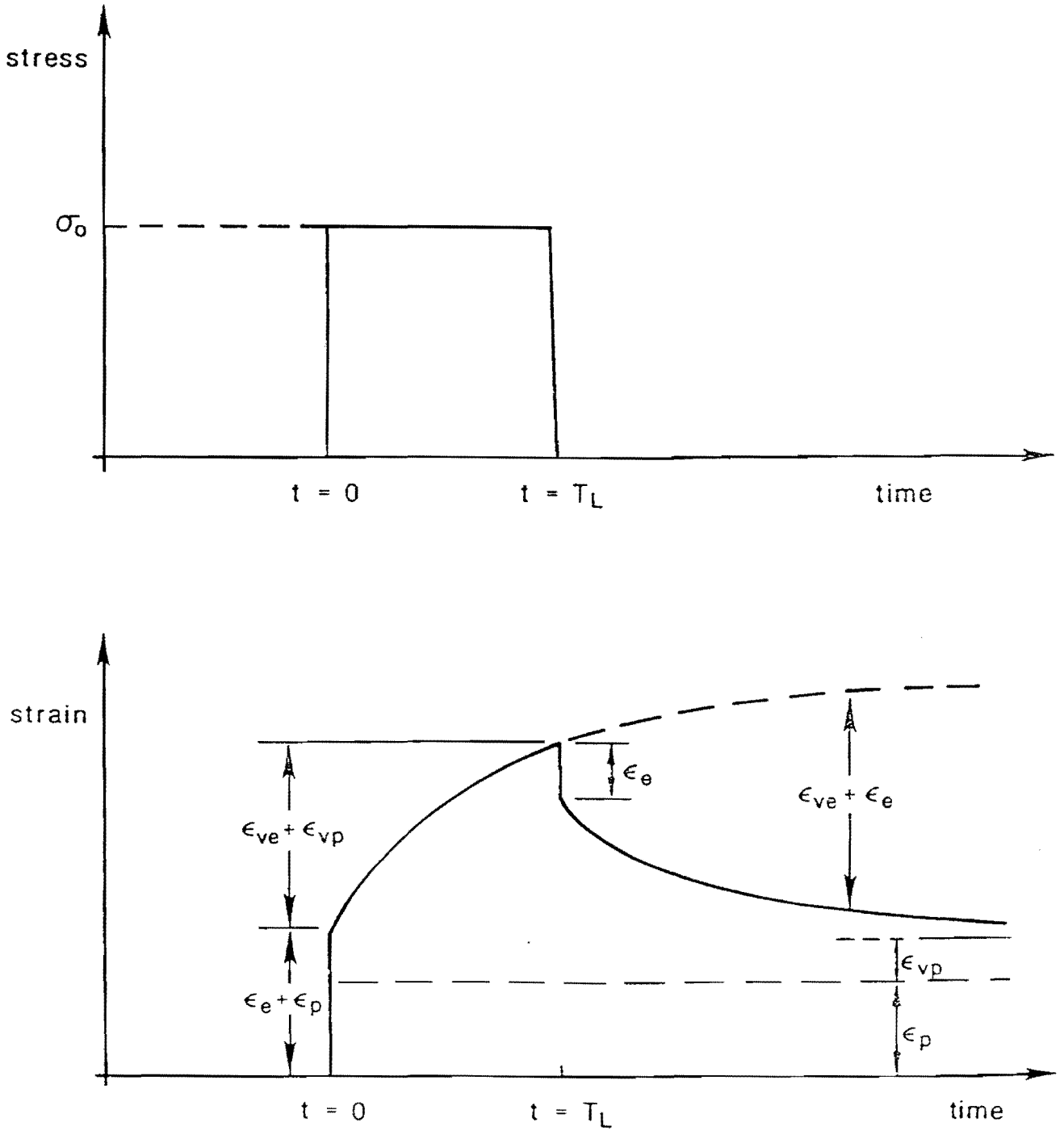

Figure 1. Visco-Elasto-Plastic Model (2).

t	=	time;
$t = 0$	=	start of loading;
$t = T_L$	=	end of loading;
σ_0	=	applied stress;
ε_e	=	elastic component of strain;
ε_{ve}	=	viscoelastic component of strain;
ε_p	=	plastic component of strain; and
ε_{vp}	=	viscoplastic component of strain.

The behavior of most pavement materials follows that of a non-linear visco-elasto-plastic model (2). This implies that the response of the material depends not only on the load applied but also on the time of loading. In granular materials, the time dependence is negligible and can be neglected. In other material types, such as fine grained materials, the time dependence cannot be neglected (2).

The use of a visco-elasto-plastic model in a primary response model is not practical to implement in a procedure for the structural evaluation of superheavy load routes due to the large number of superheavy load permit applications received by TxDOT each year (2). However, a good approximation of the time-dependent response may be achieved through the use of a quasi-elastic approach. Schapery (4) and Chua and Lytton (5) have shown that the use of material properties appropriate for a given loading time in an elastic model leads to a good approximation of the time-dependent response. Researchers use this quasi-elastic approach in the structural evaluation procedure for superheavy loads.

Recent mechanistic analysis has established a relationship between the resilient modulus of paving materials and the first and second stress invariants. The equation, developed by Uzan (6), has been used in many instances to obtain the resilient parameters, K_1 to K_3, of pavement materials (7). The equation is as follows:

$$E = K_1 P_a \left(\frac{I_1}{P_a}\right)^{K_2} \left(\frac{\tau_{oct}}{P_a}\right)^{K_3} \quad (1)$$

where E = resilient modulus;

P_a = atmospheric pressure;

I_1 = first stress invariant ($\sigma_1 + \sigma_2 + \sigma_3$ with σ_i = stress);

τ_{oct} = octahedral shear stress; and

K_i = material constants.

Equation (1) is referred to as a universal material model (2). It is simplified in certain instances. In granular materials, for example, K_3 is set to zero. Equation (1) thus reduces to

$$E = K_1 P_a \left(\frac{I_1}{P_a}\right)^{K_2} \quad (2)$$

As the material changes from granular to fine grained, the K_2 value approaches zero. The model is flexible and is capable of a resilient modulus decrease as the octahedral shear stress increases and a resilient modulus increase as the first stress invariant increases. These phenomena are observed in practice. It also fairly represents the stiffening effect observed in laboratory tests that results in an increase of resilient modulus as both the first stress invariant and the octahedral shear stress increase at large deviatoric stresses or large octahedral shear stresses. This stiffening effect is believed to be a characteristic of a granular material in a dense state, and is related to the dilation phenomenon in granular materials.

Equation (1) has been used extensively to represent pavement material behavior. It is generally used with the assumption of a constant Poisson's ratio. However, several studies have shown that Poisson's ratio increases with increasing stress ratio (σ_1/σ_3) reaching values greater than 0.5 (2).

According to Lade and Nelson (8) the following differential equation governs the relationship between resilient modulus and Poisson's ratio:

$$\frac{2\partial v}{3\partial J_2}+\frac{1\partial v}{I_1\partial I_1}=-\frac{1-2v}{3}\frac{\partial lnE}{\partial J_2}+\frac{1+v}{I_1}\frac{\partial lnE}{\partial I_1} \tag{3}$$

where: υ = Poisson's ratio;

I_1 = first stress invariant;

J_2 = second deviatoric stress invariant (= $3\tau^2_{oct}/2$); and

E = resilient modulus.

The solution of Equation (3) was obtained for the Poisson's ratio using Equation (1) as a solution of the resilient modulus. This is believed to be a good assumption and fits laboratory results well (2). Substituting Equation (1) into Equation (3) leads to a partial differential equation where the Poisson's ratio, υ, is the dependent variable, I_1 and J_2 are the independent variables, and K_2 and K_3, the material constants. Equation (1) is rewritten as

$$\ln E=\ln[K_1P_a]+K_2\ln\left[\frac{I_1}{P_a}\right]+\frac{K_3}{2}\ln\left[\frac{2J_2}{3P_a}\right] \tag{4}$$

Substituting Equation (4) into Equation (3) leads to the following partial differential equation:

$$\frac{2}{3}\frac{\partial v}{\partial J_2}+\frac{1}{I_1}\frac{\partial v}{\partial I_1}=v\left(\frac{2}{3}\frac{K_3}{J_2}+\frac{K_2}{I_1^2}\right)+\left(-\frac{1}{3}\frac{K_3}{J_2}+\frac{K_2}{I_1^2}\right) \tag{5}$$

Solving the partial differential equation yields two solutions U_1 and U_2 which include the boundary conditions (2). They are expressed as follows:

$$U_1 = 3J_2 - I_1^2 \tag{6}$$

$$U_2 = \frac{\upsilon}{I_1^{K_2} J_2^{K'_3}} - \frac{3^{K'_3}}{2(I_1^2 - 3J_2)^{\frac{K_2}{2}+K'_3}} \left[-K_2 B_\nu \left(\frac{K_2}{2}+K'_3, -K'_3+1 \right) + K'_3 B_\nu \left(\frac{K_2}{2}+K'_3, -K'_3 \right) \right] \tag{7}$$

where

	U_i	=	arbitrary constants;
	$B_\nu(a,b)$	=	incomplete beta function with parameters a and b;
	I_1	=	first stress invariant;
	J_2	=	second deviatoric stress invariant;
	υ	=	Poisson's ratio;
	K_i	=	material constants; and
	K'_3	=	$K_3/2$.

It was found that U_1 and U_2 are related through an exponential form where K_4 and K_5 are additional material constants, as follows (2):

$$U_2 = K_4(-U_1)^{K_5} \tag{8}$$

From Equations (6), (7) and (8), the following expression for Poisson's ratio, υ, can be derived:

$$\upsilon = K_4(I_1^2 - 3J_2)^{K_5} I_1^{K_2} J_2^{K'_3} + \frac{I_1^{K_2} J_2^{K'_3} 3^{K'_3}}{2(I_1^2 - 3J_2)^{\frac{K_2}{2}+K'_3}} \left[-K_2 B_\nu \left(\frac{K_2}{2}+K'_3, -K'_3+1 \right) + K'_3 B_\nu \left(\frac{K_2}{2}+K'_3, -K'_3 \right) \right] \tag{9}$$

The above formulation and solution permits the derivation of the resilient material properties K_1 to K_5 from laboratory test results. Researchers analyzed the results of compressive creep and recovery tests using a nonlinear regression procedure to fit the resilient modulus and Poisson's ratio results from the laboratory tests. Although the resilient modulus and Poisson's ratio are two independent material properties in the linear elastic case, they appear to be related in the non-linear case (2). Figures 2 and 3 show plots of the measured resilient modulus and Poisson's ratio versus the predicted resilient modulus and Poisson's ratio, respectively. The observed values were obtained from the laboratory testing and the calculated values were determined using the method already described to obtain K_1 to K_5. It is evident that a good correlation exists between the observed values from the laboratory testing and the calculated values. The vertical and lateral strains used to calculate the resilient modulus and the Poisson's ratio were obtained by fitting a creep compliance equation to the laboratory data.

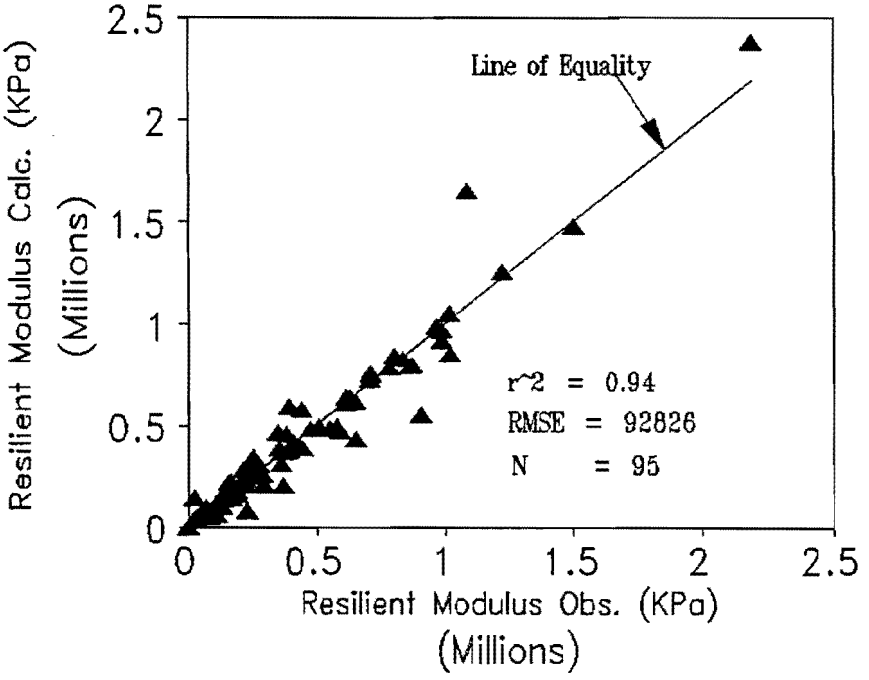

Figure 2. Observed Versus Predicted Resilient Modulus.

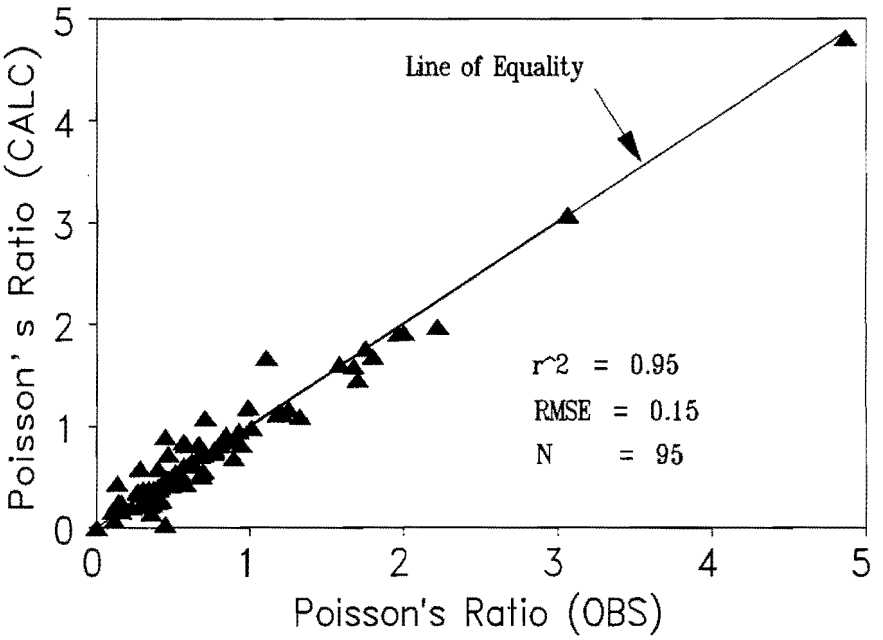

Figure 3. Observed Versus Predicted Poisson's Ratio.

Creep compliance is defined as the reciprocal of Young's modulus (9):

$$D(t) = \frac{\varepsilon(t)}{\sigma} \tag{10}$$

where $\varepsilon(t)$ = the time dependent strain under a constant stress and

σ = constant stress.

A general form of the creep compliance equation is as follows (9):

$$D(t) = \frac{1}{E_0}\left(1+\frac{t}{T_0}\right) + \sum_{i=1}^{n} \frac{1}{E_i}\left[\left(1-\exp\left(-\frac{t}{T_i}\right)\right)\right] \tag{11}$$

where E_i = viscoelastic constants;

t = time; and

T_i = viscoelastic constants.

Equation (11) is often simplified and used in the form shown below (9):

$$D(t)=D_0+D_1at^m \tag{12}$$

In the case of soil materials which can be described as nonlinear visco-elasto-plastic materials, researchers derived the creep compliance equation using a modification outlined by Sides et al. (10), in which the strain is separated into the four components shown in Figure 1. The instantaneous response upon loading is time independent and includes both an elastic and plastic component (11). The time dependent response, under a constant sustained stress also has two components, the viscoelastic and viscoplastic. Upon the removal of the stress, an instantaneous response, which is the elastic response, occurs. The time dependent response after unloading is due to viscoelasticity only. After a long time of unloading, the response of the material tends to be asymptotic to the sum of the viscoplastic and plastic deformation which are the irrecoverable components. Using the power law to describe the viscoelastic and viscoplastic components, the following expression is obtained for creep compliance (10):

$$D\ (t)\ -\ D_e\ +\ D_{ve}\left[\frac{t^m}{1\ +\ at^m}\right]\ +\ D_p\ +\ D_{vp}\left[\frac{t^q}{1\ +\ bt^q}\right] \tag{13}$$

where t is time and D_e, D_{ve}, D_p, D_{vp}, m, q, a, and b are creep compliance coefficients. Figures 4 and 5 show creep compliance curves measured from the laboratory and a matching curve obtained from Equation (13) above. Figures 6 and 7 show plots of the measured versus predicted compliance for all of the data obtained from the laboratory tests conducted in this project. As the figures show, the creep compliance model given by Equation (13) fits the observed creep compliance data very well.

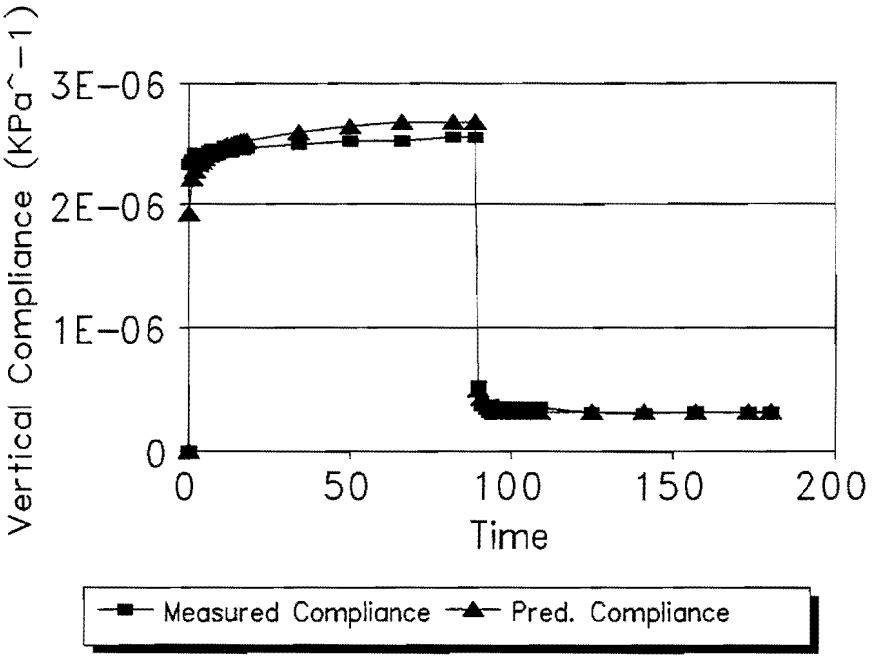

Figure 4. Vertical Creep Compliance Curve from Laboratory Data and Fitted Compliance Equation.

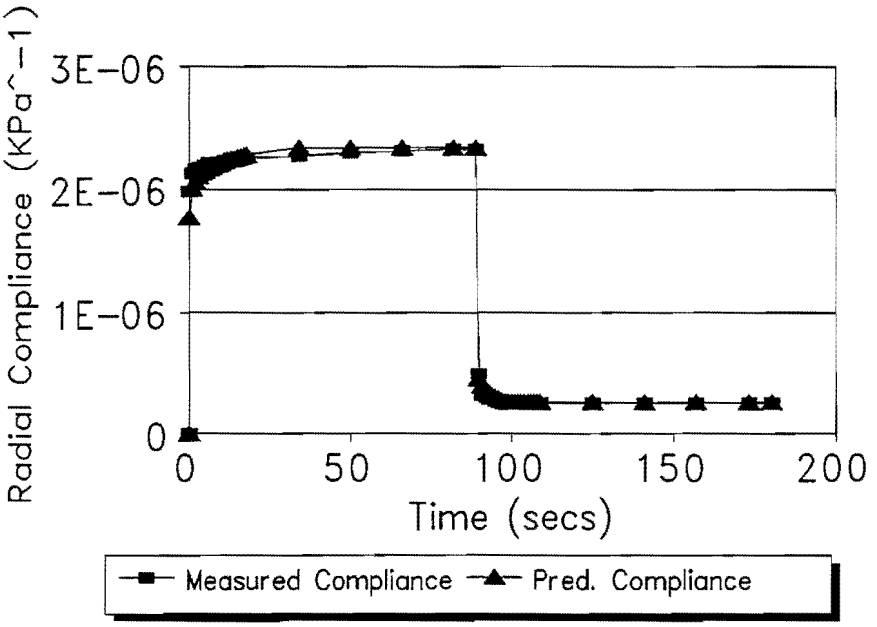

Figure 5. Radial Creep Compliance Curve from Laboratory Data and Fitted Compliance Equation.

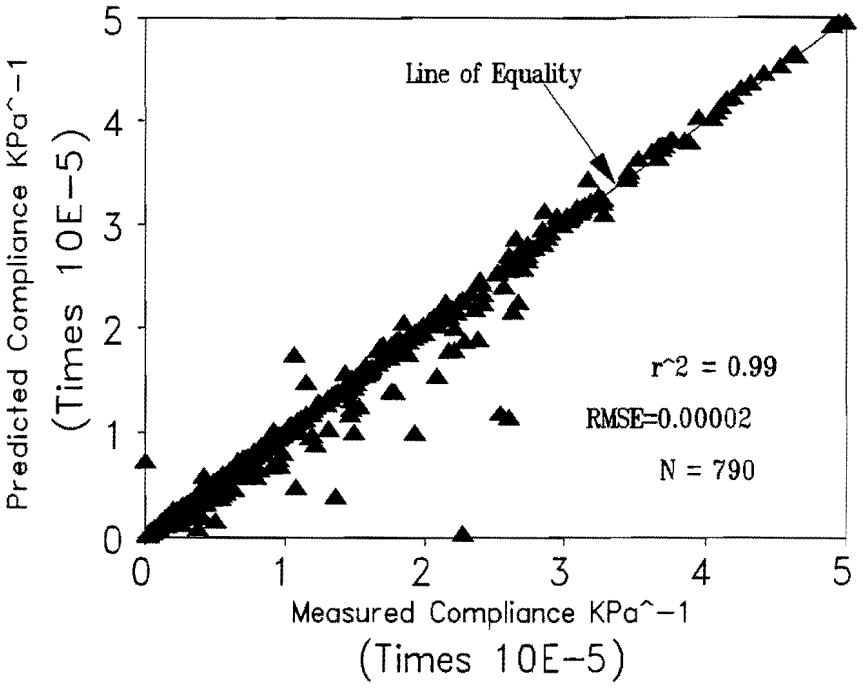

Figure 6. Vertical Creep Compliance from Laboratory Data and Compliance Equation.

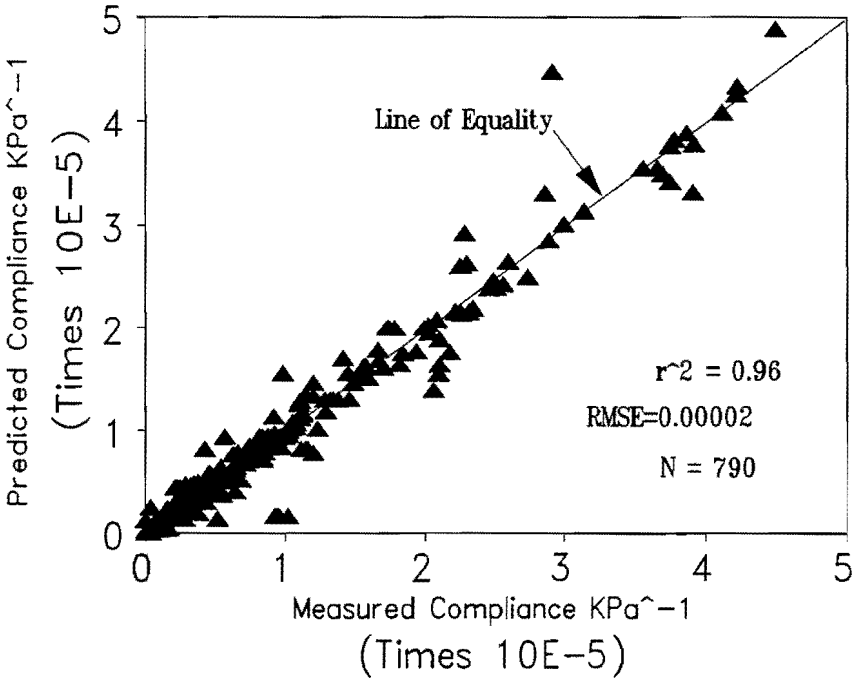

Figure 7. Radial Creep Compliance from Laboratory Data and Compliance Equation.

STRENGTH PARAMETERS

Traditionally, triaxial test results produce the strength parameters C, and ϕ. The test provides a basis upon which to evaluate stress - strain characteristics at different confining pressures. The stress at failure σ_1 and the confining pressure σ_3 can be used to construct Mohr circles and, hence, a failure envelope. The equation for the failure envelope which is the shear strength equation for a saturated material (1) is shown below:

$$\tau = C + \sigma_n \tan\phi \tag{14}$$

where τ = shear stress;

σ_n = normal stress $= (\sigma_f - U_a)_f$;

C = total cohesion;

ϕ = angle of internal friction;

σ_f = applied pressure at failure; and

U_a = pore air pressure.

Figure 8 shows Mohr's diagram and failure envelope.

A more accurate procedure for obtaining C, and ϕ, is to use the equation

$$\frac{\sigma_1}{\sigma_3} = \frac{2C\cos\phi + (1+\sin\phi)\sigma_3}{\sigma_3(1-\sin\phi)} \tag{15}$$

where the variables are as defined already (12). Equation (15) can be determined for any level of stress at failure σ_1 and confining pressure σ_3 combinations. These equations are then solved simultaneously using a pattern search approach to obtain the strength parameters C, and ϕ. Various researchers in the past have shown a relationship between the resilient modulus, M_R, and soil suction, U (3). This is also true for cohesion, C, and soil suction, U.

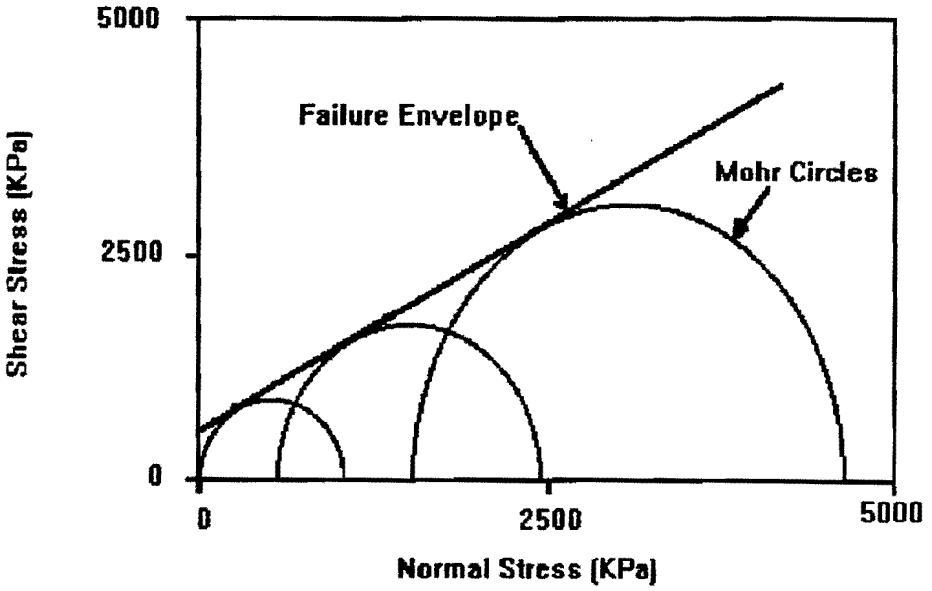

Figure 8. Mohr Circles and Failure Envelope.

SOIL SUCTION

Soil suction is the energy with which water is attracted to soil and is measured by the work required to move this water from its existing state to a pressure free distilled state (3). The soil suction or the soil water potential consists of five major components:

a) osmotic potential;
b) matrix potential;
c) gas pressure potential;
d) gravitational potential; and
e) overburden pressure potential.

The sum of these comprises the total soil suction (3). Overburden pressure is the influence of depth on the soil water potential, which is only important for fine grained soils at great depth.

For the problem of interest, the gas pressure potential, gravitational potential and the overburden pressure potential have little effect on the total soil water potential and need not be considered (3). Therefore the total suction consists of the osmotic and the matrix suction. The osmotic suction is the suction due to the dissolved salts in the pore fluids, and the matrix suction is the suction due to the hydrostatic tension of the pore water. The total suction can be measured as the negative gauge pressure relative to the external gas pressure of the soil water, which in turn, can be determined by measuring the vapor pressure in equilibrium with the soil water. Thus, the total suction can be quantitatively expressed by the Kelvin equation, which expresses suction, U, in grams-centimeter/gram of water vapor (centimeters of water) (3). The Kelvin equation is (3)

$$U = -\frac{RT}{gm} \ln\left(\frac{P}{P_o}\right) \tag{16}$$

where R = gas constant;
T = absolute temperature;
g = gravitational force acceleration;
m = molecular weight of water;
P = vapor pressure of soil water;
P_o = vapor pressure of free water; and
P/P_o = the relative humidity which can also be described as the relative vapor pressure.

Researchers use repetitive load testing and triaxial tests in research to develop a better understanding of soil behavior. Most of the studies have been concerned with determining the dynamic properties of granular base and subgrade materials. Nearly all of the studies have tried to simulate the conditions that occur within the pavement

system. Most of these studies tried to relate the resilient modulus and residual strain to the moisture properties of the soil. Culley (13) reported the effect of several moisture properties on the resilient and residual strains of a glacial till material subjected to repeated loading. Some of the moisture properties used were volumetric moisture content and saturation. Soil suction directly relates to moisture content and saturation along with the internal stress states in the soil (3). Thus, there should be a good relationship between soil suction and the resilient properties of soil materials. It is known that the failure stress, σ_1, of a given material at a given confining pressure, σ_3, with other factors such as compactive effort remaining constant, correlates to the moisture content. The strength parameter cohesion, C, also has some correlation with soil suction (1).

According to Freduland and Rahardjo, (1), the shear strength of an unsaturated soil can be formulated in terms of the normal stress and matrix suction (1). The shear strength equation thus becomes

$$\tau = c' + (\sigma_f - U_a)_f \tan\phi' + (U_a - U_w)_f \tan\phi^b \qquad (17)$$

where τ = shear stress;

c' = effective cohesion which is the intercept of the Mohr-Coulomb failure envelope on the shear stress axis when the normal stress and the matrix suction are equal to zero;

$(\sigma_f - U_a)_f$ = net normal stress on the failure plane at failure;

ϕ' = angle of internal friction associated with the normal stress variable $(\sigma_f - U_a)$;

$(U_a - U_w)_f$ = matrix suction on the failure plane at failure;

ϕ^b = angle indicating the rate of increase in shear strength relative to matrix suction;

U_a = pore air pressure; and

U_w = pore water pressure.

This reveals that the shear strength equation for an unsaturated soil is an extension of equation (14), the shear strength equation for a saturated soil. For an unsaturated soil, two stress state variables are used to describe shear strength while one stress state variable $(\sigma_f - U_a)_f$, which is the normal stress, is required for a saturated soil. This is because as the soil approaches saturation the pore water pressure, U_w, approaches the pore air pressure, U_a, and the matrix suction component vanishes. Equation (17) reverts to equation (14), the equation for a saturated soil. A comparison of equations (14) and (17) reveals that the total cohesion, C, of the material is defined as

$$C = c' + (U_a - U_w)_f \tan\phi^b \tag{18}$$

This shows that the cohesion of a material determined from the triaxial test of an unsaturated soil material is the total cohesion and is made up of two components, namely, the effective cohesion and the cohesion due to matrix suction. A model for predicting the total cohesion can be constructed based on this relationship.

Lytton and Germann (14) have demonstrated theoretically that the natural logarithm of the resilient modulus is a function of the natural logarithm of the absolute value of suction, U. Suction, as already mentioned, is correlated to the degree of saturation, the volumetric moisture content, the gravimetric moisture content and other moisture and stress properties of the soil materials.

For the gradations typically used in base courses, it is reasonable to expect that an unsaturated or partially saturated condition will most often prevail (3). Therefore, the matrix suction or moisture tension will need to be considered in predicting the resilient properties of soil materials.

According to Lamborn (15) the term $3\theta_w(U_a - U_w)$ should be subtracted from the first stress invariant where,

θ_w	=	volumetric moisture content
$(U_a - U_w)$	=	matrix suction

to take the effect of matrix suction into consideration in predicting the resilient modulus. Since suction is expressed as a negative force, Equation (1) will then take the form:

$$E = K_1 P_a \left[\frac{I_1 + 3(U_a - U_w)\theta_w}{P_a}\right]^{K_2} \left[\frac{\tau_{oct}}{P_a}\right]^{K_3} \tag{19}$$

This shows that there is some correlation between the resilient properties of soil materials and the moisture, stress and other physical properties of soil materials. This research seeks to construct prediction equations for the strength and resilient properties of soil materials based on moisture states and other physical properties.

CHAPTER 3
LABORATORY INVESTIGATION AND RESULTS

INTRODUCTION

Researchers used nine different materials that make up the base course or the subgrade of pavements in the laboratory investigation in order to establish a database of material properties for establishing models and prediction equations to obtain the strength and resilient properties of materials. The base course materials are

Limestone,
Iron Ore Gravel,
Caliche, and
Shellbase.

The subgrade materials are

Sandy Gravel,
Sand,
Silt,
Lean Clay, and
Fat Clay.

Lean Clay is clay with a liquid limit of less than 30% and Fat Clay is one with a liquid limit greater than 30%. The shellbase was made up of 60% oyster shell and 40% sand by weight based on information given by the Beaumont District. Although shellbase is not used as a pavement material in current practice, there are roadways in counties near the Gulf Coast where stabilized or unstabilized shellbase layers are found. Consequently, this material was included in the laboratory test program. Researchers carried out the following tests to determine the material properties.

SPECIFIC GRAVITY

The specific gravity, G_{sb}, of a soil is defined as the ratio of the weight in air of a given volume of soil particles to the weight in air of an equal volume of distilled water at a temperature of 4 °C (16). The test for the specific gravity was performed using TEX-108-E (16). In these tests, the specific gravity of the soil binder, consisting of the particles passing the No. 40 sieve, was determined for each soil type. Table 1 shows the results obtained from these tests.

Table 1. Specific Gravity of Binder Content for Each Soil Type Tested.

Soil Type	Specific Gravity (G_{sb})
Limestone	2.650
Iron Ore Gravel	2.703
Sandy Gravel	2.464
Caliche	2.744
Shellbase	2.703
Sand	2.421
Silt	2.882
Lean Clay	2.506
Fat Clay	2.422

PARTICLE SIZE ANALYSIS

Researchers conducted the particle size analysis of the base and subgrade materials in accordance with TEX-110-E. Samples of the materials were obtained from various parts of Texas. Tables 2 and 3 show the results of the particle size analysis. The analysis showed that the granular materials were well graded. Figures 9 to 17 show the gradation curves.

Table 2. Sieve Analysis of Base Materials.

Soil Type (Percent Passing)

Sieve Size (mm)	Limestone	Iron Ore Gravel	Caliche	Shellbase
50.800	100.00	100.00	100.00	100.00
25.400	100.00	100.00	90.35	95.10
19.05	84.47	97.60	72.32	90.78
9.525	64.71	90.98	58.92	87.33
4.750	52.71	76.08	51.33	82.12
2.000	42.29	56.12	45.56	77.51
0.420	30.10	40.36	39.24	40.36
0.250	26.93	37.34	38.39	11.05
0.149	23.51	32.91	35.16	6.08
0.106	19.77	28.15	27.81	4.57
0.075	17.61	21.95	25.87	4.02

Table 3. Sieve Analysis of Subgrade Materials.

Soil Type (Percent Passing)

Sieve Size(mm)	Sand	Silt	Lean Clay	Fat Clay	Sandy Gravel
25.400	-	-	-	-	100.00
19.05	-	-	-	-	97.50
9.525	-	-	-	-	80.28
4.750	100.00	100.00	100.00	100.00	63.66
2.000	86.90	100.00	100.00	100.00	47.15
0.420	31.76	100.00	100.00	100.00	21.42
0.250	8.12	99.99	99.80	98.35	14.28
0.149	3.33	99.66	92.44	95.53	9.09
0.106	2.41	98.77	71.74	92.03	6.83
0.075	2.14	94.08	55.36	88.48	6.02

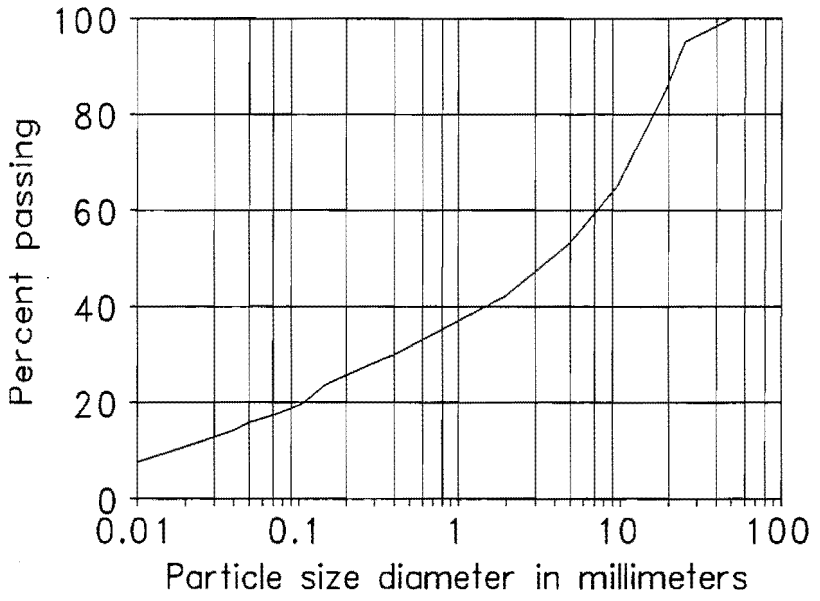

Figure 9. Gradation Curve of Limestone.

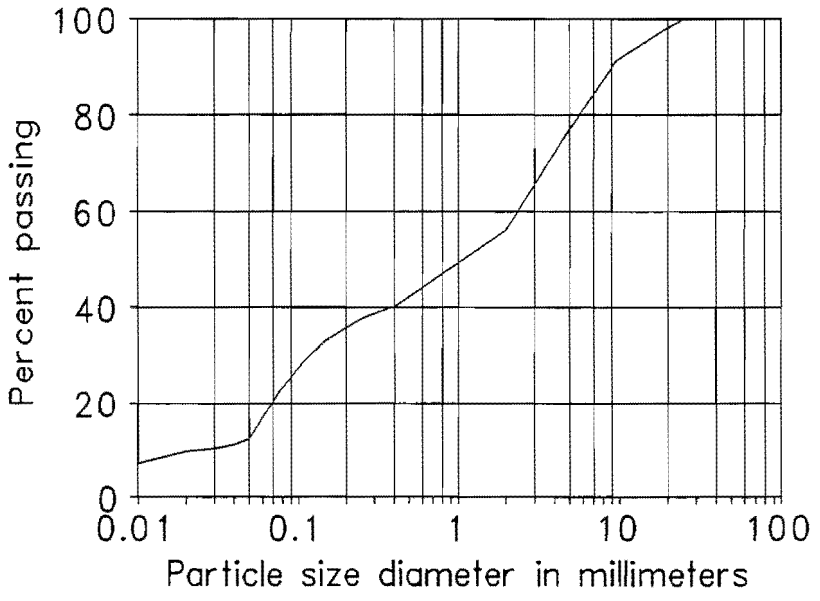

Figure 10. Gradation Curve of Iron Ore Gravel.

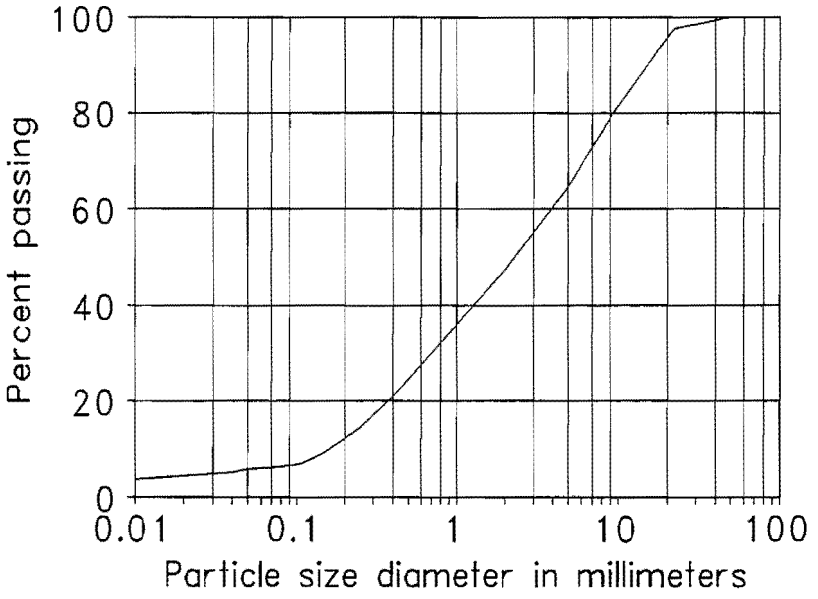

Figure 11. Gradation Curve of Sandy Gravel.

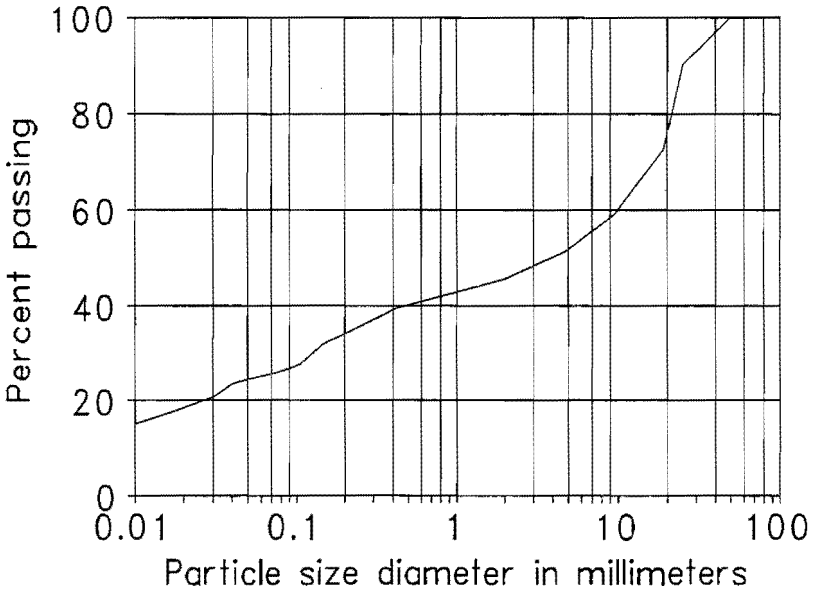

Figure 12. Gradation Curve of Caliche.

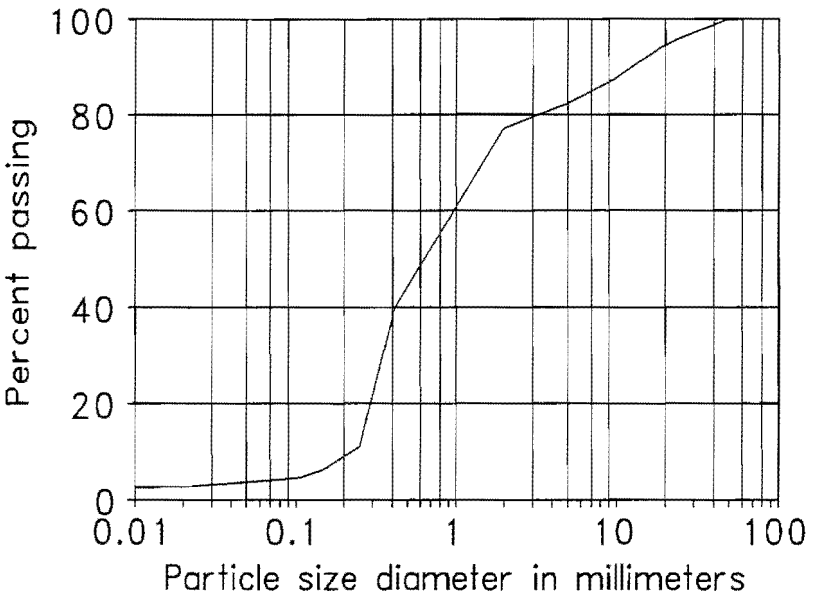

Figure 13. Gradation Curve of Shellbase.

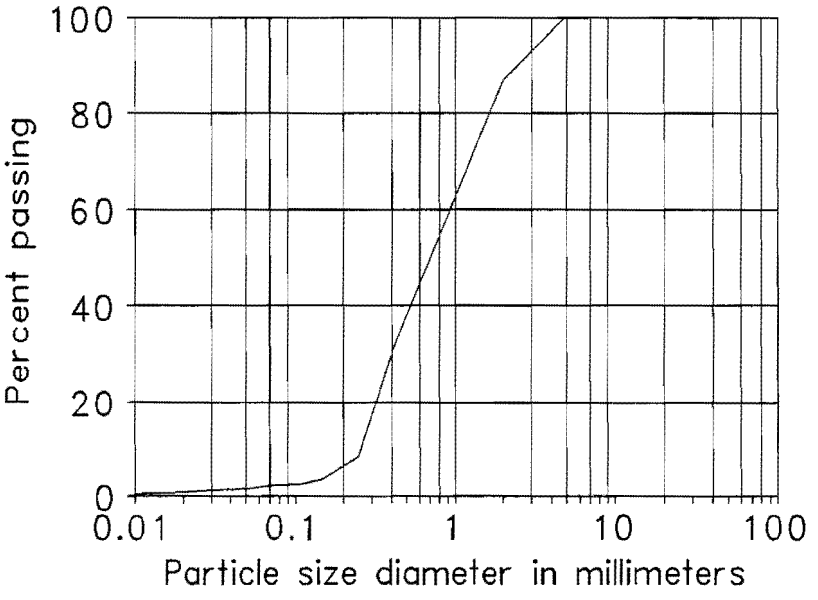

Figure 14. Gradation Curve of Sand.

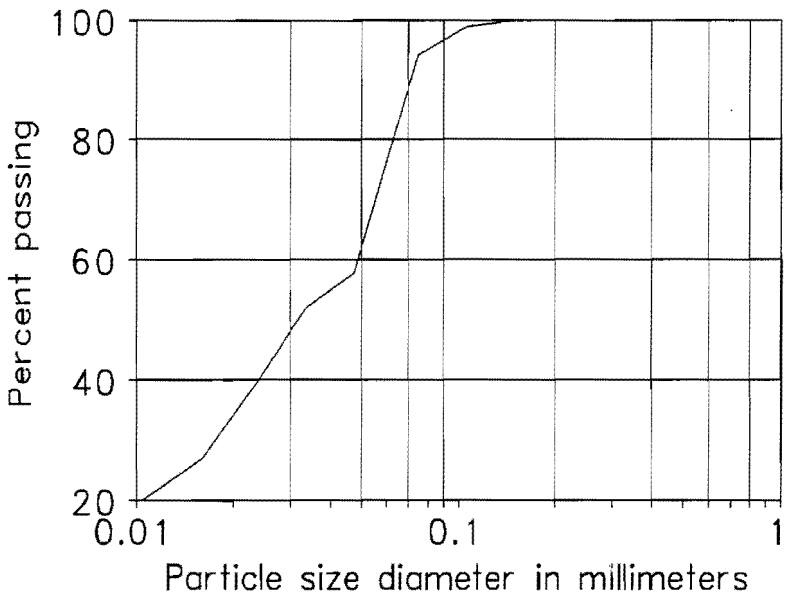

Figure 15. Gradation Curve of Silt.

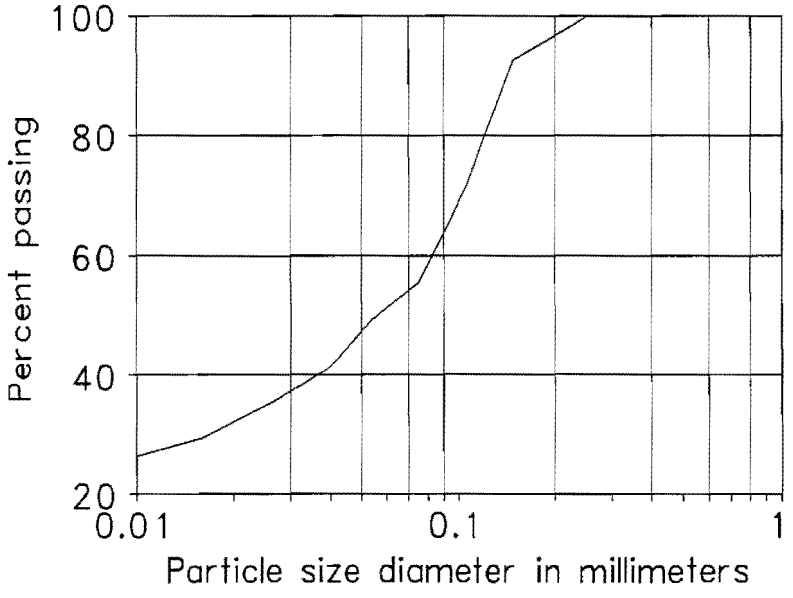

Figure 16. Gradation Curve of Lean Clay.

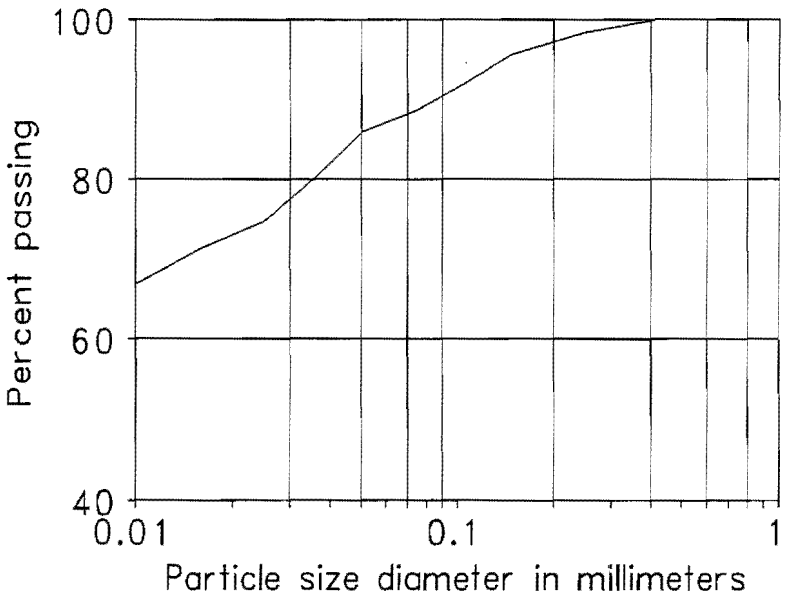

Figure 17. Gradation Curve of Fat Clay.

MOISTURE - DENSITY CHARACTERISTICS

Optimum moisture content and maximum dry density of the base and subgrade materials were determined in accordance with TEX-113-E (16). A mold with a diameter of 152 mm and a height of 203 mm was used in all cases with a compactive effort of 50 blows per layer. Table 4 summarizes the optimum moisture content and the corresponding maximum dry density. Figures 18 and 19 illustrate the moisture content versus dry density curves for a base and a subgrade material.

Table 4. Optimum Moisture Content and Maximum Dry Density.

Soil Type	Optimum Moisture (%)	Max. Dry Density (Kg/m^3)
Limestone	9.095	1736.4
Iron Ore Gravel	10.65	1814.6
Sandy Gravel	6.147	1910.8
Caliche	6.734	1831.8
Shellbase	5.013	1625.9
Sand	3.970	1485.3
Silt	11.718	1434.6
Lean Clay	10.230	1633.9
Fat Clay	19.760	1331.5

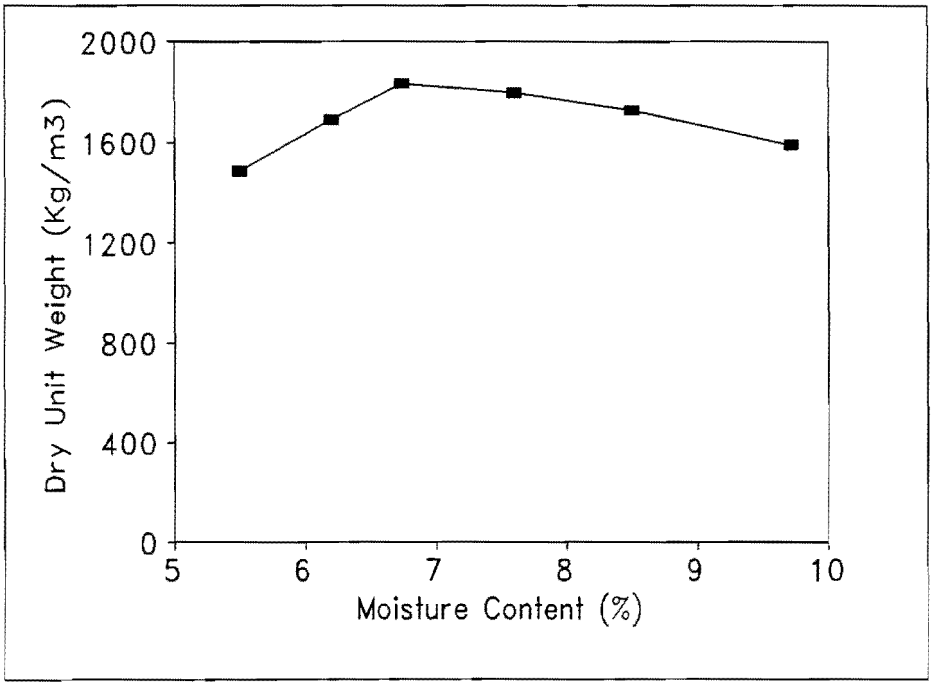

Figure 18. Moisture Density Curve for Caliche.

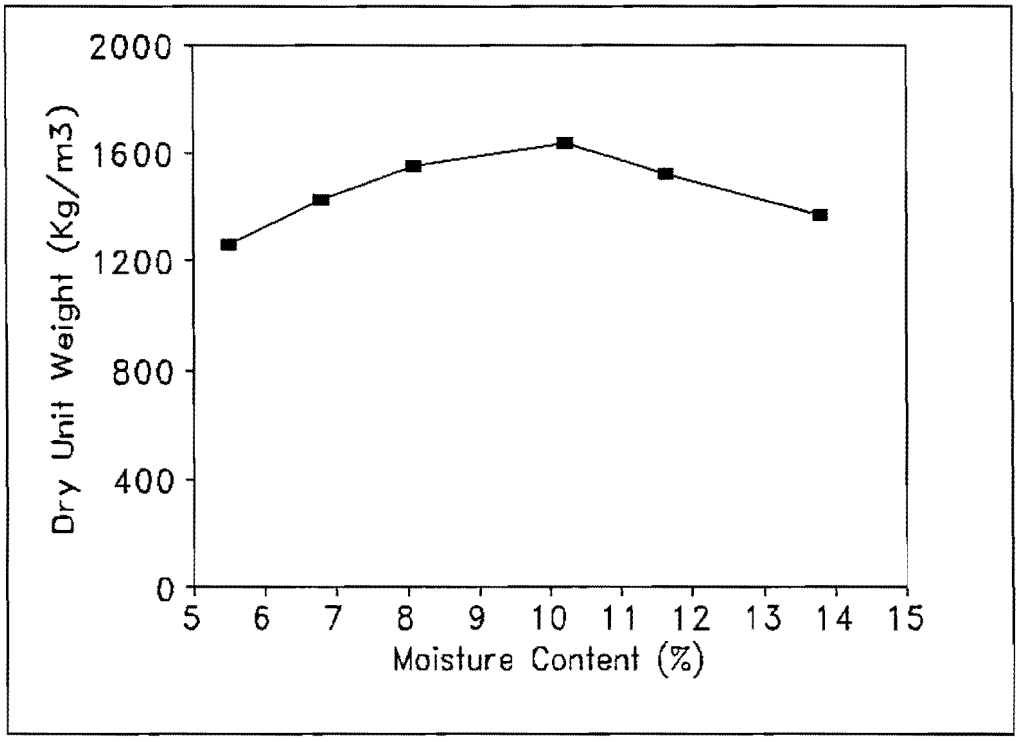

Figure 19. Moisture Density Curve for Lean Clay.

ATTERBERG LIMITS

The Atterberg limits (liquid and plastic limits) and the plasticity index were determined in accordance with TEX-104, TEX-105 and TEX-106 (16). The tests utilized only the material passing the 0.42 mm sieve size. The liquid limit was determined, from a plot of water content versus the corresponding number of blows, as the moisture content at 25 blows. The plastic limit was determined as the moisture content at which the material molded into a 3.2 mm thread breaks up. Table 5 gives a summary of the Atterberg limits.

Table 5. Atterberg Limits of Base and Subgrade Materials.

Soil Type	Liquid Limit	Plastic Limit	Plasticity Index
Limestone	20.70	11.30	7.90
Iron Ore Gravel	18.35	16.63	1.72
Sandy Gravel	20.40	12.50	8.70
Caliche	33.26	18.37	14.69
Shellbase	20.06	16.74	3.33
Sand	19.66	18.42	1.24
Silt	23.00	17.00	6.00
Lean Clay	28.00	18.00	10.00
Fat Clay	35.00	13.90	21.10

MEASUREMENT OF SOIL SUCTION (FILTER PAPER METHOD)

Since TxDOT has no standard procedure for the suction test, the procedure used for this test is given below (17).

(a) Calibrate the filter paper. Prepare 200 ml of different reagent grade sodium chloride, NaCl, which have molalities of 0.01, 0.05, 0.5, 0.1, 1.0 and 2.0 respectively. These concentrations will allow for the construction of a calibration curve that covers a practical range of suction values.

(b) Measure 20 ml of each of the NaCl solutions and put them into separately labeled, self-sealing plastic containers. Place a rubber stopper at the center of the containers. The rubber stopper will act as a pedestal for the filter paper during the moisture equilibrium phase. Place three filter papers on the rubber stopper and keep the sealed containers in a temperature controlled room for seven to ten days.

(c) Determine the moisture content of the filter paper as accurately as possible after seven days and obtain the suction value corresponding to the salt concentration and temperature from standard tables (17).

(d) Plot suction value versus filter paper moisture content. This plot serves to convert moisture contents of the papers used (from the same package of filter papers as used in the calibration) in steps (b) and (c) into suction values for the soil being tested.

(e) After putting a soil sample in a jar, put three filter papers each at the top and bottom of the soil sample. This is for the determination of matrix suction.

(f) Keep the jar in an environmentally controlled room where the temperature is set at 20 °C for at least seven days.

(g) After seven to ten days, determine the moisture content of the filter paper. To allow the filter paper to dry, place it in an oven in which the temperature is 43 °C for 48 hours. The balance used in this test should be very accurate and precise (on the order of 0.0001 gram).

(h) Use the moisture content of the filter paper from step (g) to determine the soil suction by using the plot generated in step (d).

Figure 20 shows a soil sample with filter papers, and Figures 21 and 22 illustrate the calibration curves of suction versus moisture content of the filter papers using the filter paper method. It should be noted that these are curves fitted to laboratory data.

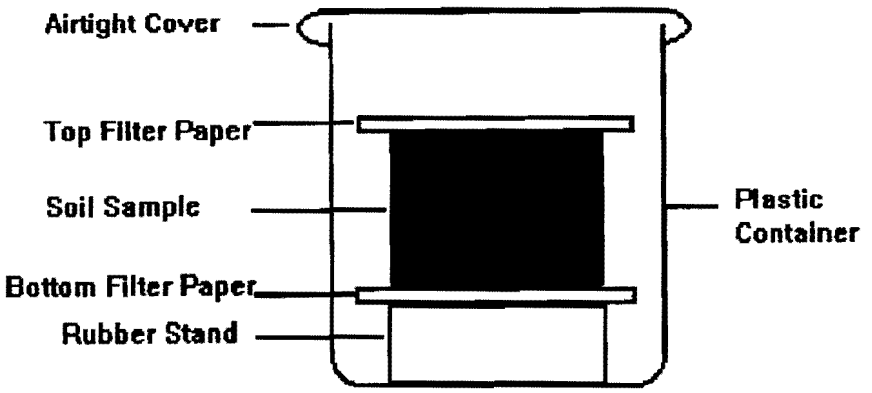

Figure 20. Soil Sample with Filter Papers.

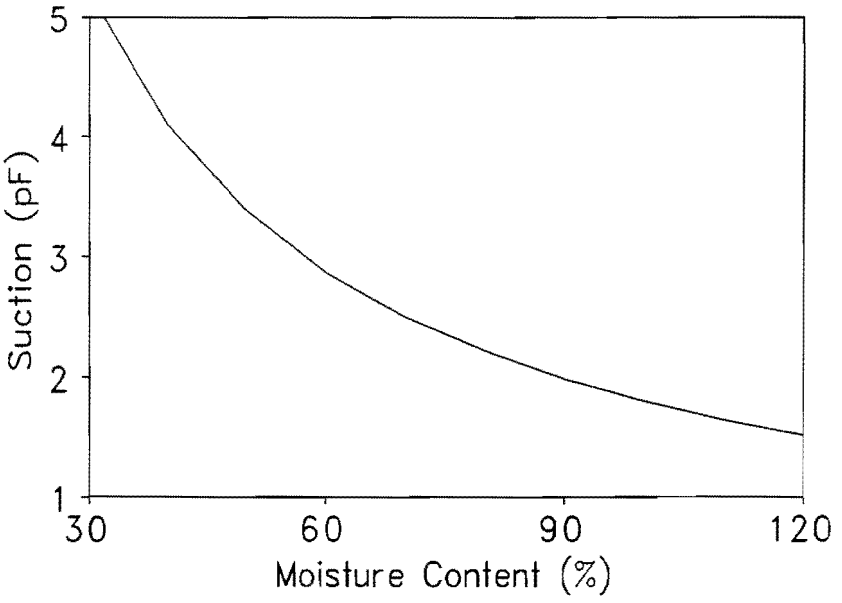

Figure 21. Suction Versus Moisture Content of Filter Paper (calibration curve 1).

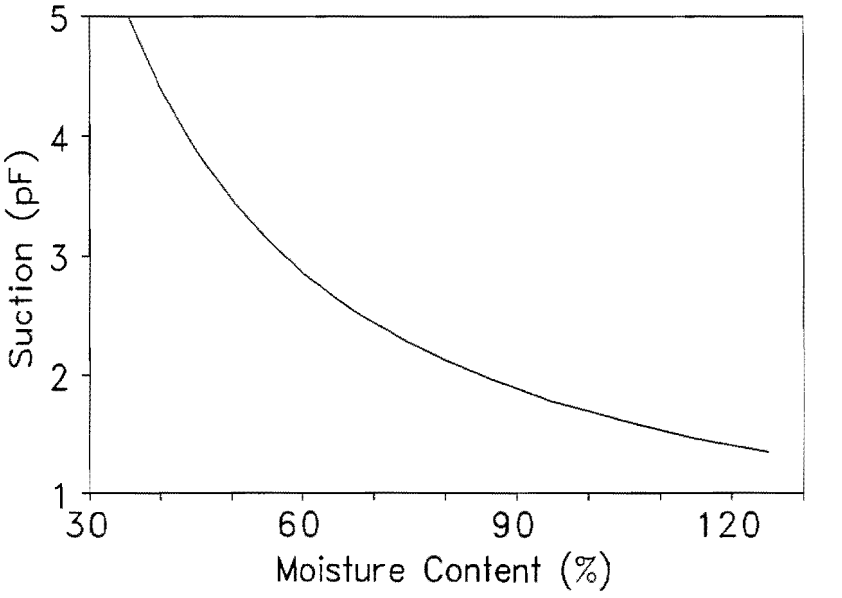

Figure 22. Suction Versus Moisture Content of Filter Paper (calibration curve 2).

MEASUREMENT OF SOIL SUCTION (PRESSURE PLATE METHOD)

There was no standard procedure for the pressure plate test. The procedure used is given below (18).

(a) Make at least two soil rings for each suction level.

(b) Start with the lowest suction level and equilibrate (that is, apply the necessary pressure for a minimum of 48 hours) at this suction level. Determine the moisture content of the soil.

(c) The six suction levels used are as follows:

1.	1/3 Bar	=	34KPa,
2.	2 Bar	=	203KPa,
3.	5 Bar	=	507KPa,
4.	8 Bar	=	811KPa,
5.	10 Bar	=	1015KPa, and
6.	15 Bar	=	1521KPa.

(d) Three suction levels are run in the 0-5 Bar pressure plate apparatus and the other three in the 0-15 Bar pressure plate apparatus. The following equation for the suction curve is fitted to the laboratory data:

$$U=(A+BW)^{-1} \tag{20}$$

where U = suction in pF,
A, B = constants, and
W = moisture content.

Table 6 presents a summary of the values of the constants A and B. Figures 23 to 31 show the suction curves for the nine different soil types determined using the pressure plate method.

Table 6. Value of Constants A and B for Suction Curves.

Material Type	A	B
Limestone	0.2350	0.011870
Iron Ore Gravel	0.1658	0.014250
Sandy Gravel	0.1410	0.027600
Caliche	0.2139	0.009505
Shellbase	0.1747	0.055170
Sand	0.1577	0.324400
Silt	0.1676	0.022740
Lean Clay	0.1236	0.017210
Fat Clay	0.1105	0.007743

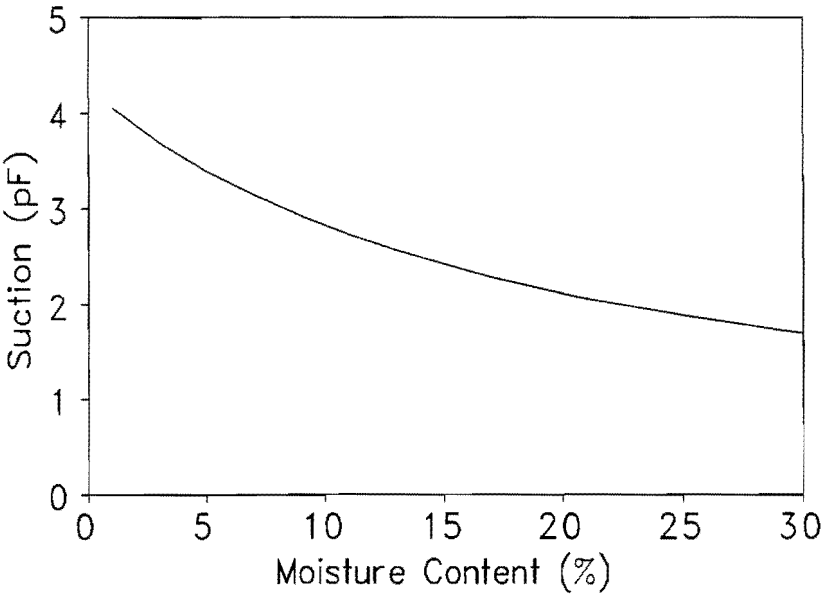

Figure 23. Suction Versus Moisture Content for Limestone.

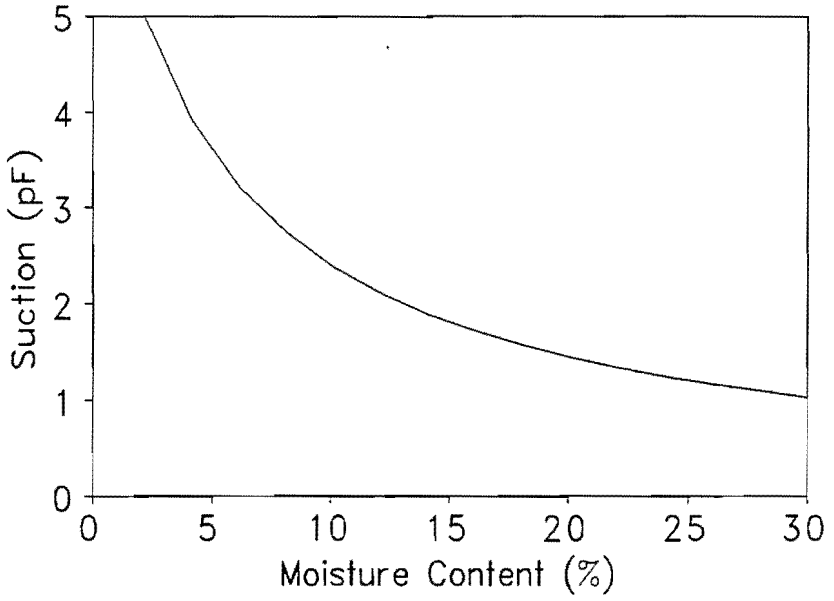

Figure 24. Suction Versus Moisture Content for Iron Ore Gravel.

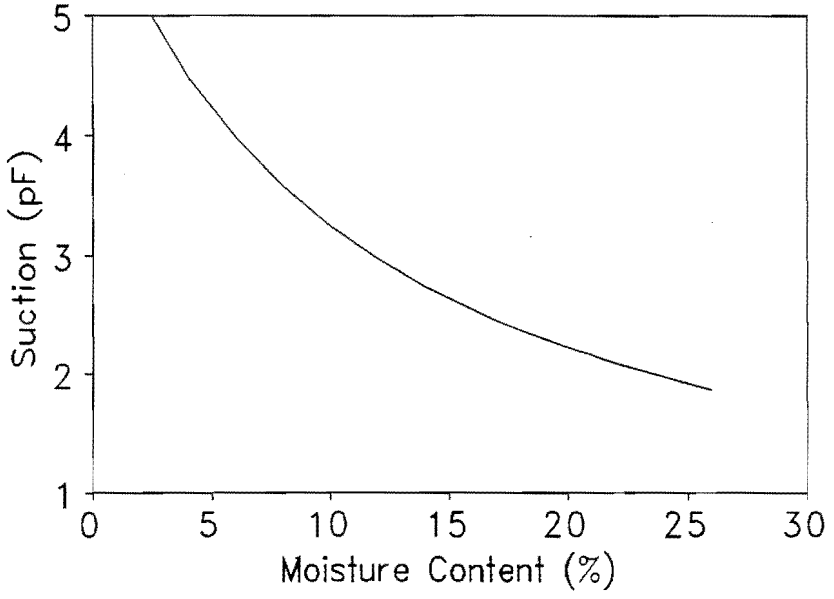

Figure 25. Suction Versus Moisture Content for Sandy Gravel.

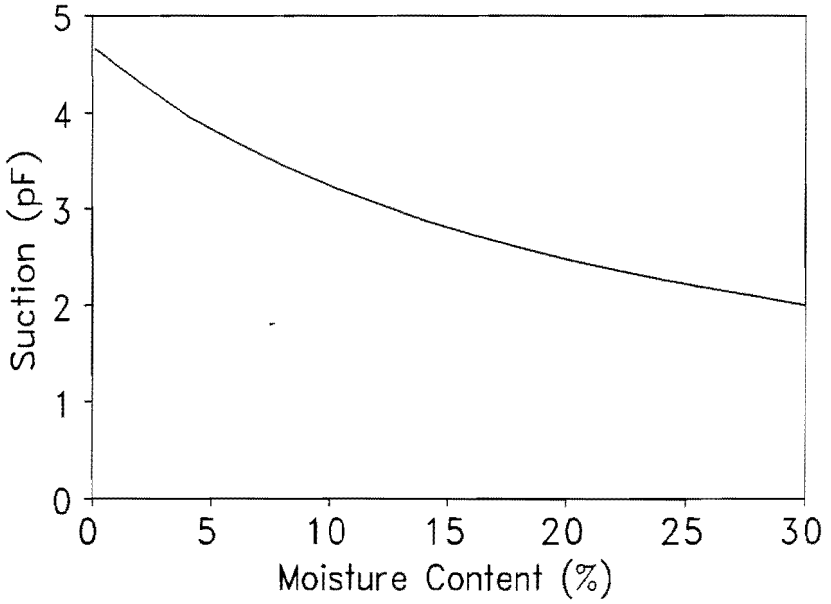

Figure 26. Suction Versus Moisture Content for Caliche.

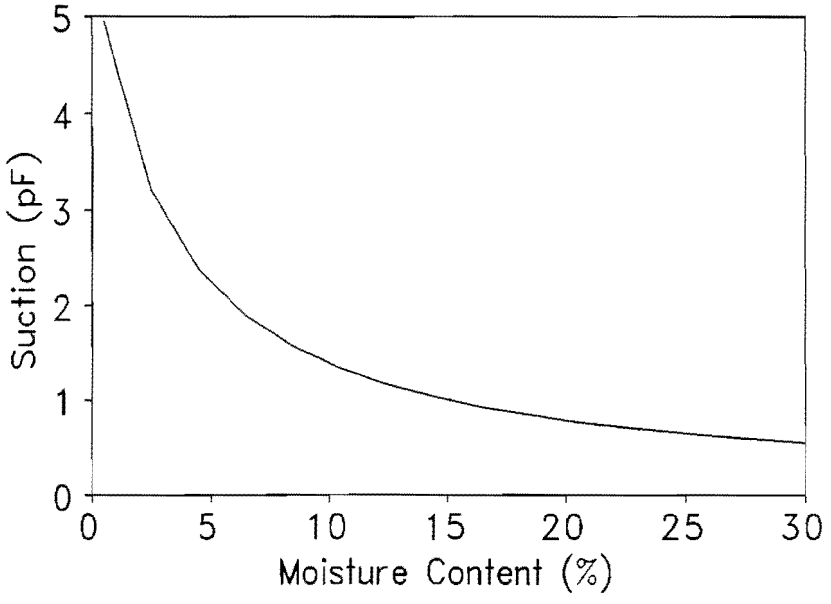

Figure 27. Suction Versus Moisture Content for Shellbase.

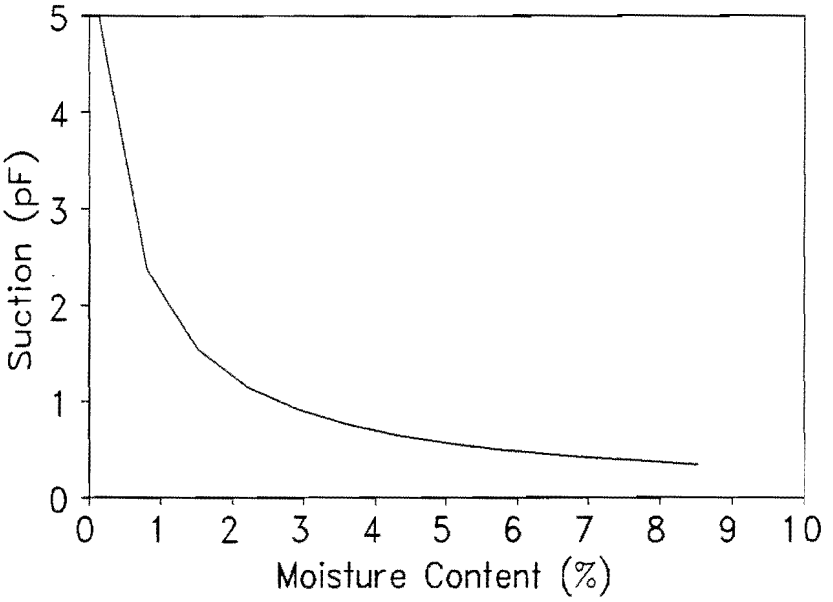

Figure 28. Suction Versus Moisture Content for Sand.

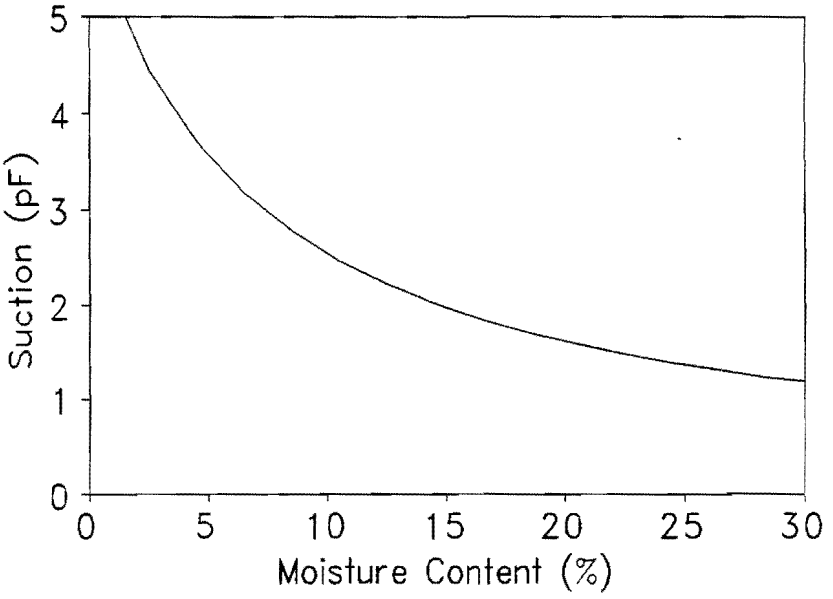

Figure 29. Suction Versus Moisture Content for Silt.

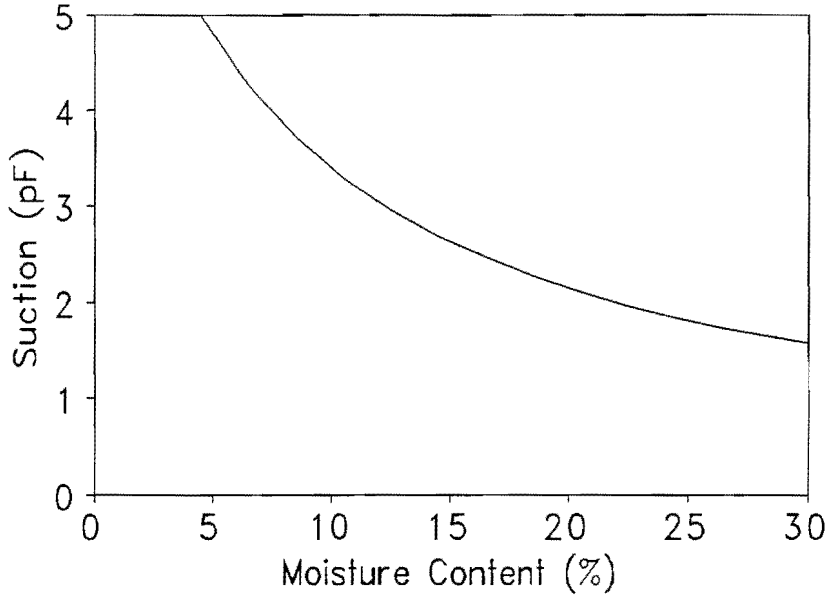

Figure 30. Suction Versus Moisture Content for Lean Clay.

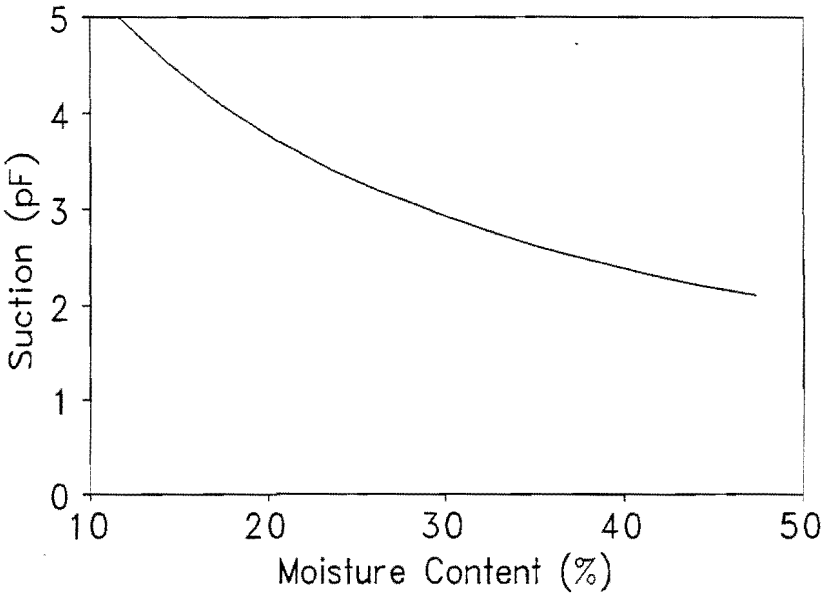

Figure 31. Suction Versus Moisture Content for Fat Clay.

TEXAS TRIAXIAL TEST (MONOTONIC LOADING)

Researchers performed this type of triaxial test according to TEX-117-E (16). The test provides a basis upon which to evaluate stress-strain characteristics at different confining pressures and was used to determine the cohesion, C, and the angle of internal friction, ϕ, for the nine base and subgrade materials. In lieu of saturating the compacted soil materials as specified in the test method, the soils were tested at three moisture contents corresponding to the optimum, and plus and minus two percent of optimum. The method of compaction was similar to that used to determine the moisture-density characteristics of the materials. A linear Mohr envelope was assumed, and the results were used to generate Mohr's failure envelope based on Equation (14). The Texas triaxial test is quite different from the other conventional tests used to obtain the strength parameters of soil materials. The main differences are listed below.

1. The use of axial cells which are lightweight stainless steel cylinders 171 mm in diameter and 305 mm in height, fitted with a standard air valve and a tubular rubber membrane 152 mm in diameter. This membrane is thicker than the membrane used in the other triaxial tests.
2. During the test, the specimens are subjected to a lateral pressure instead of an all around confining pressure used in other triaxial tests.

Figures 32 to 40 show Mohr's failure envelopes for the base and subgrade materials evaluated. In addition, Table 7 summarizes the strength parameters determined from the triaxial test results. The strength parameters were determined by the pattern search technique using the failure stresses from the tests and Equation (15) (given in Chapter 2).

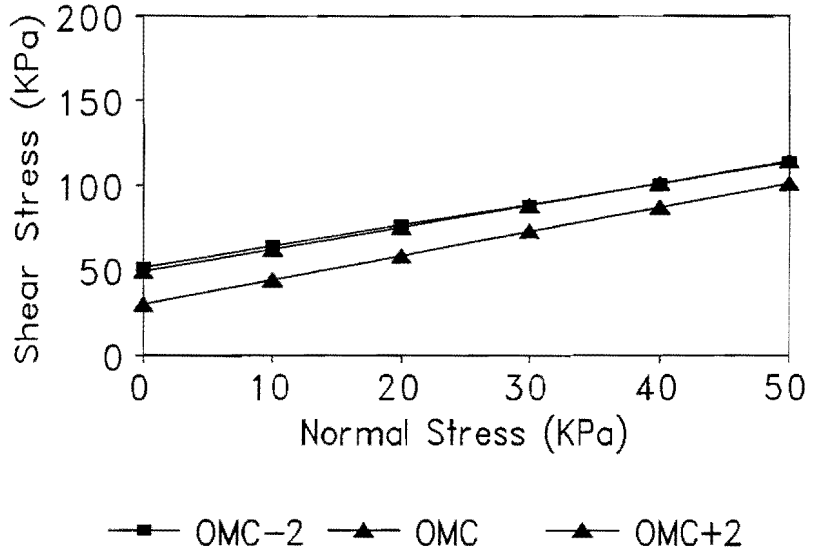

Figure 32. Mohr Failure Envelopes for Limestone.

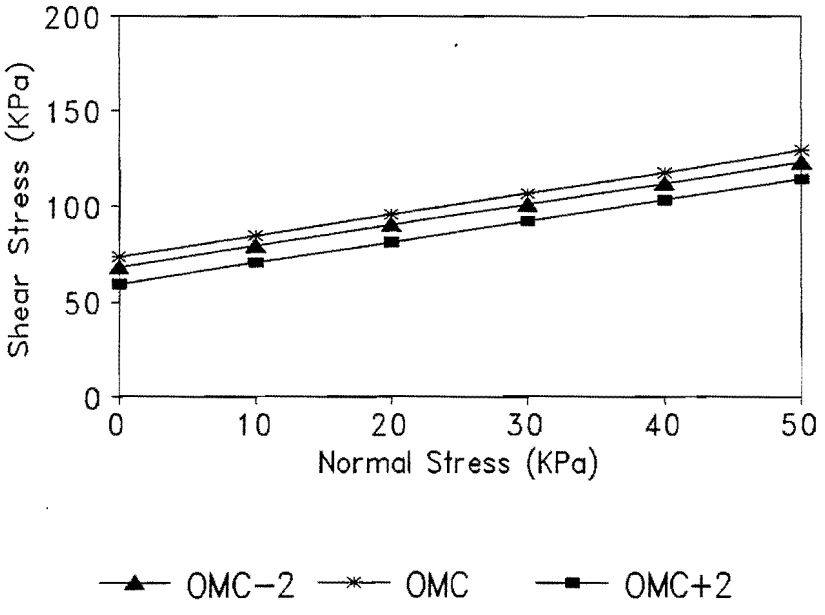

Figure 33. Mohr Failure Envelopes for Iron Ore Gravel.

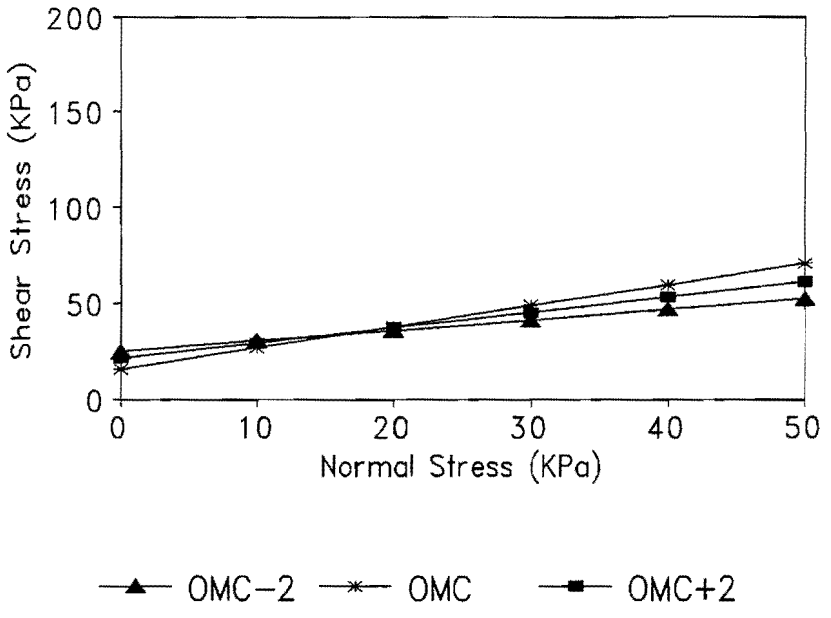

Figure 34. Mohr Failure Envelopes for Sandy Gravel.

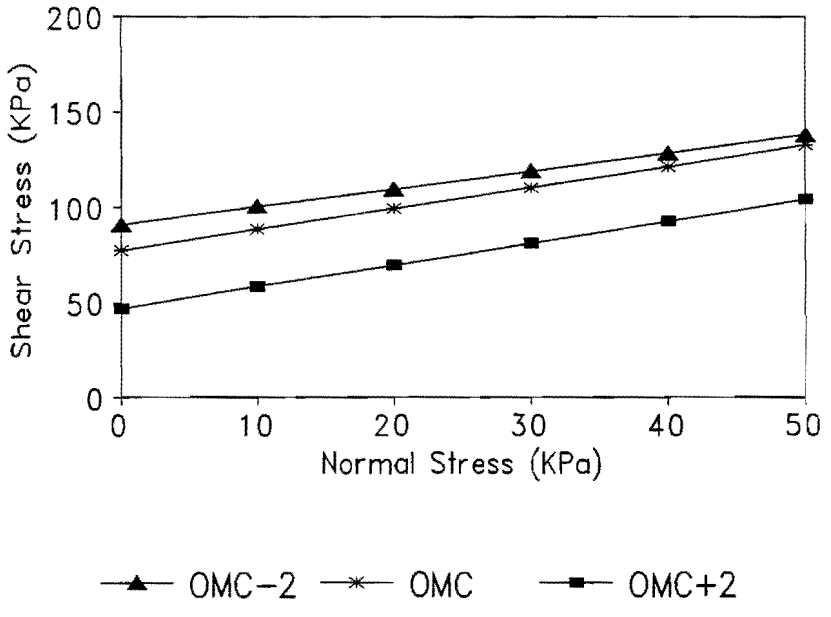

Figure 35. Mohr Failure Envelopes for Caliche.

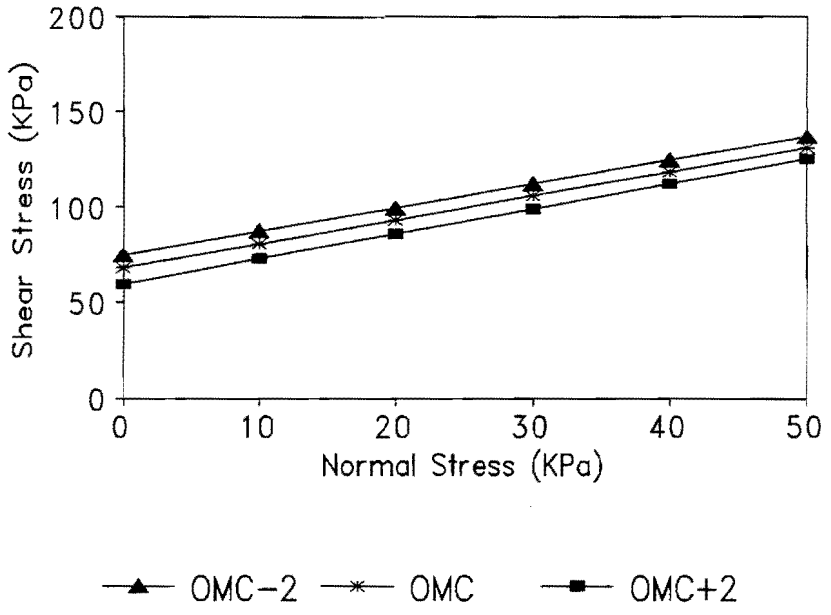

Figure 36. Mohr Failure Envelopes for Shellbase.

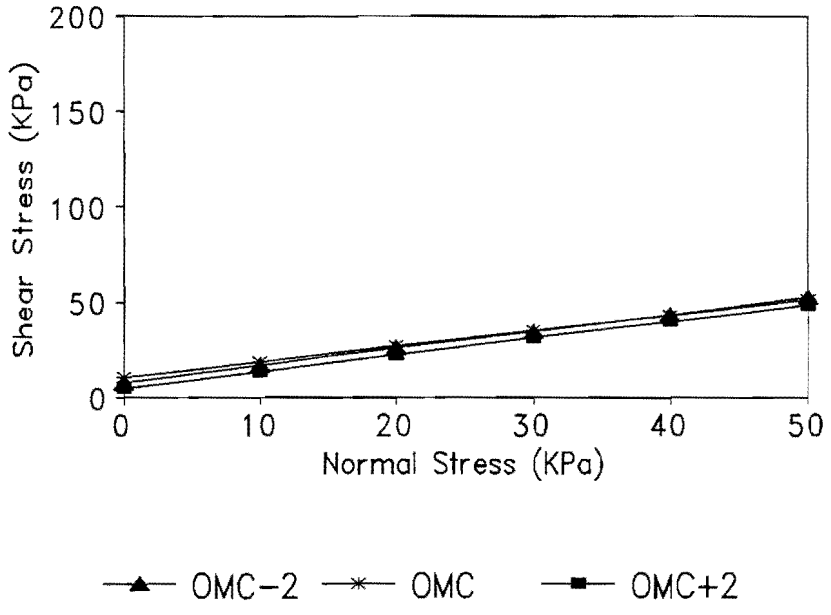

Figure 37. Mohr Failure Envelopes for Sand.

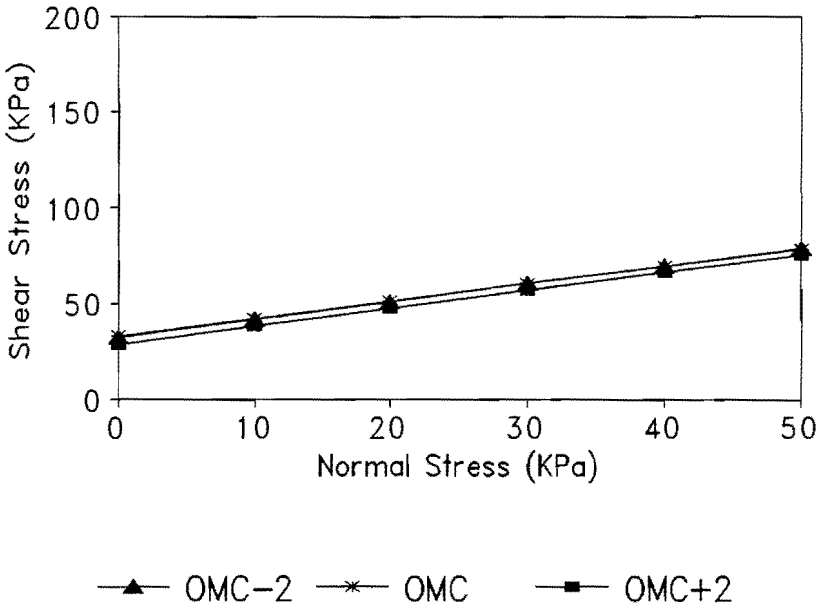

Figure 38. Mohr Failure Envelopes for Silt.

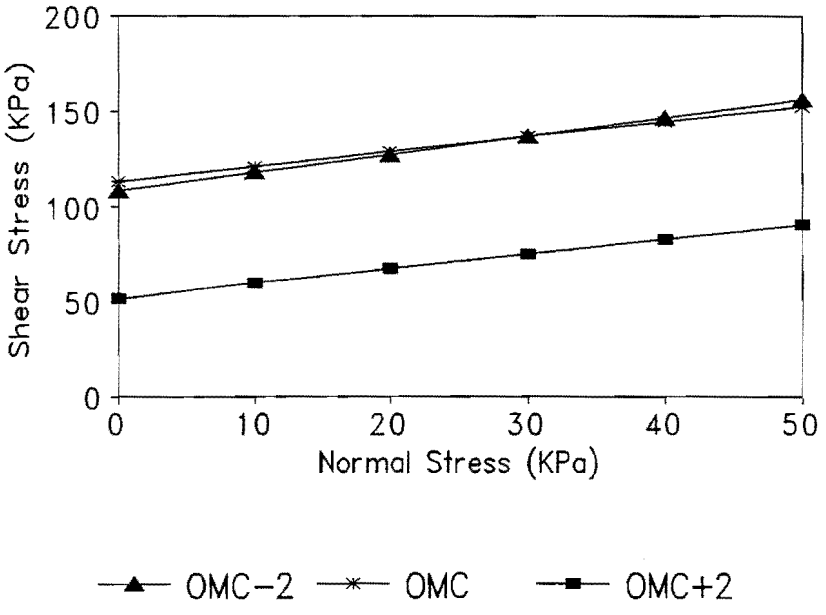

Figure 39. Mohr Failure Envelopes for Lean Clay.

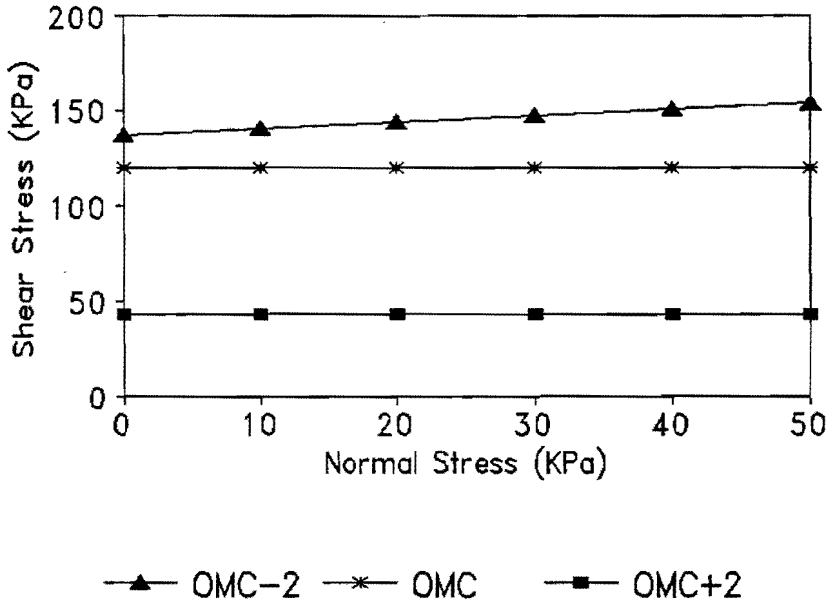

Figure 40. Mohr Failure Envelopes for Fat Clay.

Table 7. Cohesion and Angle of Internal Friction Results for Materials.

Soil Type	Minus 2% Optimum		Optimum		Plus 2% Optimum	
	C (kPa)	$\phi°$	C (kPa)	$\phi°$	C (kPa)	$\phi°$
Limestone	30	55	49	53	54*	51*
I.O. Gravel	68	48	73	48	59	48
S. Gravel	25	29	16	48	21	39
Caliche	91	43	77	48	47	49
Shellbase	75	51	68	51	60	52
Sand	8	42	52	39	4	41
Silt	33	43	33	42	29	43
Lean Clay	109	44	113	38	52	38
Fat Clay	137	18	120	0	43	0

* Limestone results at - 4 percent of optimum.

MODIFIED TEXAS TRIAXIAL TEST

The modified triaxial test is similar to the Texas triaxial test in everything except the sequence of loading. The modified sequence is as follows:

(a) The specimen is conditioned with a sinusoidal load pulse of about 10% of the failure load obtained from the triaxial test.
(b) A square wave load pulse with a magnitude of about 33% of the failure load obtained from the triaxial test is applied to the specimen for 90 seconds.
(c) The specimen is then unloaded and allowed to recover for 180 seconds.
(d) The specimen is then loaded monotonically till failure.

The objective of this test is to determine if the resilient properties of the specimen can be obtained in addition to the strength parameters. The materials were tested at the optimum moisture content. Figures 41 to 49 show the Mohr failure envelopes.

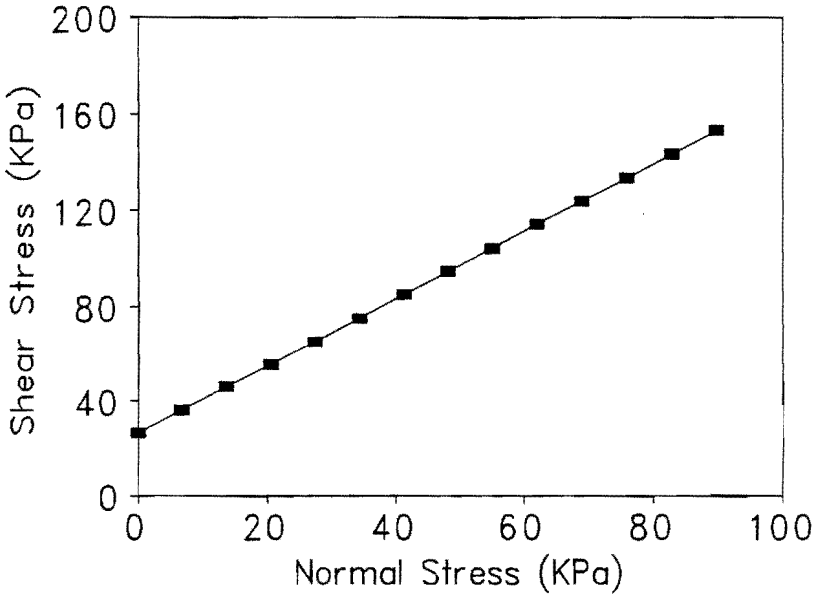

Figure 41. Mohr Failure Envelope for Limestone.

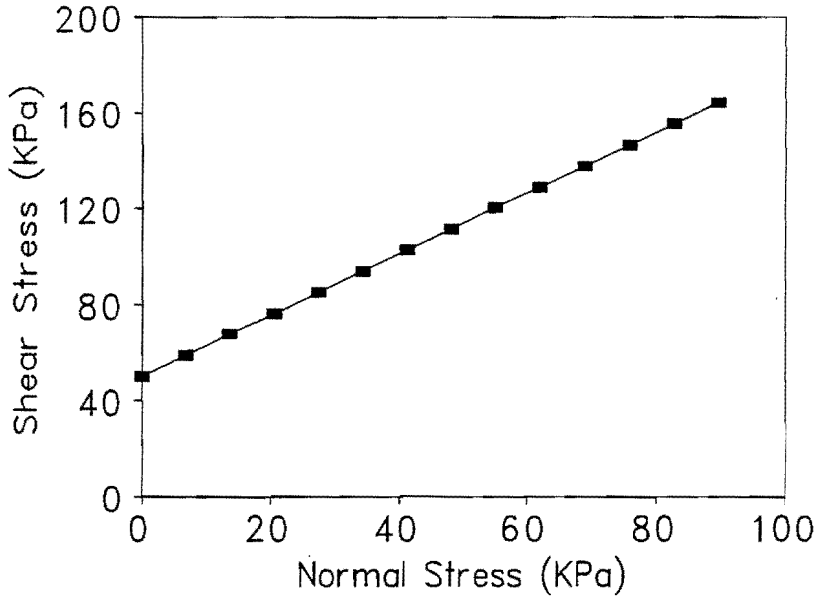

Figure 42. Mohr Failure Envelope for Iron Ore Gravel.

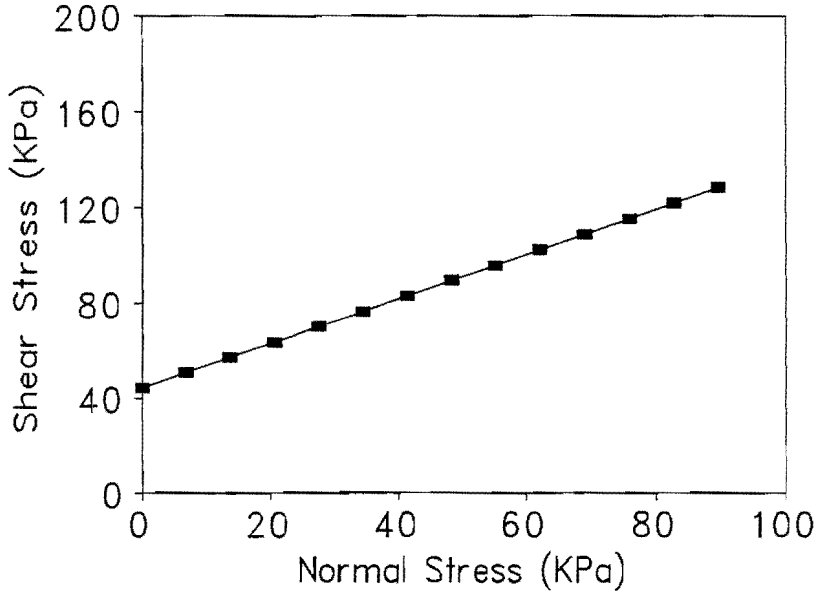

Figure 43. Mohr Failure Envelope for Sandy Gravel.

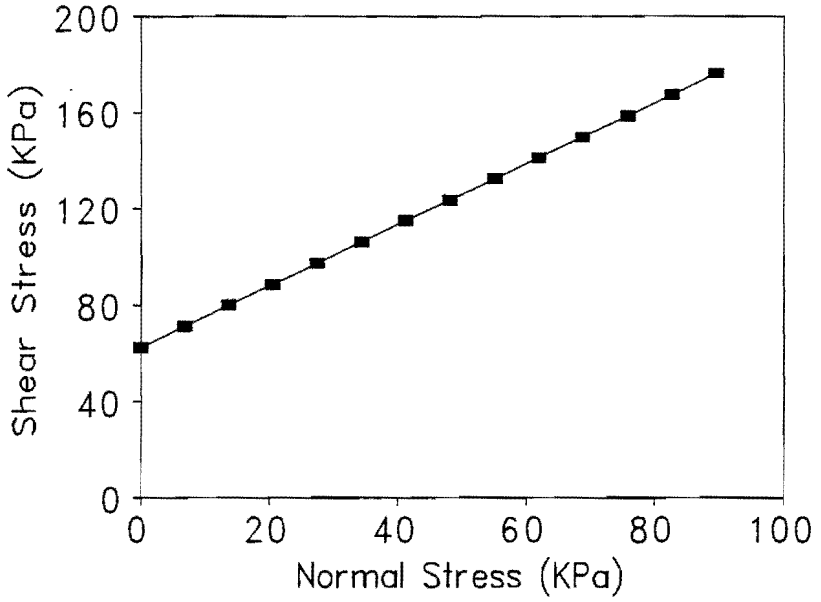

Figure 44. Mohr Failure Envelope for Caliche.

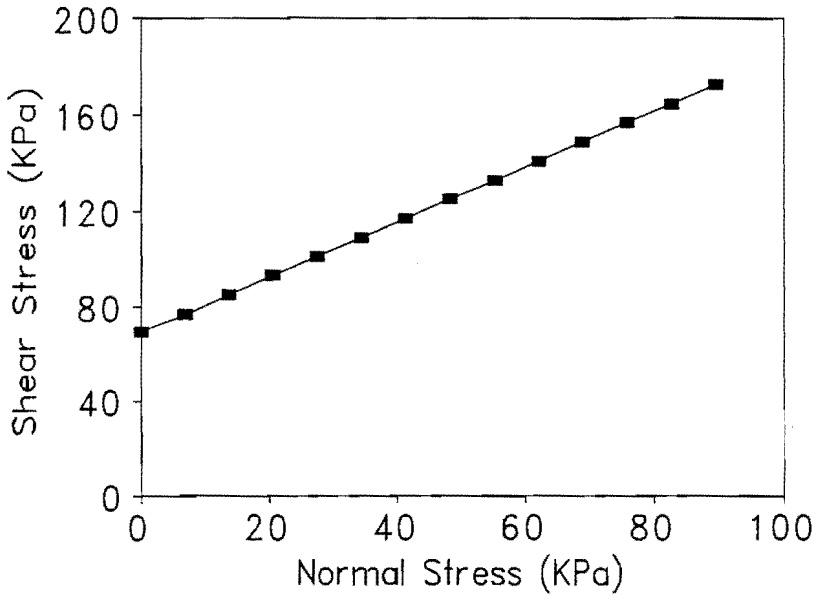

Figure 45. Mohr Failure Envelope for Shellbase.

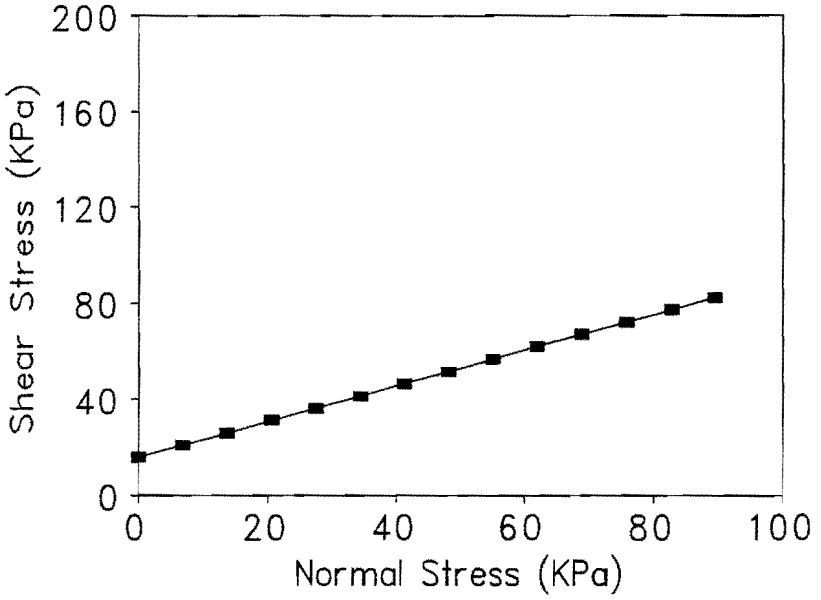

Figure 46. Mohr Failure Envelope for Sand.

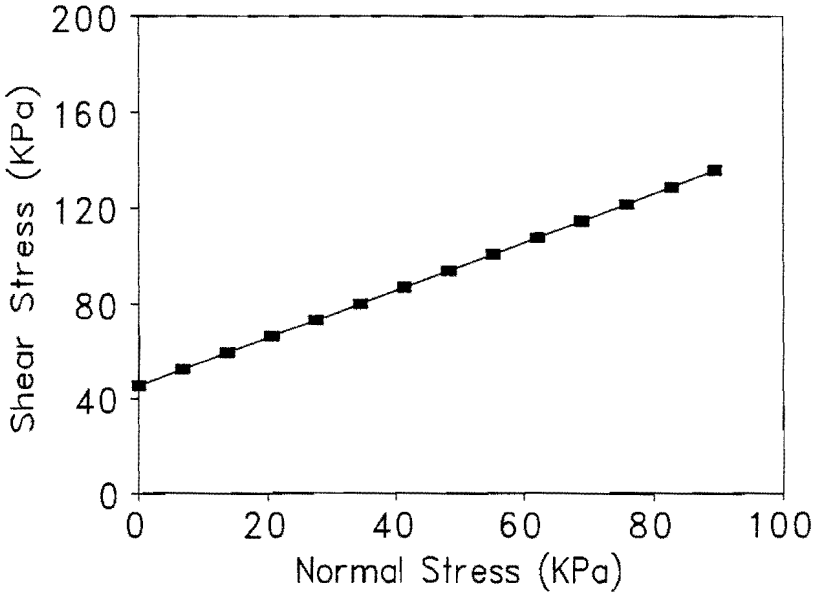

Figure 47. Mohr Failure Envelope for Silt.

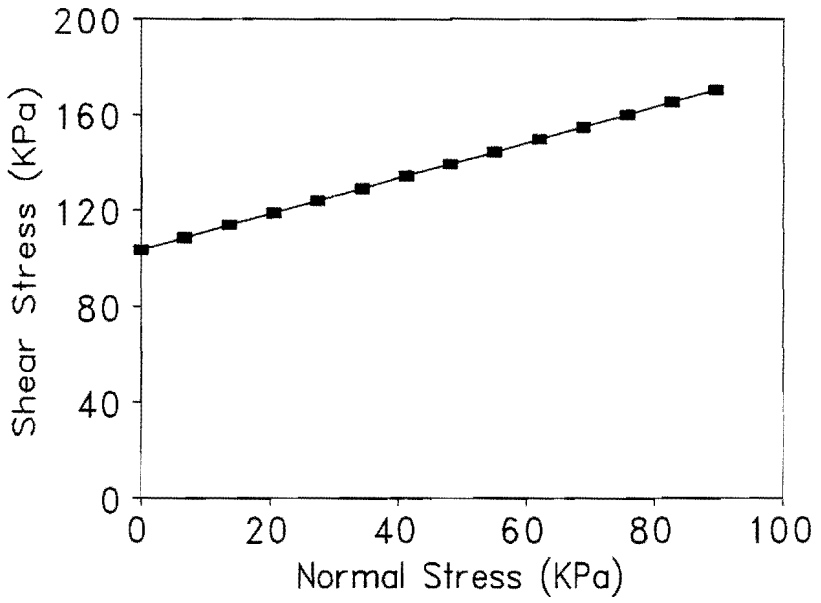

Figure 48. Mohr Failure Envelope for Lean Clay.

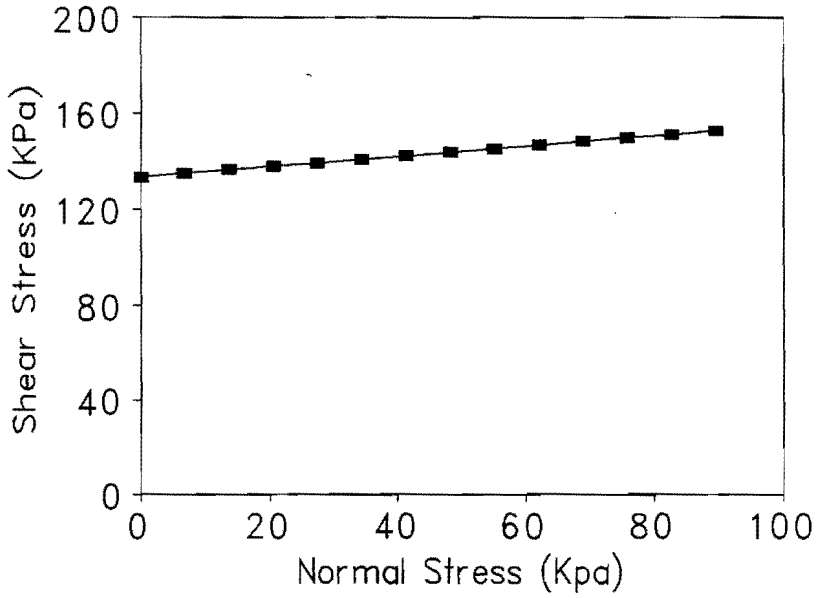

Figure 49. Mohr Failure Envelope for Fat Clay.

The strength parameters C, and ϕ, and the material properties K_1 to K_3 are summarized in Table 8 for the subgrade and base materials tested according to the modified triaxial test procedure. The resilient properties, K_1 to K_3, were determined from the creep and recovery data taken during the load and unload cycle of the modified Texas triaxial test. These properties were backcalculated following the procedure used for analyzing the compressive creep and recovery test results presented subsequently. Figure 50 shows an example of the loading profile and its corresponding deformation.

Table 8. Summary of Strength and Resilient Parameters from Modified Texas Triaxial Test.

Materials	Cohesion***	F.	K_1	K_2	K_3
Limestone	26	55	243	0.95	$-6.5*10^{-5}$
Iron Ore	50	52	75	1.01	$-2.2*10^{-5}$
Sandy Gravel	44	43	152	0.88	$-2.9*10^{-4}$
Caliche	62	52	322	0.88	$-9.8*10^{-5}$
Shellbase	69	49	318	0.80	$-9.8*10^{-5}$
Sand	15	40	498	0.77	-0.01
Silt	45	45	195	0.71	$-6.5*10^{-5}$
Lean Clay	103	37	195	0.68	-0.19
Fat Clay	133	12	122	0.19	-0.36

* Cohesion is in KPa. + Friction angle is in degrees.

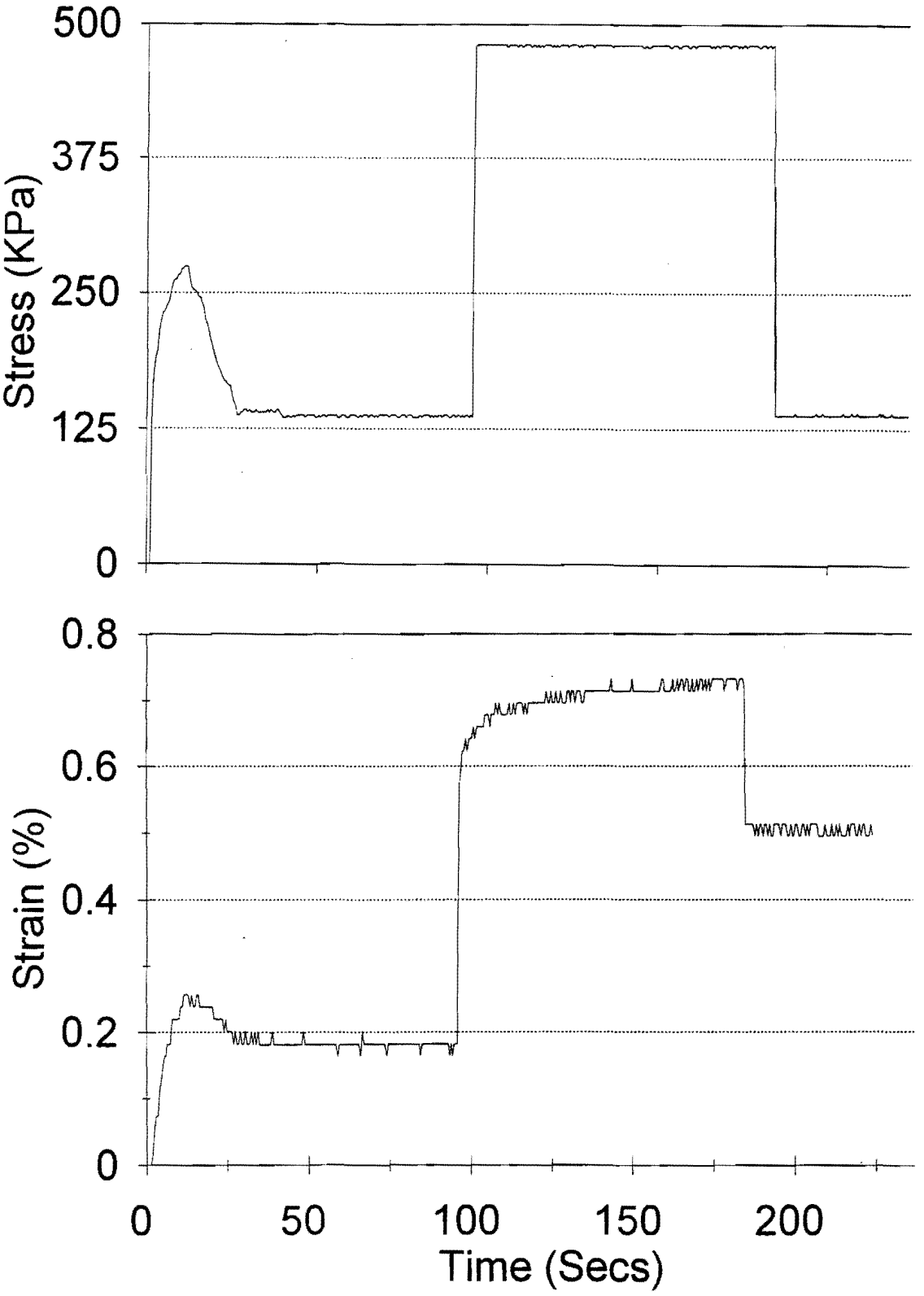

Figure 50. Load and Deformation Profiles for Modified Texas Triaxial Test.

COMPRESSIVE CREEP AND RECOVERY TEST

Researchers performed this test without a reference standard or specification but using the procedure from the Strategic Highway Research Program (SHRP) A005 project and also using AASHTO T-274 (19) as a guide. The pressure chamber, shown in Figure 51, was used in place of the conventional triaxial pressure chamber because of the size of the samples and the attachment of both radial and vertical linear variable differential transformers (LVDT's) which took up a lot of space (as shown in Figure 52). The samples were preconditioned using the AASHTO recommended procedure (19). Due to the small nature of the applied stresses, the load cell to record the deviator load was mounted inside the pressure chamber to reduce the occurrence of errors from friction, etc. A computerized data acquisition system allowed simultaneous recordings from six channels, that is, three for the radial LVDT's and three for the vertical LVDT's. Data were recorded at every 0.1 of a second for the conditioning phase and 1.0 second for the creep test.

The procedure for the compressive creep and recovery test is as follows:

(a) The specimen was prepared and molded using a metal cylinder 305 mm high and 152 mm in diameter. It was then extruded and placed in a rubber membrane as recommended by AASHTO (19).

(b) To condition the specimen, 200 repetitions of a square wave were initially applied to the test specimen. The specimen was loaded for 0.1 seconds and then allowed to recover for 0.9 seconds. This was done starting at the highest confining pressure and then at subsequent confining pressures.

(c) After conditioning, a single load and unload cycle was applied to the specimen using a prescribed deviatoric stress. This was in the form of a square wave load pulse applied for 90 seconds, after which the specimen was unloaded and allowed to recover.

(d) The confining pressure was reduced to the next prescribed level and steps (b) and (c) repeated until the final and lowest confining pressure was run. Note that AASHTO T-274 (19) was used as a guide in conducting this test.

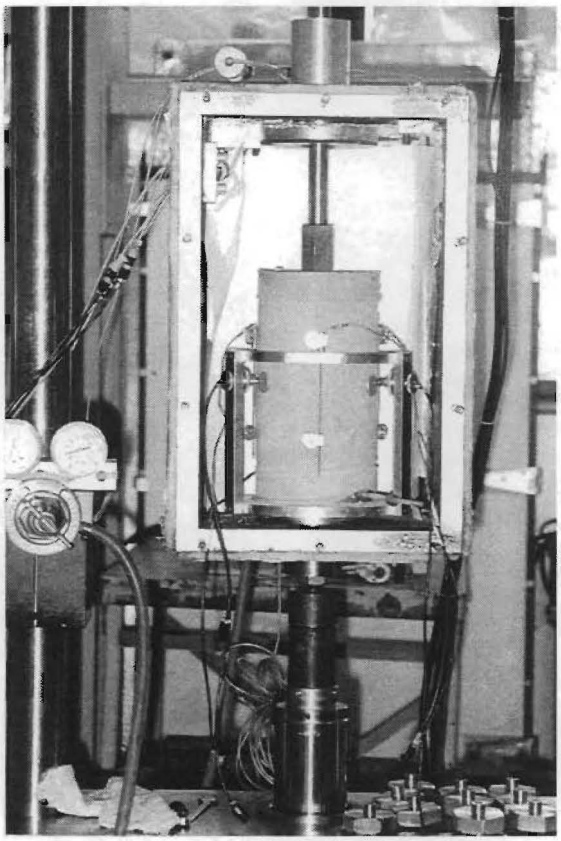

Figure 51. Pressure Chamber with Specimen.

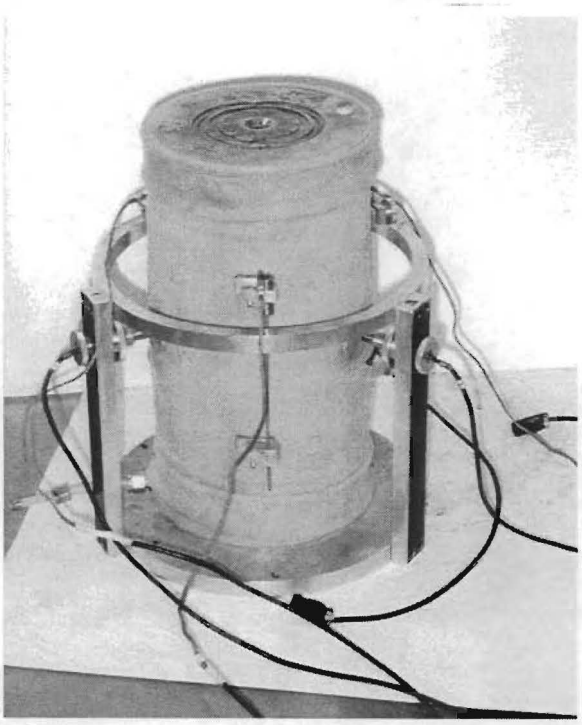

Figure 52. Specimen with Vertical and Radial LVDT's.

(e) Three LVDT's were used for measuring axial deformation and three LVDT's were used to measure the radial deformation. In both cases, these were placed 120° apart and a 130-mm gauge length centered along the height of the cylindrical mold was used for vertical deformations. Figures 53 and 54 illustrate the sensors used to measure vertical and radial displacements.

(f) The strains (vertical and radial) and the applied load were used to obtain vertical and radial compliance curves.

Equation (13), given in Chapter 2, was fitted to the compressive creep and recovery data for the different confining pressures and soil types. Researchers used the compliance equations to obtain the resilient strains at specified times and stress states, which they then used to obtain the resilient moduli and the Poisson's ratios corresponding to the different stress states. The resilient moduli at the different stress states were used as input data in Equation (1) to backcalculate the resilient parameters, K_1, K_2, and K_3. An estimate of suction, U, was also obtained since it acts as a confining pressure as shown in Equation (19). Finally, the Poisson's ratios at different stress states were also used in backcalculating the resilient parameters K_2 to K_5 using Equation 9. Tables 9 to 11 summarize the resilient parameters.

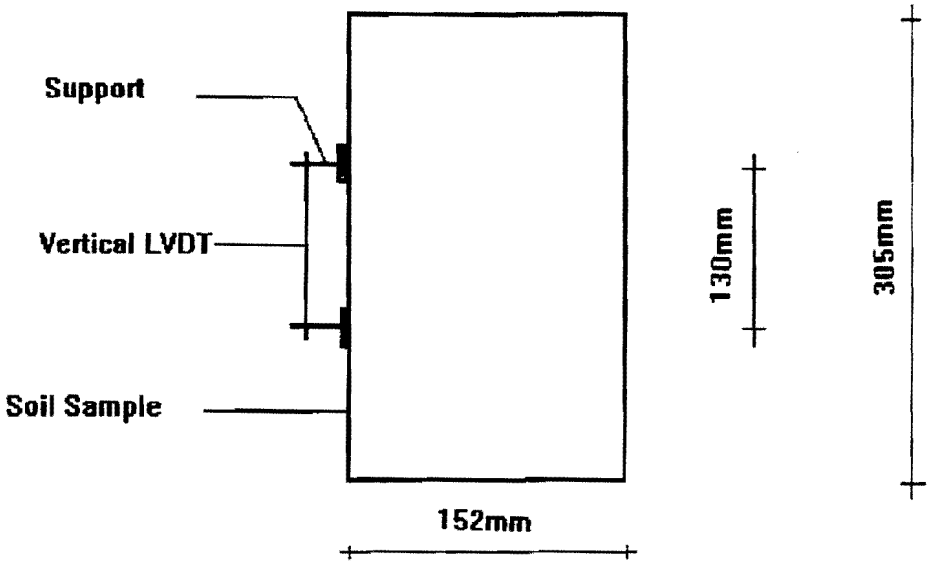

Figure 53. Vertical Displacement Measuring System.

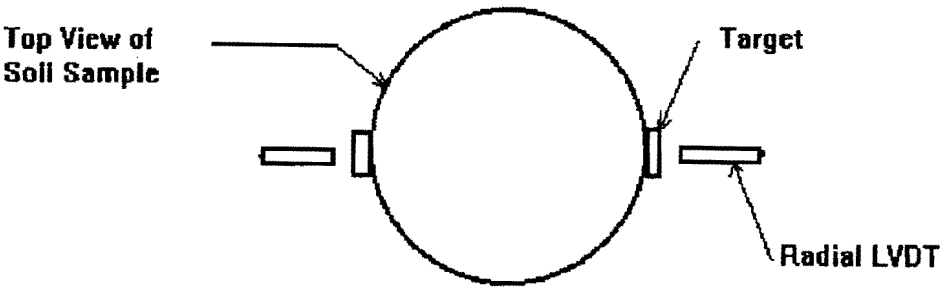

Figure 54. Radial Displacement Measuring System.

Table 9. Material Properties K_1 to K_5 and Suction for Material at -2% of Optimum.

Material	K_1	K_2	K_3	K_4	K_5	U (KPa)
Limestone	1498	0.904	-0.326	2.297	-0.339	-11
I.O. Gravel	2816	0.603	0	3.584	-0.503	-17
S. Gravel	11288	0.631	-0.102	1.645	-1.646	0
Caliche	1443	1.184	0	0.791	-0.437	-12
Shellbase	827	1.101	0	0.588	-0.201	0
Sand	3118	0.439	0	1.537	-0.335	-2
Silt	824	1.195	-0.111	1.034	-0.325	-10.
Lean Clay	4096	0	-0.267	0.020	-0.755	0
Fat Clay	200	0.659	-1.473	-0.944	0.368	-15

Table 10. Material Properties K_1 to K_5 and Suction for Material at Optimum.

Material	K_1	K_2	K_3	K_4	K_5	U (KPa)
Limestone	1657	0.904	-0.326	2.297	-0.339	-11
I.O. Gravel	3271	0.492	-0.001	0.886	-0.006	-60
S. Gravel	1574	0.670	-0.285	2.223	-0.185	-22
Caliche	888	0.829	-0.005	1.623	-0.277	-27
Shellbase	815	0.597	-0.003	0.929	-0.213	-2
Sand	6434	0.512	0	1.337	-0.119	-2
Silt	1172	0.518	-0.204	1.720	-0.099	0
Lean Clay	105	0.322	-0.100	1.489	-0.011	-102
Fat Clay	263	1.249	-0.498	1.214	-0.236	-59

Table 11. Material Properties K_1 to K_5 and Suction for Material at +2% Optimum.

Material	K_1	K_2	K_3	K_4	K_5	U (KPa)
Limestone*	3853	0.429	-0.024	3.435	-0.385	-9
I.O. Gravel	211	0.558	0	1.036	-0.237	-45
S. Gravel**	-	-	-	-	-	-
Caliche	477	0.186	-0.002	1.200	-0.084	-32
Shellbase	753	0.776	0	0.853	-0.269	-2
Sand	6319	0.404	-0.028	1.332	-0.040	-5.
Silt	998	0.502	-0.100	1.955	-0.283	-1
Lean Clay	776	0.104	-0.549	-0.248	0.312	0
Fat Clay	440	0.664	-0.174	1.561	-0.210	-85

* Limestone was tested at minus four percent of the optimum moisture content.

** Sandy Gravel was not tested at plus two percent of optimum.

DIELECTRIC AND CONDUCTIVITY TEST

The dielectric constant, ϵ_r, and electrical conductivity, ρ, of each of the compacted soil samples used in the compressive creep and recovery test were determined before the actual testing was done. The properties were determined at three different locations at the top and bottom of the soil samples. Researchers used a tubular probe of a dielectric and conductivity meter produced by Adek Ltd. in Estonia (Figure 55). Table 12 summarizes the results.

The dielectric constant affects the travel time of electromagnetic waves within a uniform medium. The higher the dielectric constant, the longer the travel time. Typical dielectric constants of highway materials are given in Table 13.

The dielectric constant is a physical quantity that may be estimated from radar survey data. It is used to estimate layer thickness non-destructively at highway speed. Pavement applications of ground penetrating radar have been investigated by TxDOT

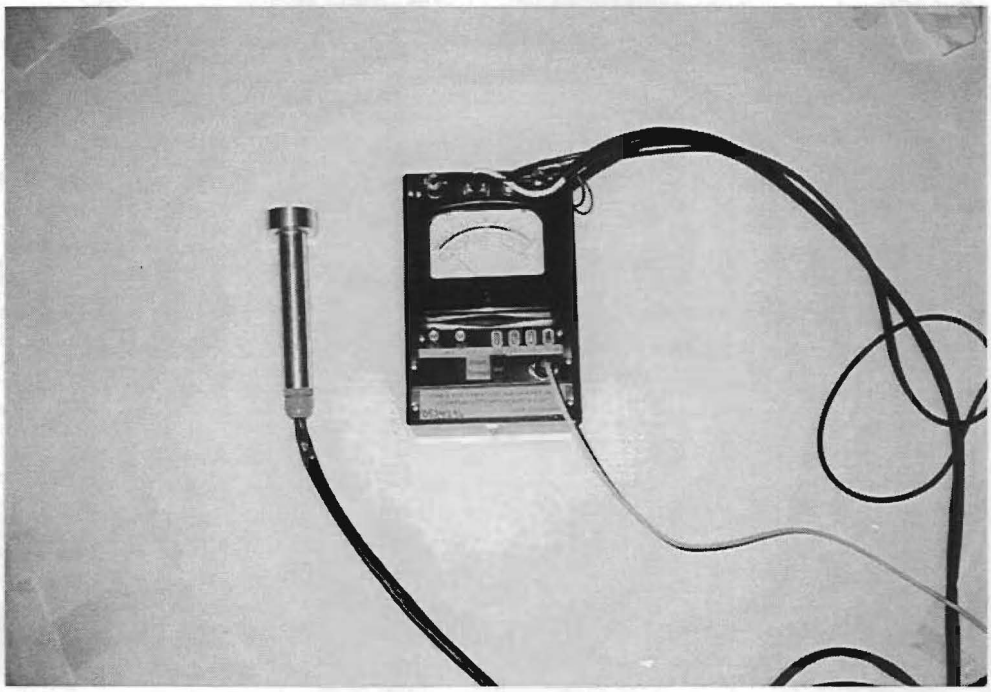

Figure 55. Dielectric Probe Used to Measure Dielectric Constants of Laboratory Molded Specimens.

through research projects with the Texas Transportation Institute (TTI). The Department has developed the capability to conduct radar surveys and to analyze the data collected. This capability is particularly useful for structural evaluation of superheavy load routes since it permits the estimation of layer thicknesses for these routes. The layer thicknesses are required input to the superheavy load evaluation procedure.

Considering the useful application of radar for route assessment, researchers also measured the dielectric constants of the soils in the laboratory to investigate the correlation between this physical quantity and the resilient and strength parameters required for assessing the structural adequacy of superheavy load routes. In this way, the application of radar for estimating these parameters may also be investigated.

Table 12. Dielectric and Conductivity Values for Materials Tested.

Soil Type	-2% of Optimum		Optimum		+2% of Optimum	
	ε_r	ρ	ε_r	ρ	ε_r	ρ
Limestone	8.95	41.20	13.85	167.55	15.55*	186.60*
I.O. Gravel	9.45	11.75	15.00	101.85	17.65	249.00
S. Gravel	17.65	249.00	11.90	229.00	**	**
Caliche	13.90	143.45	16.00	270.70	16.90	262.30
Shellbase	5.85	10.95	5.25	14.70	6.90	43.30
Sand	4.90	16.15	5.90	32.20	6.75	31.20
Silt	11.05	158.00	12.70	140.50	15.40	306.00
Lean Clay	9.80	57.25	11.15	34.00	15.70	104.65
Fat Clay	22.65	516.05	21.60	689.65	25.75	808.40

* Limestone was tested at minus 4% of optimum.

** Sandy Gravel was not tested.

Table 13. Typical Dielectric Constants.

Material	Dielectric Constant
Air	1
Water	81
Asphalt	3- 6
Concrete	6 - 11
Crushed Limestone	10 - 23
Dry Sand	3 - 5
Clays	5 - 40

CHAPTER 4
ANALYSIS OF THE MODIFIED TEXAS TRIAXIAL TEST RESULTS

INTRODUCTION

As indicated in the beginning of this report, TTI researchers investigated a number of alternative procedures for determining the resilient and strength parameters required for conducting the structural evaluation of superheavy load routes. Indeed, this report documents the specific efforts made in this regard. The objective was to develop alternative procedures that TxDOT engineers may use to estimate the required parameters in the absence of actual laboratory data from triaxial tests on soils. Alternatively, researchers sought to identify modifications to existing test methods that may simplify the task of determining the required material parameters. All of these efforts were done as part of developing the superheavy load analysis procedure, and to facilitate its implementation within the department.

One approach investigated by researchers was a modification of the existing Texas triaxial test that offered the potential of just one test method determining both the strength and resilient parameters. Another approach taken was to develop prediction equations for estimating the required parameters using soil properties determined from simpler tests. The succeeding chapter presents the results from this work. The present chapter discusses the analysis of the modified Texas triaxial test data.

Recall that the standard Texas and modified Texas triaxial tests differed only in their loading sequence. A load and hold sequence was added to the standard Texas triaxial loading sequence in order to allow the specimen to creep. This provided data for estimating the resilient parameters, K_1, K_2 and K_3 of the material, in addition to the strength parameters, cohesion, C, and the angle of internal friction, ϕ. Figures 56 to 61 compare the strength parameters of the materials from the two tests. Also, researchers performed a statistical analysis to determine if there are any significant differences between the two results obtained.

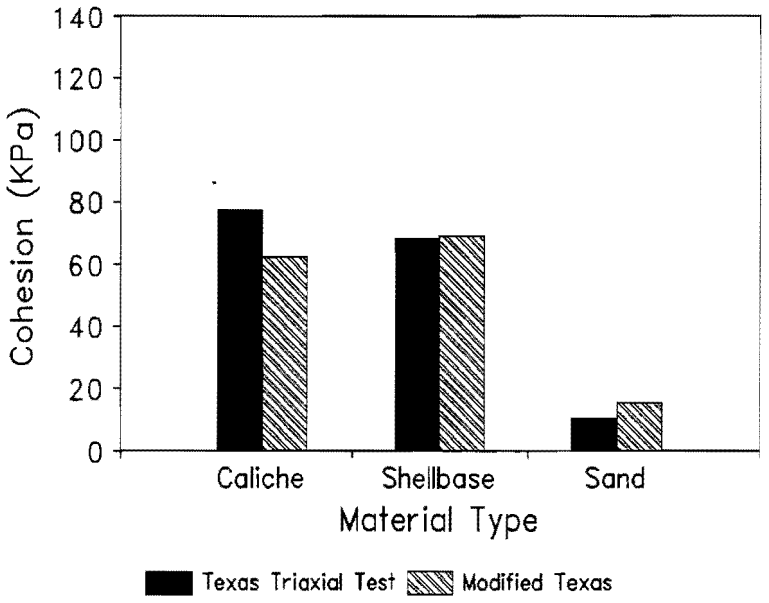

Figure 56. Cohesion Results from Standard and Modified Texas Triaxial Tests for Caliche, Shellbase and Sand.

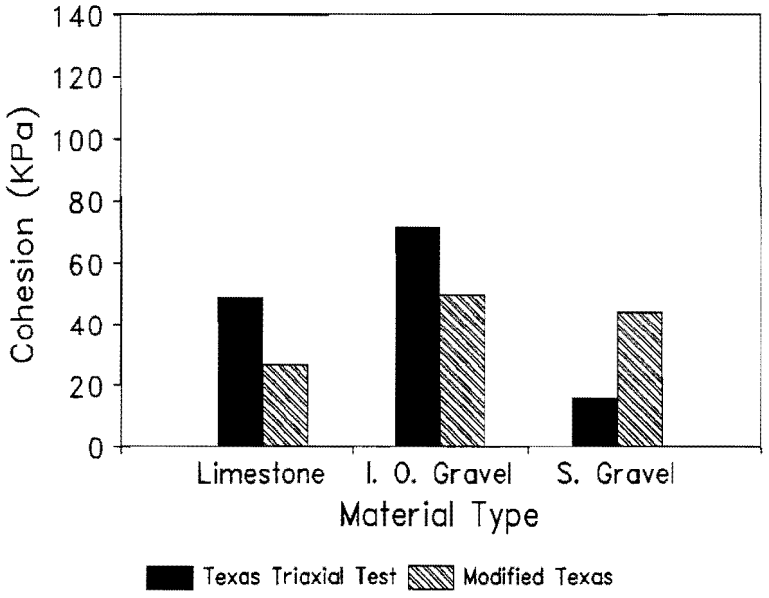

Figure 57. Cohesion Results from Standard and Modified Texas Triaxial Tests for Limestone, Iron Ore Gravel and Sandy Gravel.

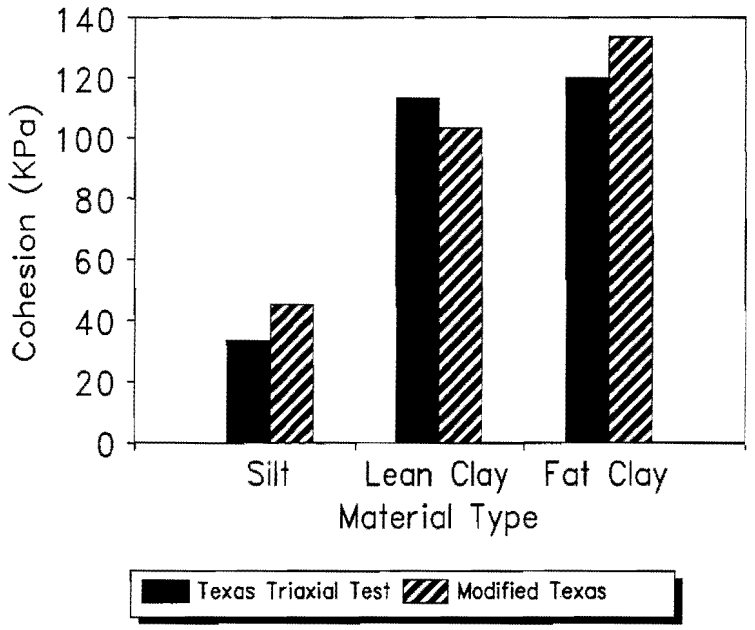

Figure 58. Cohesion Results from Standard and Modified Texas Triaxial Tests for Silt, Lean Clay and Fat Clay.

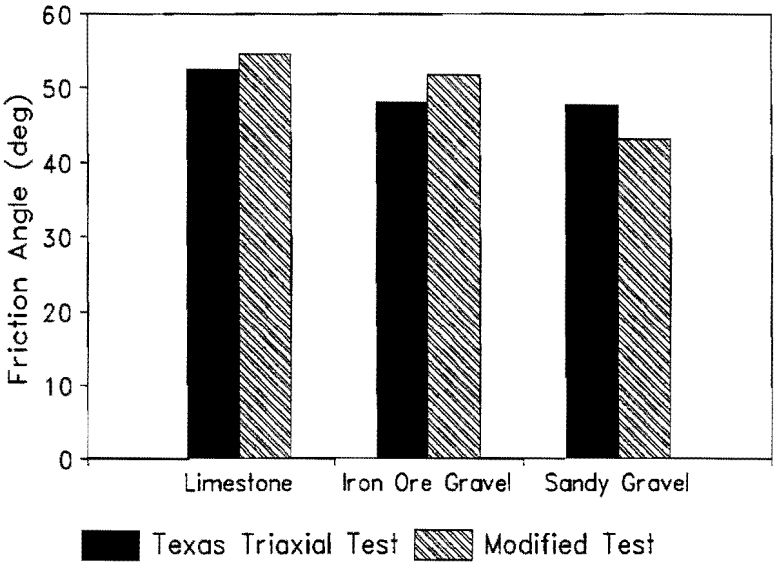

Figure 59. Angle of Internal Friction Results from Standard and Modified Texas Triaxial Tests for Limestone, Iron Ore Gravel and Sandy Gravel.

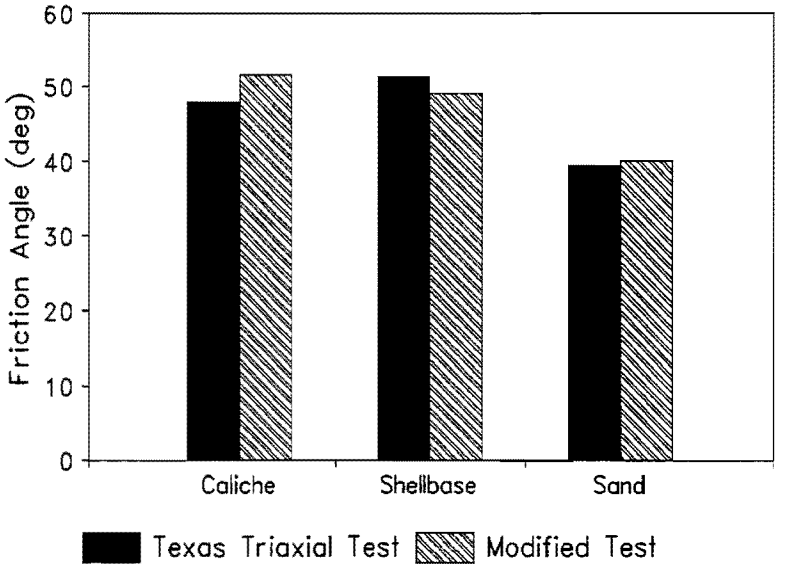

Figure 60. Angle of Internal Friction Results from Standard and Modified Texas Triaxial Tests for Caliche, Silt and Sand.

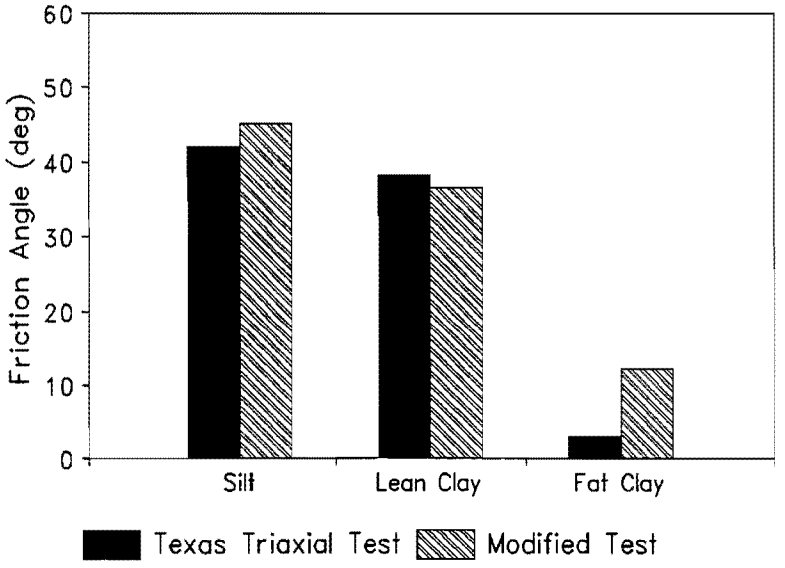

Figure 61. Angle of Internal Friction Results from Standard and Modified Texas Triaxial Tests for Silt, Lean Clay and Fat Clay.

STATISTICAL ANALYSIS

Researchers conducted the statistical analysis of the data using the PC version of SAS release 6.03 (20). The primary considerations in the analysis were the coefficient of determination (r^2), which is a measure of how well the results from the two different methods were correlated, and the error sum of squares, which is an indication of the level of error occurring in the modified test procedure. Researchers performed an analysis of variance (AOV) to determine if there was a significant difference between cohesion and the angle of internal friction obtained from the standard and modified procedures. The experiment was designed as a randomized block design (21) in which the two test procedures were referred to as the treatments, Trt. The standard Texas triaxial test was designated Trt(S) and the modified Texas triaxial test, Trt(M). The nine different soil types were referred to as the blocks. We can expect some differences in the cohesion and the angle of internal friction results between the various soil types or blocks since these soils have very different physical properties. In here, we are interested in determining if there is a significant difference in the material properties between the two treatments or test procedures. We can do this statistically by using the randomized block design (21). This enables us to make a more precise comparison of the two different treatments which are the standard and modified triaxial tests. Listed below are some of the statistical advantages of this experimental design (21).

a) The statistical analysis is quite simple.
b) The design is easy to construct.
c) It is a useful design for comparing different treatment means in the presence of a single source of variability which in this case is the soil type.

A level of significance, α, of five percent (α=0.05) was used in this analysis. Tables A.1 and A.2 in the Appendix show the AOV table for cohesion, C, and the angle of internal friction, ϕ. Figures 62 and 63 show plots of the cohesion and the angle of internal friction from the two test procedures.

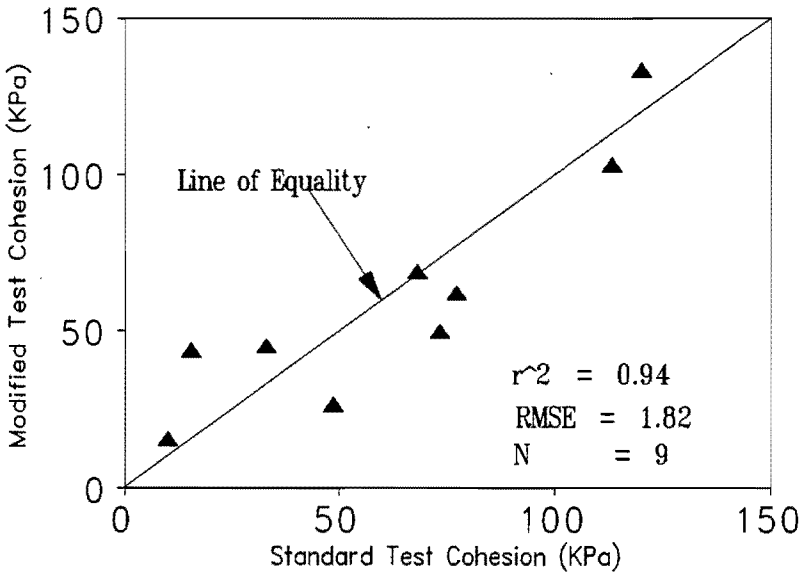

Figure 62. Standard Cohesion Versus Modified Cohesion.

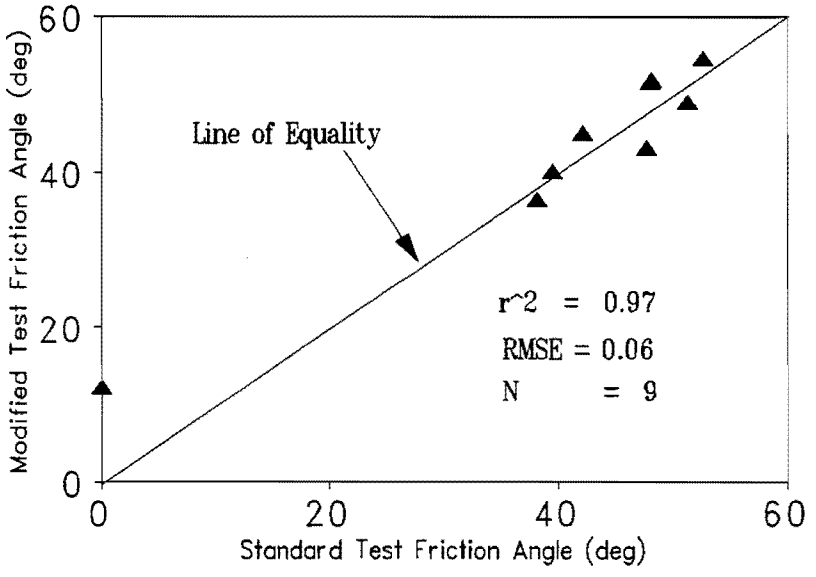

Figure 63. Standard Friction Angle Versus Modified Friction Angle.

From the results of the analysis of variance summarized in Tables A.1 and A.2 we can test the hypothesis as to whether there is a significant difference in the mean response of cohesion and the angle of internal friction from the two test procedures. The null and alternate hypotheses are as follows:

H_o :Difference in mean μ_s-$\mu_m = 0$

H_A :Difference in mean μ_s-$\mu_m \neq 0$

For this research, we will reject the null hypothesis, H_o, if the calculated F value is greater than $F_{\alpha,df1,df2}$,

where $\alpha = 0.05$

$df_1 = 1.00$

$df_2 = 8.00$

$F_{0.05,1,8} = 5.123$. For cohesion, the calculated F value was 0.05, and for the angle of internal friction, it was 1.12 as shown in Tables A.1 and A.2. We can therefore conclude that there was not enough statistical evidence to reject the null hypothesis, and there is no significant difference in the results obtained from the two tests.

Researchers also made a similar analysis for the resilient properties, K_1 and K_2. In this instance, the resilient parameters from the modified triaxial test were compared with the corresponding estimates from the compressive creep and recovery test. It was not necessary to analyze K_3 since it plays quite a marginal role in the prediction of the resilient modulus in granular base and subgrade materials and the database for fine grained materials was limited. It must be stated, however, that the K_3 values observed from the two methods were close. Figures 64 and 65 show plots of K_1 and K_2 from the two different methods. A simple regression analysis was made with the data to develop equations for calibrating the K_1 and K_2 values estimated from the modified triaxial test, to values representative of compressive creep and recovery test results. Equations (21)

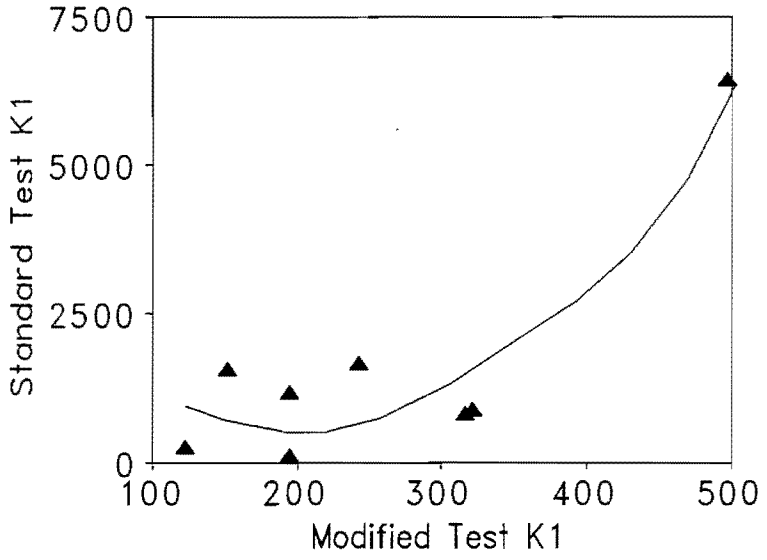

Figure 64. Modified Texas Triaxial Test K_1 Versus Compressive Creep and Recovery Test K_1.

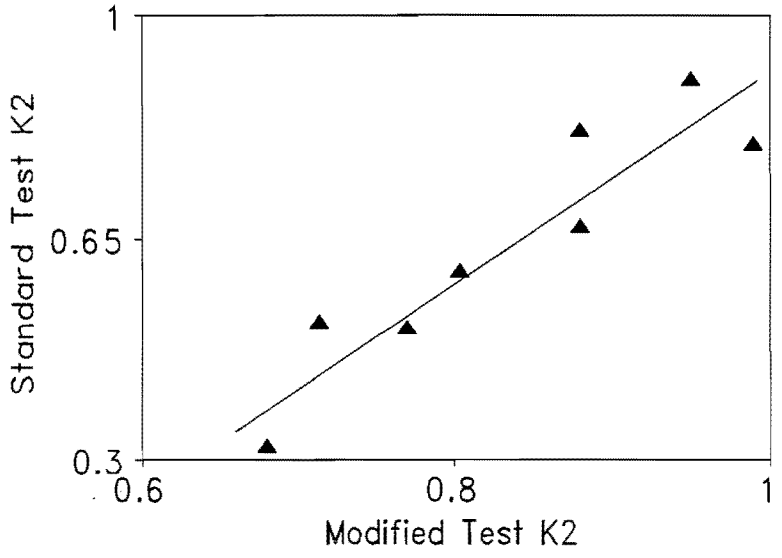

Figure 65. Modified Texas Triaxial Test K_2 Versus Compressive Creep and Recovery Test K_2.

and (22) were developed with coefficients of determination (r^2) of 0.81 and 0.88 respectively:

$$K_1 = 3737 - 28.81X + 0.06794X^2 \quad (21)$$

where X = K_1 obtained from the modified triaxial test

$$K_2 = -0.9018 + 1.905Y \quad (22)$$

where Y = K_2 obtained from the modified triaxial test

Equations 21 and 22 were used to calibrate the K_1 and K_2 values from the modified triaxial test. Table 14 shows a summary of the calibrated K_1 and K_2 values, and Figures 66 and 67 present the information graphically.

Table 14. Calibrated K_1 and K_2 Values from Modified Texas Triaxial Test.

Material	Legend	K_1	K_2
Fat Clay	1	1234	0.19
Sandy Gravel	2	930	0.77
Iron Ore Gravel	3	712	0.54
Lean Clay	4	703	0.32
Silt	5	703	0.45
Limestone	6	749	0.91
Shellbase	7	1439	0.59
Caliche	8	1508	0.77
Sand	9	6202	0.46

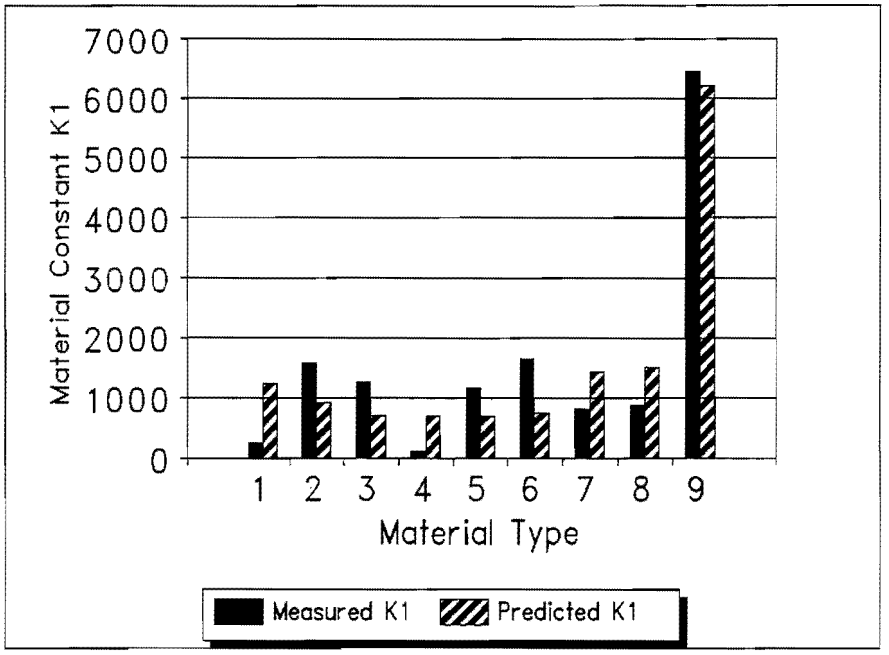

Figure 66. Measured K_1 from Compressive Creep and Recovery Test Versus Predicted K_1 from Calibration Equation.

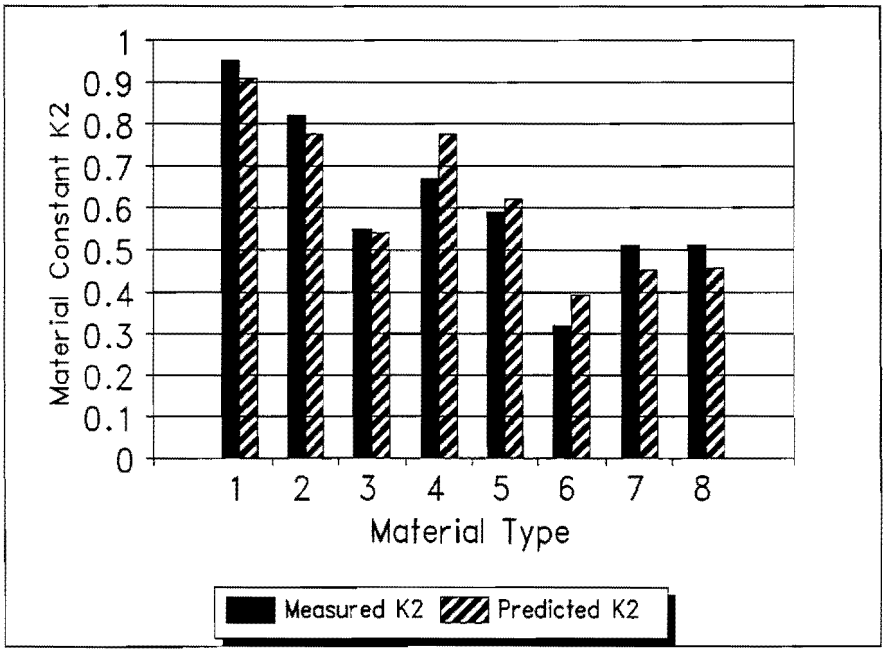

Figure 67. Measured K_2 from Compressive Creep and Recovery Test Versus Predicted K_2 from Calibration Equation.

From the results of the analysis of variance summarized in Tables A.3 and A.4, we can test the hypothesis as to whether there is a significant difference in the mean resilient parameters from the compressive creep and recovery test, and the modified triaxial test after calibration. The null and alternate hypotheses are

H_o : Difference in mean μ_s-μ_m = 0

H_A : Difference in mean μ_s-μ_m $\neq$ 0

For this research we will reject the null hypothesis H_o if the calculated F value is greater than $F_{\alpha,df1,df2}$,

where α = 0.05

df_1 = 1.00

df_2 = 8.00

$F_{0.05,1,8}$ = 5.123. For K_1, the calculated F value was 0.15, and for K_2 it was 0.0. We can therefore conclude that there was not enough statistical evidence to reject the null hypothesis, and there is no significant difference in the calibrated results from the modified triaxial test and the results from the compressive creep and recovery test.

CHAPTER 5
PREDICTIVE RELATIONSHIPS

INTRODUCTION

To develop relationships for predicting the resilient parameters K_1, K_2, and K_3, and the strength parameters, C and ϕ, it is necessary to determine the important terms that make up the database of material properties from which the independent variables will be selected as input into the proposed relationships. These terms can be divided into four groups, namely,

Moisture Variables:

- Gravimetric moisture content;
- Volumetric moisture content;
- Soil Suction;
- Saturation;

Strength Variables:

- Cohesion;
- Angle of Internal Friction;

Resilient Variables:

- Resilient Modulus;
- Poisson's ratio;
- Resilient parameters K_1 to K_5 ;

Physical Variables:

- Specific gravity;
- Maximum dry density;
- Gradation;
- Conductivity and dielectric constant; and
- Atterberg limits.

Researchers selected the input variables for the prediction equations based on the ability of personnel to measure these properties without much difficulty in-situ or in the laboratory and with the required accuracy. Figure 68 shows a flow chart of the strategy for the regression analysis (22).

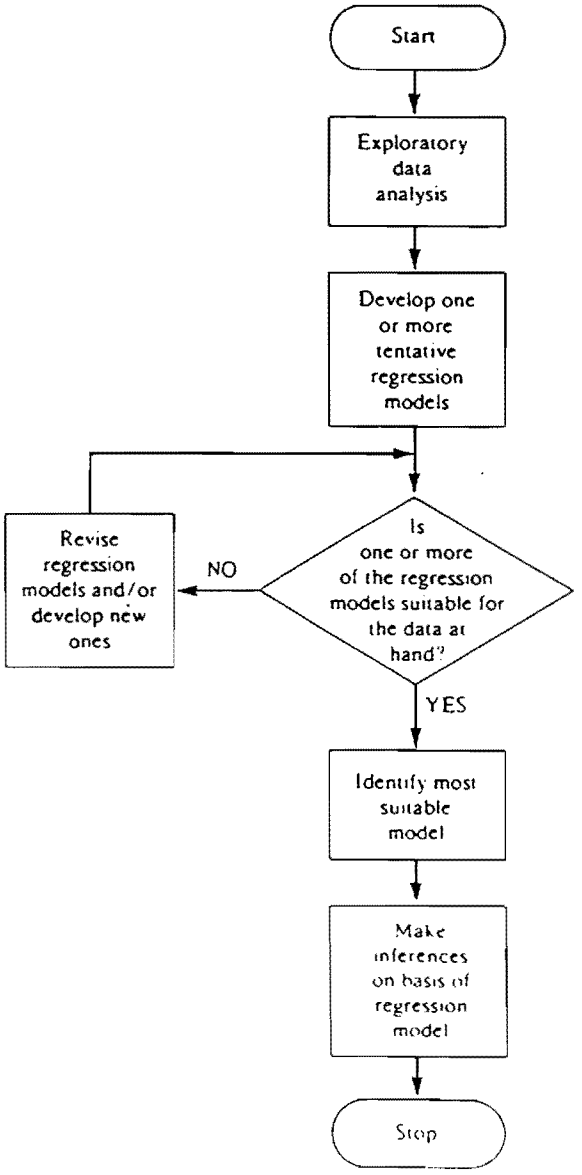

Figure 68. Flow Chart of Regression Analysis (22).

EXPLORATORY ANALYSIS

Before any regression was run on the data, researchers conducted an exploratory analysis in order to identify potential problems in the data which may have been due to miscellaneous factors such as data entry mistakes. Also, the exploratory analysis was aimed at identifying those observations which may be outliers. Researchers reviewed scatter plots of all combinations of the independent and dependent variables to identify obvious trends that may need further investigation at a later stage. Another reason for the scatter plots was to ensure that the data appear to be consistent with what is logically expected from mechanistic analysis and previous research.

TEST FOR NORMALITY, INDEPENDENCE AND CONSTANT VARIANCE

The three main assumptions made in regression analysis are (21)

- The residuals are independent;
- The residuals have a constant variance; and
- The residuals are normally distributed.

These assumptions were checked for their validity by using scatter plots and other diagnostic statistics. To test for independence, the Durbin-Watson test statistic, d, was used (21). A value of d ranging from 1.5 to 2.5 was considered adequate for concluding that the variables were independent. A plot of the residuals ($Y-\hat{Y}$), where Y is the observed value and $\hat{Y}$ is the predicted value, versus $\hat{Y}$ was analyzed to check for constant variance (21). A plot of the residuals plotted in the form of a histogram was used to check for normality (21).

DIAGNOSTIC STATISTICS

A number of diagnostic statistics were used in the regression analysis to check for the significance of parameter estimates, errors, and multicollinearity, and the assumptions already discussed. Table 15 summarizes these diagnostic statistics and their critical values (21).

Table 15. Critical Values of Diagnostic Statistics.

Diagnostic Statistic	Diagnostic Objective	Critical Values
Variance Inflation Factor	Multicollinearity	< 10
Eigenvalues	Multicollinearity	Small Values
Condition Index	Multicollinearity	< 30
Durbin-Watson T. S., d	Serial Correlation	1.5 < d < 2.5
C_p	Optimum number of Independent variables	Minimize
MSE	Goodness of fit	Minimize
$PRESS_p$	Ability to predict outside of dataset	Minimize
Prob > F-Statistic	Significance of Parameter Estimate	< 0.05

MODEL SELECTION

The selected independent variables were used as the final database from which the regression equations were developed. Researchers used the SAS procedures Stepwise, Rsquare and Rsreg (20) to obtain different possible models which were later refined to obtain the final prediction equations by eliminating multicollinearity and using the $PRESS_p$ test statistic. This statistic is computed by calculating the squares of the differences between the predicted values using first, a regression equation developed without the i^{th} observation and then an equation developed with the i^{th} observation. This process is repeated (N-1) times and summed up, where N is the total number of observations (20). The model with the lowest $PRESS_p$ statistic is preferred. Some of the independent variables used in the models were normalized. The purpose of normalizing the variables was to enable those variables to be added or omitted from the statistical models without adversely affecting the remaining model coefficients or, in other words, to reduce the occurrence of multicollinearity. They were normalized as follows (22):

$$X_N = X - X_{mean} \tag{23}$$

where X_N = normalized X variable,

X = variable X, and

X_{mean} = grand mean of variable X.

The SAS procedures, REG and GLM, were used to determine the parameter estimates and the necessary diagnostic statistics for the prediction equations. Researchers selected the model which best satisfies all the diagnostic statistics discussed.

RESILIENT PARAMETER K_1

The final form of the prediction equation for the resilient parameter, K_1, is

$$K_1 = 28659 - 417.297PL - 5706.38G_s + 12780\theta_w - 75.443N40 - 5462.069\tan\phi + 58.975N40_N*U_N + 256.002N40_N*\tan\phi_N - 309.3217U_N*\varepsilon_{rN} \quad (24)$$

where PL = plastic limit of material,

G_{sb} = specific gravity of soil binder,

θ_w = volumetric moisture content,

$\tan\phi$ = tangent of friction angle, ϕ,

N40 = % of material passing the 0.42mm sieve size,

$N40_N$ = normalized N40 = N40 - 57.215,

$\tan\phi_N$ = normalized $\tan\phi$ = $\tan\phi$ - 0.92877,

U = suction in pF,

U_N = normalized suction = U - 2.12231,

ε_r = dielectric constant, and

ε_{rN} = normalized dielectric constant ε_r - 12.5981.

Table A.5 in the Appendix gives a summary of the output of the regression and general linear model procedures from SAS. Figure 69 shows a plot of the measured versus the predicted K_1 values from the prediction equation.

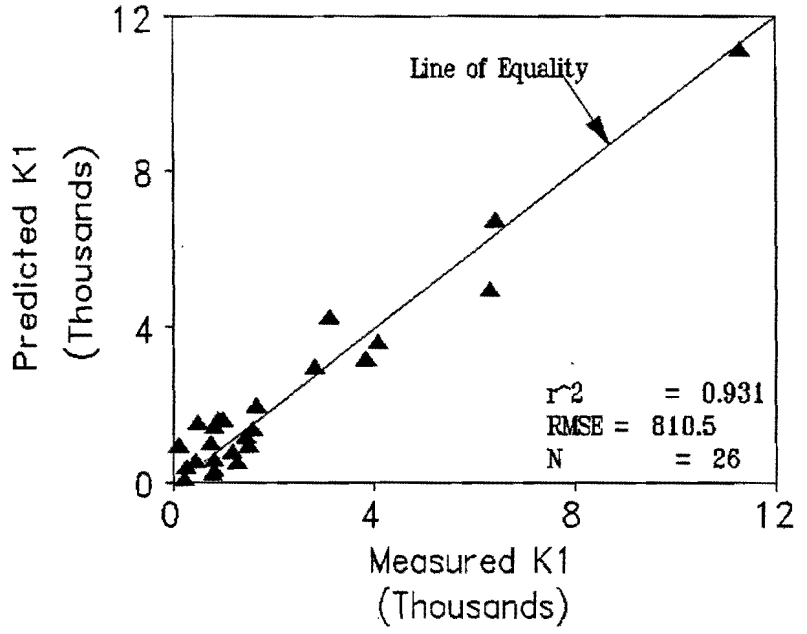

Figure 69. Measured Versus Predicted K_1 Values.

SUMMARY

Researchers have developed a prediction equation for predicting K_1, which is an input parameter used in Uzan's model (6) to predict the resilient modulus of pavement materials. Sensitivity analysis by Jooste and Fernando (23) shows that this is the most influential of the three material parameters K_1, K_2 and K_3 in the model. The coefficient of determination for the prediction equation is 0.93, which is good enough to obtain a reasonably accurate estimate of K_1 in the absence of actual test data from compressive creep and recovery or resilient modulus tests. The input variables for this equation are suction, plastic limit, specific gravity, volumetric moisture content, angle of internal friction, material dielectric constant, and the percentage of materials passing the 0.42 mm sieve size. All of the input variables are obtained from simple laboratory tests and analysis of material sampled from the field. The dielectric constant may be obtained from radar measurements along a proposed superheavy load route which is a capability TxDOT already has. References, published research, or local experience can provide

the angle of internal friction. They tend not to vary much, and, for most granular materials, are in the range of 43° to 55°. The effects of multicollinearity among the input variables were acceptable. This prediction equation should therefore give a reasonable estimate of the resilient parameter, K_1, for a wide range of material types and moisture conditions.

RESILIENT PARAMETER K_2

The final form of the prediction equation for the resilient parameter, K_2, is

$$K_2 = -0.127927 + 0.515759G_{sb} - 0.084802W + 0.00027N40_N^2 - 0.009607LL_N*W_N - 0.192586LL_N*\tan\phi_N + 0.003981LL_N^2 \quad (25)$$

where G_{sb} = specific gravity of binder content of soil,
W = gravimetric moisture content,
W_N = normalized gravimetric moisture content,
= W - 8.94172, and
LL_N = normalized liquid limit = LL - 24.4188.

All other variables are defined already. Table A.6 in the Appendix is a summary of the output of the regression and general linear model procedures from SAS. Figure 70 shows a plot of the measured versus the predicted K_2 values from the prediction equation.

SUMMARY

Researchers have developed a prediction equation for K_2. The influence of K_2 in Uzan's model is limited (23). The coefficient of determination of this equation is 0.75 which is considered acceptable since K_2 does not significantly affect the estimation of the Mohr-Coulomb yield criterion in the superheavy load analysis procedure. The input variables for this equation are similar to those for the prediction equation of K_1, and

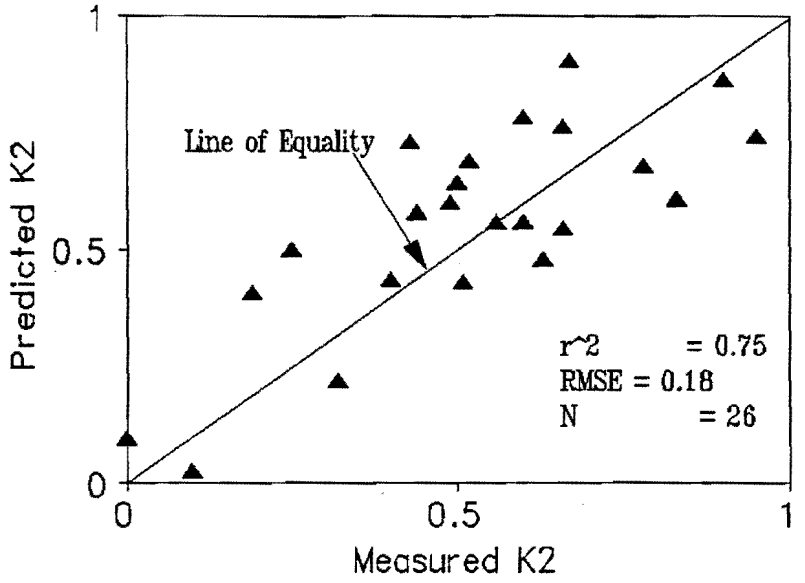

Figure 70. Measured Versus Predicted K_2 Values.

they should therefore be obtained quite easily. The effects of multicollinearity among the input variables are within the acceptable range. The prediction equation should therefore give an acceptable estimate of K_2.

RESILIENT PARAMETER K_3

The final form of the prediction equation for the resilient parameter, K_3, is

$$K_3 = 1.807384 - 0.181851\epsilon_r - 2.808291LL_N*W_N - 0.016342\ LL_N*\epsilon_r \qquad (26)$$

where ϵ_r = dielectric constant,

LL_N = normalized liquid limit = (LL - 28.6667),

W_N = normalized gravimetric moisture content, and

= (W - 13.451).

Note that this equation is based on data from fine grained soils and, therefore, is most suitable for only fine grained soils. This is because K_3 for granular materials is approximately zero. Table A.7, in the Appendix, is a summary of the output of the regression and general linear model procedures from SAS. Figure 71 shows a plot of the measured versus the predicted K_3 values from the prediction equation.

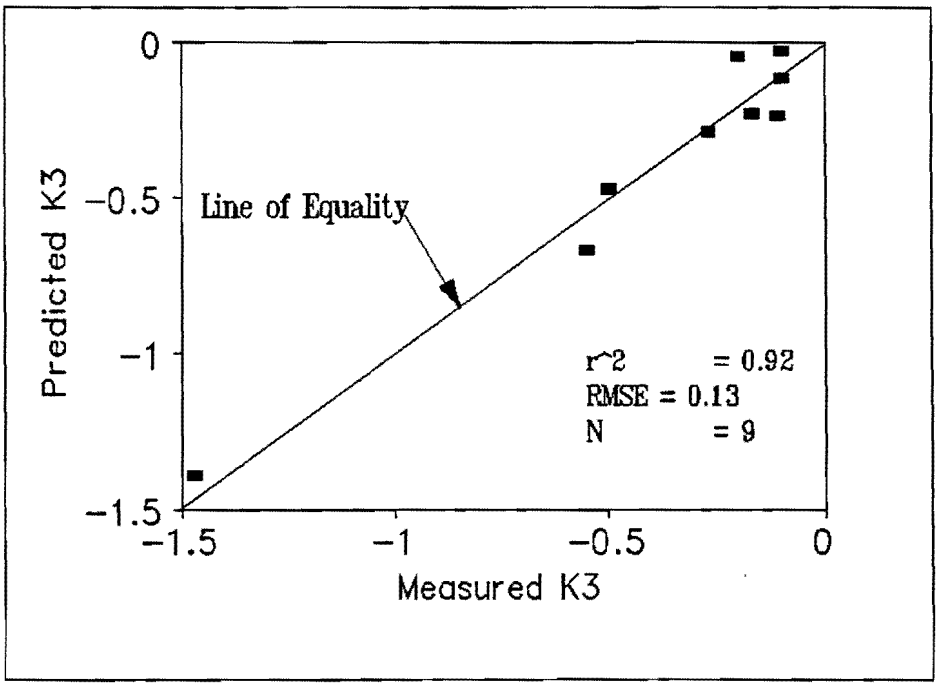

Figure 71. Measured Versus Predicted K_3 Values.

SUMMARY

Researchers have developed a prediction equation for K_3. The resilient parameter K_3 is significant only for estimating the resilient modulus of fine grained materials such as silt and clay. The coefficient of determination for the prediction equation is 0.92. The maximum value of the variance inflation factor which is an indication of the effects of multicollinearity among the input variables is 11.21. This is slightly above the acceptable limit of 10.0 but not significant enough to adversely affect the estimation of

K_3 by the prediction equation. The input variables are similar to those for the prediction equations for K_1 and K_2 and should be obtained quite easily in the laboratory.

EFFECT OF LOADING TIME ON THE RESILIENT MODULUS OF PAVEMENT MATERIALS

As discussed in Chapter 2 of this report, the strain response of most pavement materials which are non-linear and visco-elasto-plastic in nature is both stress and time dependent. This means that the resilient modulus of such materials tends to decrease with an increase in the time of loading. An advantage of the compressive creep and recovery test is that the resilient strain and, hence, the resilient modulus can be calculated for different times of loading. The prediction equations for estimating the values of the resilient parameters K_1, K_2 and K_3 are based on a loading time of 0.1 second which is typical of highway traffic speed. There will be the need for a transformation equation to estimate the resilient modulus of the pavement materials if the vehicular speed and hence the loading time on the pavement differs from the assumed speed. This equation is based on a reference resilient modulus calculated from a loading time of 0.1 seconds. Other inputs into this equation are the time of loading and the material properties. The transformation equation from compressive creep and recovery data is given by

$$\ln E_{r,t} = 3.0286 + 0.8721 * \ln E_{r,0.1} - 1.14914 * t - 0.0654 * LL + 0.00107 * \rho \quad (27)$$

where $\ln E_{r,t}$ = natural logarithm of resilient modulus at a loading time, t;

$\ln E_{r,0.1}$ = natural logarithm of resilient modulus at a loading time of 0.1 seconds;

LL = liquid limit; and

ρ = conductivity.

Table A.8, in the Appendix, is a summary of the output of the regression and general linear model procedures from SAS. Figure 72 is a plot of the measured resilient modulus at various times of loading versus the predicted resilient modulus from the prediction equation.

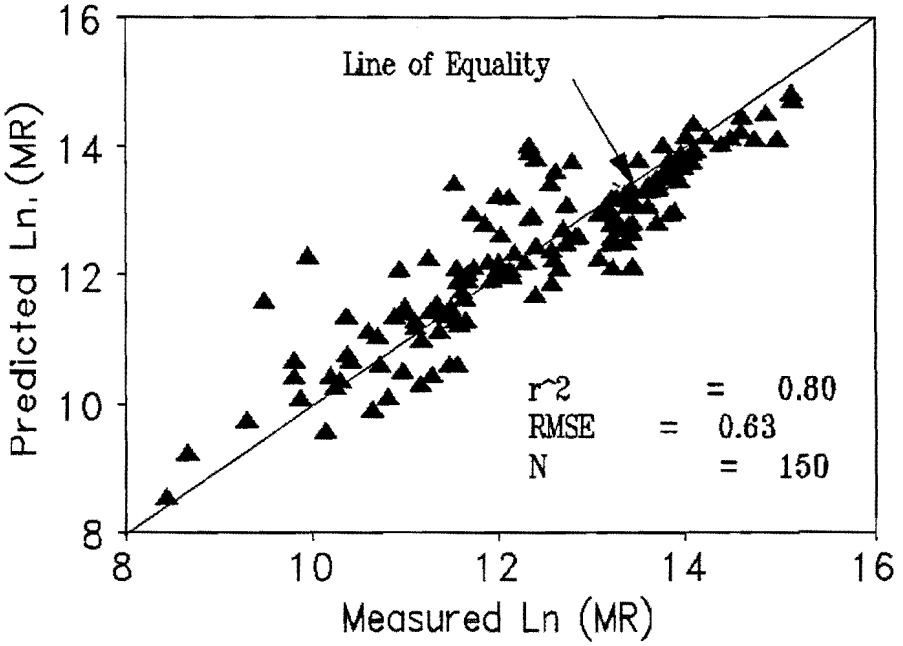

Figure 72. Measured Versus Predicted Natural Logarithm of Resilient Modulus.

By algebraic manipulation, the following equations for estimating the resilient parameters $K_{1,t}$, $K_{2,t}$ and $K_{3,t}$, for some other loading time, t, are obtained:

$$K_{1,t}=K_{1,0.1}^{0.8721}P_a^{-0.1279}e^{3.0286-1.149t-0.0654LL+0.00107\rho} \quad (28)$$

$$K_{2,t}=0.8721K_{2,0.1} \quad (29)$$

$$K_{3,t}=0.8721K_{3,0.1} \quad (30)$$

In the preceding equations $K_{1,0.1}$, $K_{2,0.1}$, and $K_{3,0.1}$ are the resilient parameters based on a 0.1 second time of loading and the other variables are as defined previously. The above equations may be derived by substituting Uzan's model, given by Equation (1) in Chapter 2, into the resilient modulus transformation equation derived from compressive creep and recovery test data.

STRENGTH PARAMETER COHESION, C

The final form of the prediction equation for C, was based on a modification of Equation (18) which was derived from mechanistic analysis. The modified form of Equation (18) is shown below:

$$C = c' + bU + dU\tan\phi \tag{31}$$

where C = total cohesion,
c' = effective cohesion,
U = suction,
ϕ = friction angle, and
b, d = constants.

The effective cohesion is a function of the plastic limit and aggregate gradation among others. The final form of the prediction equation for cohesion, C, is shown below:

$$C = 83.952 + 1.58127N40 - 2.574n - 0.0426N40_N^2 - 6.8837PL_N*G_{sN} + 0.1412U - 0.8073U*\tan\phi \tag{32}$$

where

C	=	total cohesion, KPa;
N40	=	% of material passing the 0.42 mm sieve size;
n	=	porosity;
$N40_N$	=	normalized N40 = (N40 - 55.8889);
PL_N	=	normalized plastic limit = (PL - 15.8956);
G_{sN}	=	normalized specific gravity of total aggregate = (G_s - 2.6083);
U	=	suction in KPa; and
ϕ	=	angle of internal friction.

Table A.9, in the Appendix, is a summary of the output of the regression and general linear model procedures from SAS. Figure 73 shows a plot of the measured versus the predicted C values from the prediction equation.

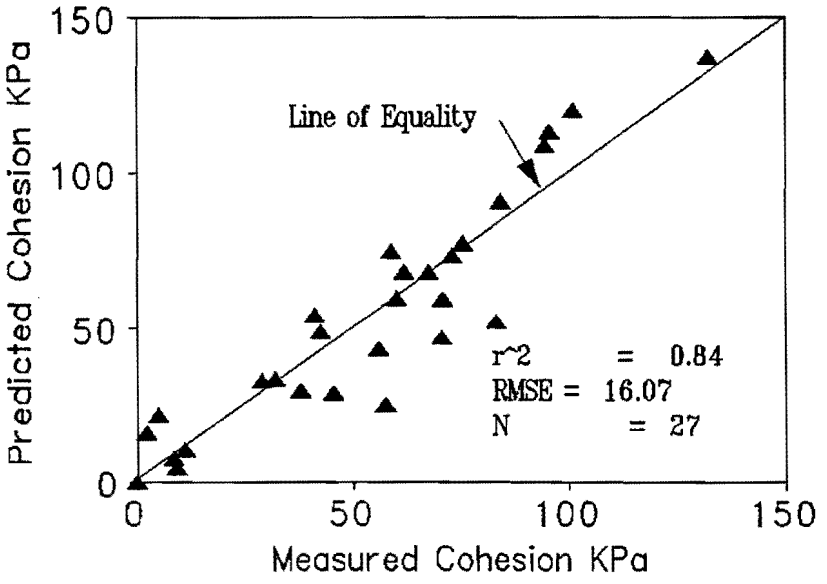

Figure 73. Measured Versus Predicted Cohesion.

SUMMARY

The prediction equation for cohesion, C, was based on mechanistic analysis. The mechanistic analysis shows that cohesion is a function of suction, the product of suction and the tangent of the angle of internal friction, and the effective cohesion which in turn is a function of the plastic limit, aggregate gradation and other soil properties. The prediction equation for cohesion verifies the mechanistic analysis. The input variables are as stated previously, and the coefficient of determination is 0.84. The effects of multicollinearity are minimal and within the acceptable range. The prediction equation should therefore give a good estimate of cohesion for soil materials in the absence of triaxial test data.

STRENGTH PARAMETER ANGLE OF INTERNAL FRICTION, ϕ

The final form of the prediction equation for the angle of internal friction, ϕ, is

$$\phi = 1.61055 - 0.95655PI - 0.881467n - 4.12995U + 31.81656G_{sb} \quad (33)$$

where PI = plasticity Index,
n = porosity,
U = suction in pF, and
G_{sb} = specific gravity of binder content.

Table A.10, in the Appendix, is a summary of the output of the regression and general linear model procedures from SAS. Figure 74 shows a plot of the measured versus the predicted angle of internal friction, ϕ, values from the prediction equation.

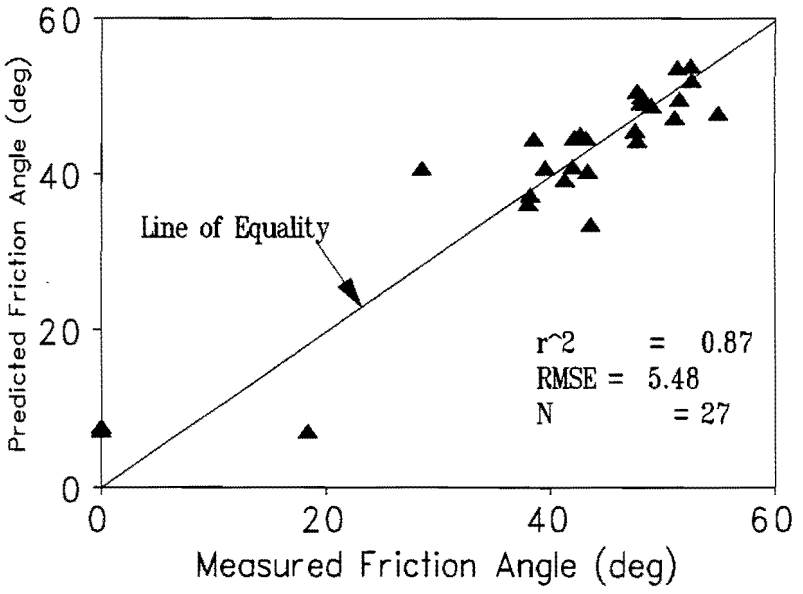

Figure 74. Measured Versus Predicted Angle of Internal Friction, ϕ, Values.

SUMMARY

Researchers have developed a prediction equation to predict, ϕ, which is the angle of internal friction. The coefficient of determination for the prediction equation is 0.87. The maximum value of the variance inflation factor, which is an indication of the effects of multicollinearity among the input variables, is 1.28. This is within the acceptable range, and the effect of multicollinearity among the input variables is minimal. The input variables are similar to those for the prediction equations for K_1, K_2 and K_3 and should be obtained quite easily in the laboratory. The prediction equation should therefore give a good estimate of ϕ.

CHAPTER 6
CONCLUSIONS AND RECOMMENDATIONS

CONCLUSIONS

Researchers investigated various alternate methods of obtaining the strength and resilient parameters of base and subgrade materials. These methods include the modified Texas triaxial test procedure and prediction equations. Based on the tests and analysis, the research team presents the following conclusions:

1. The strength parameters cohesion, C, and the angle of internal friction, ϕ, obtained from the modified triaxial test, were not significantly different from those of the standard Texas triaxial test.
2. The resilient parameters K_1 and K_2, obtained from the modified triaxial test procedure, should be calibrated using Equations (21) and (22), respectively, to obtain K_1 and K_2 values which are not significantly different from those obtained from the compressive creep and recovery test.
3. Three prediction equations to predict the resilient parameters K_1, K_2 and K_3, and two prediction equations to predict the strength parameters C, and ϕ, have been developed. The coefficient of determination for the equations ranged from 0.75 to 0.93. The independent variables differed for the different equations although suction, the dielectric constant, gradation and the Atterberg limits were among the prominent variables which were used in these equations. Using the methods presented in this report, it is possible to obtain good estimates of the resilient parameters K_1 to K_3 and the strength parameters C, and ϕ. While the goodness of fit of the prediction equation for K_2 was not as high as those obtained for the other equations, an r^2 of 0.75 is considered to be acceptable on the basis of the relatively smaller sensitivity of the predicted Mohr-Coulomb yield function to this parameter. The prediction equations have been incorporated into the structural evaluation procedure for superheavy loads in order to provide TxDOT engineers with a way of estimating the

resilient and strength parameters of unbound pavement layers from results of simpler laboratory tests.

RECOMMENDATIONS

The procedures for determining the resilient and strength parameters of soils should be implemented within the Department. TTI researchers can assist with this implementation by providing training on the use of the structural evaluation procedure for superheavy loads and on the laboratory and field tests to collect data for evaluating the resilient and strength parameters of soils. These tests include soil suction measurements, compressive creep and recovery, the modified Texas triaxial test, and dielectric measurements. There will be a need to establish standard TxDOT procedures for these tests. This task may be done as part of the implementation effort. In the development of standard test procedures, researchers recommend the following tasks:

1. Further testing should be done with the modified Texas triaxial test procedure to obtain a broader database to establish the effect of moisture on determining K_1 and K_2 and to investigate further the relationships between the resilient parameters from the modified test procedure and the compressive creep and recovery test.
2. A laboratory program should be established and executed to compare resilient parameters from the compressive creep and recovery test to the corresponding parameters determined from the resilient modulus test described in AASHTO T-274.
3. The resilient parameters estimated from the modified Texas triaxial test should also be compared with corresponding parameters from the resilient modulus test (AASHTO T-274).
4. A laboratory program should be conducted to evaluate the resilient and strength parameters for TxDOT asphalt concrete mixtures and stabilized base materials.
5. A standard laboratory test for measuring soil suction should be adopted by TxDOT. Assistance in evaluating and selecting a standard test procedure can be provided by TTI.

REFERENCES

1. Freduland, D. G. and H. Rahardjo. *Soil Mechanics for Unsaturated Soils*, A Wiley-Interscience Publication, John Wiley and Sons, Inc. New York, 1993.
2. Lytton, R. L., J. Uzan, E. G. Fernando, R. Roque, D. Hiltunen, and S. Stoffels. *Development and Validation of Performance Prediction Models and Specifications for Asphalt Binders and Paving Mixes*. Report SHRP-A-357. Strategic Highway Research Program, National Research Council, Washington, D. C., 1993.
3. Edris, E. V. and R. L. Lytton. *Dynamic Properties of Subgrade Soils Including Environmental Effects*. Research Report No. 164-3. Texas Transportation Institute, Texas A&M University, College Station, Texas, 1976.
4. Schapery, R. A., "A Method of Viscoelastic Stress Analysis Using Elastic Solutions," Journal of the Franklin Institute, Vol. 279, No 4, pp 268-289, 1965.
5. Chua, K. M., and R. L. Lytton, "A Method of Time-Dependent Analysis Using Elastic Solutions for Non-Linear Materials," International Journal for Numerical and Analytical Methods in Geomechanics, A Wiley-Interscience Publication, John Wiley and Sons, Inc. New York, 1987, Vol 11, pp 421-431, 1987.
6. Uzan, J. Characterization of Granular Materials, Analysis and Testing of Granular Bases and Subbases. In *Transportation Research Record* 1022, Transportation Research Board, National Research Council, Washington, D.C., 1985, pp. 52-59.
7. Uzan, J. and T. Scullion. Verification of Backcalculation Procedures. *Proceedings, Third International Conference on Bearing Capacity of Roads and Airfields*, Trondheim, Norway, July 3-5, 1990, pp. 447-458.
8. Lade, P. V. and R. B. Nelson. Modeling and Elastic Behavior of Granular Materials. *International Journal for Numerical and Analytical Methods in Geomechanics*, A Wiley-Interscience Publication, John Wiley and Sons, Inc., New York, 1987, pp 21-42.
9. Huang, Y. H. *Pavement Analysis and Design*. Prentice Hall, Englewood Cliffs, N.J., 1993.

10. Sides, A., J. Uzan et al., A Comprehensive Visco-Elasto-Plastic Characterization of Sand Asphalt Under Compression and Tension Cycle Loading. *Journal of Testing and Evaluation*, Vol. 13, No. 1, American Society for Testing and Materials, Philadelphia, Pennsylvania, 1985, pp 94-102.
11. Seed, H. B. and R. L. McNeil. Soil Deformations under Repeated Stress Applications. *Proceedings, Conference on Soils for Engineering Purposes*, STP 232, American Society for Testing Materials, Philadelphia, Pennsylvania, 1957, pp 62-71.
12. Crockford, W. W., L. J. Bendana et al. *Modeling Stress and Strain States in Pavement Structures Incorporating Thick Granular Layers*. Final Report Contract F08635-87-C-0039, U.S Air Force, Tyndall Air Force Base, Florida, 1990.
13. Culley, R. W. Effects of Freeze Thaw Cycling on Stress Strain Characteristics and Volume Change of a Till Subjected to Repeated Loading. *Canadian Geotechnical Journal*, Vol. 8, No. 3, National Research Council of Canada, Ottawa, 1971, pp 57-78.
14. Lytton, R.L. and F. P. Germann, Y. J. Chou, and S. M. Stoffels, "Determination of Asphaltic Concrete Pavement Structural Properties by Nondestructive Testing," NCHRP Report 327, National Cooperative Highway Research Program, Transportation Research Board, Washington, D.C, 1990.
15. Lamborn, M. J. *A Micromechanical Approach to Modeling Partly Saturated Soils*. M.S. Thesis. Texas A&M University, College Station, Texas, 1986.
16. Texas State Department of Highways and Public Transportation. *Manual of Testing Procedures*. Vol. 1 & 2, Austin, Texas, 1983.
17. Lytton, R. L. and S. Jooste. *Determination of Moisture Suction Relationships Using Filter Paper*. (Unpublished Laboratory Procedures Manual) Texas Transportation Institute, Texas A&M University, College Station, Texas, 1993.
18. Lytton, R. L. and S. Jooste. *Determination of Moisture Suction Relationships Using Pressure Plate*. (Unpublished Laboratory Procedures Manual) Texas Transportation Institute, Texas A&M University, College Station, Texas, 1993.

19. AASHTO *Guide for Design of Pavement Structures*, American Association of State Highway and Transportation Officials, Washington, D. C., 1986.
20. SAS Institute Inc., *SAS Procedures Guide*. Version 6, Third Edition, Cary, N.C., 1990.
21. Ott, R. L. *An Introduction to Statistical Methods and Data Analysis*. Fourth Edition, Marion Merrell Dow, Inc, Duxbury Press, Belmont, California, 1993.
22. Casella, G. and R. L. Berger. *Statistical Inference*. Second Edition, Wadsworth and Brooks/Cole Statistics/Probability Series, New York, 1990.
23. Jooste, F. and E. G. Fernando. Development of a Procedure for the Structural Evaluation of Superheavy Load Routes, Research Report 1335-3F, Texas Transportation Institute, Texas A&M University, College Station, Texas, 1995.

APPENDIX

STATISTICAL OUTPUT FOR PREDICTION EQUATIONS

Table A.1. Analysis of Variance for Cohesion.

Analysis of Variance N = 18 r^2 = 0.945

Class	Levels	Values
Treatment	2	m s
Block	9	1 2 3 4 5 6 7 8 9

Dependent Variable: Cohesion

Source	DF	Sum of Squares	Mean Square	F Value	Pr > F
Model	9	461.524	51.280	15.49	0.0004
Error	8	26.479	3.309		
C. Total	17	488.004			

Cohesion Mean	R-Square	C.V.	Root MSE
8.9245	0.945739	20.385	1.81933

Dependent Variable: Cohesion

Source	DF	Anova SS	Mean Square	F Value	Pr > F
Block	8	461.349	57.668	17.42	0.0003
Treatment	1	0.175	0.175	0.05	0.8239

Table A.2. Analysis of Variance for Angle of Internal Friction.

Analysis of Variance N = 18 r^2 = 0.975

Class	Levels	Values
Block	9	1 2 3 4 5 6 7 8 9
Treatment	2	m s

Dependent Variable: Friction angle

Source	DF	Sum of Squares	Mean Square	F Value	Pr > F
Model	9	1.023	0.113	32.64	0.0001
Error	8	0.027	0.003		
C. Total	17	1.051			

Friction Angle Mean	R-Square	C.V.	Root MSE
0.73126	0.973491	8.072186	0.05903

Dependent Variable: Friction angle

Source	DF	Anova SS	Mean Square	F Value	Pr > F
Block	8	1.019	0.127	36.58	0.0001
Treatment	1	0.00389	0.00389	1.12	0.3211

Table A.3. Analysis of Variance for Resilient Parameter K_1.

Analysis of Variance N = 18

Class	Levels	Values
Block	9	1 2 3 4 5 6 7 8 9
Treatment	2	m s

Dependent Variable: K_1

Source	DF	Sum of Squares	Mean Square	F Value	Pr > F
Model	9	52626299.7	5847366.6	26.95	0.0001
Error	8	1735491.4	216936.4		
C. Total	17	54361791.1			

R-Square	C.V.	Root MSE	K_1 Mean
0.968075	30.37961	465.764	1533.15

Dependent Variable: K_1

Source	DF	Anova SS	Mean Square	F Value	Pr > F
Block	8	52594206.9	6574275.9	30.31	0.0001
Treatment	1	32092.8	32092.8	0.15	0.7105

Table A.4. Analysis of Variance for Resilient Parameter K_2.

Analysis of Variance Procedure N = 18 r^2 = 0.973

Class	Levels	Values
Block	8	1 2 3 4 5 6 7 8
Treatment	2	m s

Dependent Variable: K_2

Source	DF	Sum of Squares	Mean Square	F Value	Pr > F
Model	8	0.50087993	0.062600	31.65	0.0001
Error	7	0.01384762	0.001978		
C. Total	15	0.51472755			

R-Square	C.V.	Root MSE	K_2 Mean
0.973097	7.231752	0.04448	0.61503

Dependent Variable: K_2

Source	DF	Anova SS	Mean Square	F Value	Pr > F
Block	7	0.50087900	0.071554	36.17	0.0001
Treatment	1	0.00000001	0.00000001	0.00	0.9981

Table A.5. Regression and General Linear Model Output for K_1.

Dependent Variable: K_1 N=26 R^2 = 0.9317

Analysis of Variance

Variable	DF	Parameter Estimate	Standard Error	T for H_0: Parameter=0	Prob > |T|
Intercept	1	28659	3728.89	7.686	0.0001
PL	1	-417.29	87.87	-4.749	0.0002
G_s	1	-5706.38	1484.97	-3.843	0.0013
θ_w	1	12780	5504.46	2.322	0.0329
N40	1	-75.44	13.21	-5.708	0.0001
tan ϕ	1	-5462.07	722.39	-7.561	0.0001
$N40_N*U_N$	1	58.97	15.69	3.757	0.0016
$N40_N*\tan \phi_N$	1	256.00	27.48	9.313	0.0001
$U_N*\varepsilon_{rN}$	1	-309.32	96.02	-3.221	0.0050

Maximum Variance Inflation Factor	6.88378964
RMSE	810.52185
C.V.	38.93927
Press Statistic	24708745.66475
Durbin-Watson, d	2.23559653

Table A.6. Regression and General Linear Model Output for K_2.

Dependent Variable: K_2 N=26 R^2 = 0.7529

Analysis of Variance

Variable	DF	Parameter Estimate	Standard Error	T for H_0: Parameter=0	Prob > |T|
Intercept	1	-0.127927	0.47268916	-0.271	0.7896
G_s	1	0.515759	0.22532700	2.289	0.0337
W	1	-0.084802	0.01543333	-5.495	0.0001
$N40_N^2$	1	0.000270	0.00005129	5.272	0.0001
LL_N*W_N	1	-0.009607	0.00254634	-3.773	0.0013
LL_N*tan ϕ_N	1	-0.192586	0.03535033	-5.448	0.0001
LL_N^2	1	0.003981	0.00152711	2.607	0.0173

Maximum Variance Inflation Factor	7.88692
RMSE	0.18528
C.V.	29.24886
Press Statistic	1.27359
Durbin-Watson D	2.35791

Table A.7. Regression and General Linear Model Output for K_3.

Dependent Variable: K_3 N=9 R^2 = 0.9224

Variable	DF	Parameter Estimate	Standard Error	T for H0: Parameter=0	Prob > |T|
Intercept	1	1.807384	0.29450281	6.137	0.0017
ε_r	1	-0.181851	0.02503517	-7.264	0.0008
LL_N*W_N	1	-2.808291	0.43124690	-6.512	0.0013
LL_N*ε_r	1	-0.016342	0.00541146	-3.020	0.0294

Maximum Variance Inflation Factor	11.21529894
RMSE	0.1328
C.V.	34.44317
Press Statistic	0.70026595
Durbin-Watson D	2.21515728

Table A.8. Regression and General Linear Model Output for $\ln(E_{r,t})$

Dependent Variable: ln(E) N=150 R^2=0.80

Analysis of Variance

Variable	DF	Parameter Estimate	Standard Error	T for H_0: Parameter=0	Prob > |T|
Intercept	1	3.028660	0.50904504	5.950	0.0001
$\ln(E_{r,0.1})$	1	0.872182	0.03871182	22.53	0.0001
t	1	-1.149148	0.17293362	- 6.645	0.0001
LL	1	-0.065402	0.01108195	- 5.902	0.0001
Conductivity	1	0.001072	0.00033300	3.220	0.0016

Maximum Variance Inflation Factor	1.87
RMSE	0.6354
C.V.	6.047
Press Statistic	62.961
Durbin-Watson D	1.345

Table A.9. Regression and General Linear Model Output for Cohesion, C.

Dependent Variable: Cohesion N=27 R^2 = 0.8436

Analysis of Variance

Variable	DF	Parameter Estimate	Standard Error	T for H0: Parameter=0	Prob > |T |
Intercept	1	12.167	3.3147	3.671	0.0015
N40	1	0.2291	0.0388	5.892	0.0001
n	1	-0.3730	0.1277	-2.919	0.0085
$N40_N^2$	1	-0.0061	0.0015	-4.009	0.0007
PL_N*G_s	1	-0.9976	0.3663	-2.723	0.0131
U	1	0.14120	0.0235	5.990	0.0001
U*tanϕ	1	-0.1171	0.0406	-2.878	0.0093

Maximum Variance Inflation Factor	7.552569
RMSE	2.3307
C.V.	28.84657
Press Statistic	230.77876
Durbin-Watson D	2.16315606

Table A.10. Regression and General Linear Model Output for Angle of Internal Friction, ϕ.

Dependent Variable: Friction Angle N=27 R^2 = 0.8714					
Analysis of Variance					
Variable	DF	Parameter Estimate	Standard Error	T for H0: Parameter=0	Prob > |T|
Intercept	1	1.610551	20.666	0.078	0.9386
PI	1	-0.956558	0.1976	-4.841	0.0001
n	1	-0.881467	0.1488	-5.922	0.0001
U	1	-4.129953	1.4436	-2.861	0.0091
G_s	1	31.816561	7.2946	4.362	0.0002

Maximum Variance Inflation Factor	1.28895710
RMSE	5.48479
C.V.	13.44787
Press Statistic	1094.51643395
Durbin-Watson D	2.11523066